

Rune H. Larsen

# Pre-rotation of inlet flow for a reversible pump turbine in pump mode

Master's thesis in Mechanical Engineering

Supervisor: Pål-Tore Selbo Storli and Petter Østby, Rainpower

June 2019



Rune H. Larsen

# Pre-rotation of inlet flow for a reversible pump turbine in pump mode

Master's thesis in Mechanical Engineering  
Supervisor: Pål-Tore Selbo Storli and Petter Østby, Rainpower  
June 2019

Norwegian University of Science and Technology  
Faculty of Engineering  
Department of Energy and Process Engineering





**MASTER WORK**

for

student Rune Haugen Larsen

Spring 2019

*Pre-rotation of inlet flow for a reversible pump turbine in pump mode*

*Prerotasjon av strømnning på innløpet av en reversibel pumpeturbin i pumpedrift*

**Background**

Norway has 50% of the European hydro reservoir energy storage, and many of these sites are highly suitable for retrofitting of pump-storage capabilities. To be able to reuse existing power plants by retrofitting with Reversible Pump Turbines (RPTs), the problem of cavitation in pumping mode must be solved. This has been proposed solved by the use of an axial booster pump in front of the RPT. A booster pump will create a rotational component in the flow leaving the booster pump. How this component will evolve as the flow approaches the RPT is uncertain, and how the rotation actually is at the inlet of the RPT is important for the operation and characteristics of the RPT, especially since it affects the cavitation properties of the unit, and might counteract the initial suggested solution by using the booster pump in the first place.

**Objective**

The candidate shall investigate how the rotational component in the outlet flow from a booster pump is distributed and evolves as the flow approaches the RPT and how this affects the pump performance curves.

**The following tasks are to be considered:**

1. Literature review of RPTs in pump mode as well as mixed-flow pump design philosophy and the outlet flow field from such pumps
2. Investigate how the flow field evolves from the outlet of a mixed-flow pump to the inlet of a prescribed RPT geometry.
3. Develop a numerical model for further analysis of the head-flow characteristics of the combined system.
4. If the student will go to Nepal for an excursion, earlier and further work will be presented as a publication and presented at the conference; 9<sup>th</sup> *International symposium on Current Research in Hydropower Technologies (CRHT-IX)* at Kathmandu University

The master work comprises 15 ECTS credits.

The work shall be edited as a scientific report, including a table of contents, a summary in Norwegian, conclusion, an index of literature etc. When writing the report, the candidate must emphasise a clearly arranged and well-written text. To facilitate the reading of the report, it is important that references for corresponding text, tables and figures are clearly stated both places.

By the evaluation of the work the following will be greatly emphasised: The results should be thoroughly treated, presented in clearly arranged tables and/or graphics and discussed in detail.

The candidate is responsible for keeping contact with the subject teacher and teaching supervisors.

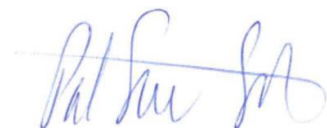
Risk assessment of the candidate's work shall be carried out according to the department's procedures. The risk assessment must be documented and included as part of the final report. Events related to the candidate's work adversely affecting the health, safety or security, must be documented and included as part of the final report. If the documentation on risk assessment represents a large number of pages, the full version is to be submitted electronically to the supervisor and an excerpt is included in the report.

According to “Utfyllende regler til studieforskriften for teknologistudiet/sivilingeniørstudiet ved NTNU” § 20, the Department of Energy and Process Engineering reserves all rights to use the results and data for lectures, research and future publications.

Submission deadline: 11 June 2019.

- Work to be done in lab (Water power lab, Fluids engineering lab, Thermal engineering lab)
- Field work

Department for Energy and Process Engineering, 11/1 2019



Pål-Tore Storli  
Supervisor

Co-Supervisor(s): Petter Østby, Rainpower

# Abstract

Pumped hydropower storage is an excellent tool for balancing the energy grid and help utilize renewable energy resources more effectively. As electrical energy needs to be used as it is created, pumped hydro technology supplies the opportunity of storing energy which is otherwise going to waste. Norway has 50% of the European hydro storage capacity [1], and much of this capacity could be used to help balance the European energy grid. To do so, retrofitting of pumping abilities to existing hydropower plants is a viable option. According to a study performed by *NVE*, many of the hydropower plants in Norway are suitable for retrofitting of pump-storage capabilities [2].

To be able to reuse existing power plants by retrofitting Francis turbines with Reversible Pump Turbines (RPTs), the obstacle of cavitation in pumping mode needs to be solved. The cavitation problem has been proposed solved by the use of a booster-pump in front of the RPT. This booster-pump could produce a rotational component in the flow approaching the RPT. How this rotational component evolves as the flow approaches the RPT is uncertain, and how the rotation is at the inlet of the RPT is important for the operation and characteristics of the RPT.

To investigate the matter of pre-rotation in an RPT; steady-state computational fluid dynamics simulations on the full geometry of an RPT have been conducted using the commercial *ANSYS CFX* software. Pump performance curves with and without pre-rotation have been obtained and investigated. The results suggest that counter pre-rotation gives additional head, following the Euler turbomachinery equation. However, efficiency does not increase. It is also observed that the secondary flows generated by the bend in the draft tube, rotate in the same direction as the induced pre-rotation.

Further, a possible solution with a mixed-flow booster-pump in series with the RPT has been studied. This machine has swirl at the outlet, acting as pre-rotation for the flow towards the RPT. The combined system is simulated with the booster-pump rotating in the same direction as the RPT, and the opposite. The results are similar to what was found when using a uniform pre-rotation. Counter pre-rotation provides additional head while pre-rotation in the same direction subtracts head from the system.



# Sammen drag

Pumpekraftverk er et utmerket verktøy for å balansere energinettet og å utnytte fornybare energikilder mer effektivt. Ettersom elektrisk energi må bli brukt samstundes som det blir produsert, gir pumpekraft-teknologi muligheten til å lagre energi som ellers ville ha gått til spille. Norge har 50% av Europas vannlagerkapasitet og mye av denne kapasiteten kan bli brukt til å balansere Europas energinett [1]. Dette kan bli gjort ved å bygge om eksisterende vannkraftverk til pumpekraftverk. I følge *NVE*, er mange av vannkraftverkene i Norge passende for å bli bygd om til pumpekraftverk [2].

For å kunne gjenbruke et eksisterende vannkraftverk med Francis-turbiner ved å ettermontere reversible pumpeturbiner (RPTer), må problemet med kavitasjon i pumpemodus løses. Dette problemet har blitt foreslått løst ved å bruke en boosterpumpe foran RPTen. Denne boosterpumpen kan muligens produsere en roterende komponent i strømmingen oppstrøms RPTen. Hvordan denne komponenten utvikles gjennom sugerøret mot RPTen er usikkert, og hvordan rotasjonen er på innløpet av RPTen er viktig for operasjonen og pumpekaraktistikken til maskinen.

Tidsuavhengige CFD-simuleringer (Computational Fluid Dynamics) på en komplett RPT-geometri har blitt gjennomført ved hjelp av den kommersielle programvaren *ANSYS CFX*. Pumpekurver, med og uten prerotasjon, har blitt generert og undersøkt. Resultatene antyder at prerotasjon i motsatt retning av rotasjonsretningen til RPTen, genererer en økning i løftehøyde. Dette samsvarer med Eulers turbomaskin ligning. Samtidig ser det ut til at virkningsgraden *ikke* øker. Det er også observert at den sekundære strømmingen som genereres nedstrøms av bendet i sugerøret, roterer i samme retning som den induserte prerotasjonen.

Videre har en mulig løsning med en *mixed-flow* boosterpumpe blitt undersøkt. Denne maskinen har en virvel ved utløpet som fungerer som prerotasjon for RPTen. Det kombinerte systemet er simulert med boosterpumpen roterende i både samme og motsatt retning som RPTen. Det samme mønsteret gjentas her. Prerotasjon i motsatt retning av rotasjonsretningen til RPTen gir økt løftehøyde, mens prerotasjon i samme rotasjonsretning gir redusert løftehøyde.



# Contents

Task Description . . . . .	i
Abstract . . . . .	iii
Sammendrag . . . . .	v
Notations . . . . .	xi
List of Figures . . . . .	xiii
List of Tables . . . . .	xvii
<b>I Introduction</b>	<b>1</b>
<b>1 Introduction</b>	<b>3</b>
1.1 Motivation . . . . .	3
1.2 Previous Work and Hypothesis . . . . .	4
1.3 Objective and Outline . . . . .	4
1.4 Limiting the Scope . . . . .	5
<b>II Theoretical Background</b>	<b>7</b>
<b>2 Pumped Hydropower Storage</b>	<b>9</b>
2.1 Energy Storage . . . . .	9
2.2 Francis Reversible Pump Turbine . . . . .	10
2.3 Multistage Reversible Pump Turbine . . . . .	11
2.4 Difference between Turbine Mode and Pump Mode . . . . .	11

2.5	Cavitation . . . . .	12
2.6	Net Positive Suction Head and Submergence . . . . .	13
2.7	Booster Pump in Series with RPT . . . . .	14
2.7.1	Booster-Pump at Roskrepp Hydropower Station . . . . .	16
<b>3</b>	<b>Pump Theory</b>	<b>17</b>
3.1	Pump Performance Curves . . . . .	17
3.2	Specific Speed and the Cordier Diagram . . . . .	18
3.3	Pump Types . . . . .	19
3.4	Impeller Approach and Pre-Rotation . . . . .	20
3.5	Diffusers and Guide Vanes . . . . .	21
<b>4</b>	<b>Numerical Theory</b>	<b>23</b>
4.1	The Incompressible Navier-Stokes Equations . . . . .	23
4.2	Rotating Frame of Reference . . . . .	24
4.3	Turbulent and Laminar Flow . . . . .	24
4.4	Reynolds-Averaged Navier-Stokes Equations . . . . .	25
4.5	Turbulence Modelling . . . . .	25
4.6	Boundary Layer Modelling . . . . .	26
4.7	Periodic Boundary Conditions . . . . .	27
<b>III</b>	<b>Method and Results</b>	<b>29</b>
<b>5</b>	<b>Reversible Pump Turbine with Uniform Pre-Rotation at Draft Tube Inlet</b>	<b>31</b>
5.1	Geometry . . . . .	31
5.2	Mesh Generation . . . . .	31
5.3	Mesh Independence Study . . . . .	35
5.4	Numerical Setup . . . . .	35
5.4.1	Inlet Boundary Conditions . . . . .	36



---

5.5	Results . . . . .	38
5.5.1	Pump Performance Curves . . . . .	38
5.5.2	Velocity Distribution . . . . .	40
5.5.3	Secondary Flows in Draft Tube . . . . .	41
5.5.4	Hydraulic Losses . . . . .	42
<b>6</b>	<b>Booster-Pump in Series with Reversible Pump Turbine</b>	<b>45</b>
6.1	Booster-Pump Geometry and Placement . . . . .	45
6.2	Selection of Booster-Pump and Rapid Prototyping . . . . .	46
6.3	Results . . . . .	47
6.3.1	Converging Nozzle Mixed-Flow Booster-Pump . . . . .	48
6.3.2	Booster-Pump Running in Opposite Direction as RPT . . . . .	50
6.3.3	Booster-Pump Running in the Same Direction as RPT . . . . .	52
6.3.4	Comparison of Options . . . . .	53
<b>IV</b>	<b>Concluding Remarks</b>	<b>55</b>
<b>7</b>	<b>General Discussion</b>	<b>57</b>
<b>8</b>	<b>Conclusion</b>	<b>59</b>
<b>9</b>	<b>Future Work</b>	<b>61</b>
	<b>References</b>	<b>64</b>
	<b>APPENDICES</b>	<b>67</b>
<b>A</b>	<b>Theory</b>	<b>67</b>
A.1	Inducers . . . . .	67
A.2	Submergence . . . . .	67
<b>B</b>	<b>Rapid Prototyping</b>	<b>69</b>

---

B.1 Axial Booster-Pump . . . . .	69
B.2 Large Diameter Mixed-Flow Booster-Pump . . . . .	70
<b>C Nepal Conference Paper</b>	<b>71</b>

# Notations

## Abbreviations

<b>BEP</b>	Best Efficiency Point
<b>BP</b>	Booster-Pump
<b>CAD</b>	Computer Aided Design
<b>CFD</b>	Computational Fluid Dynamics
<b>DNS</b>	Direct Numerical Simulation
<b>DT</b>	Draft Tube
<b>GVO</b>	Guide Vane Opening
<b>GV</b>	Guide Vane
<b>HL</b>	High Load
<b>IGV</b>	Inlet Guide Vane
<b>PL</b>	Part Load
<b>RPT</b>	Reversible Pump Turbine
<b>SC</b>	Spiral Casing
<b>SV</b>	Stay Vane

## Normalized Numbers

$\bar{\eta}$	Normalized Efficiency	$\bar{\eta} = \frac{\eta_{CFD}}{\eta_{experiment,BEP}}$
$\bar{H}$	Normalized Head	$\bar{H} = \frac{H_{CFD}}{H_{experiment,BEP}}$
$\bar{Q}$	Normalized Mass Flow	$\bar{Q} = \frac{Q_{CFD}}{Q_{experiment,BEP}}$
$\tilde{H}$	Percent of RPT Head	$\tilde{H} = \frac{H_{CFD}}{H_{experiment,BEP}} * 100\%$

## Definitions

**NPR** Negative Pre-Rotation: Pre-rotation in the same direction as the impeller rotational direction. Defined as a negative amount of degrees

**PCPR** Positive Counter Pre-Rotation: Pre-rotation in the opposite direction as the impeller rotational direction. Defined as a positive amount of degrees

## Nomenclature

$\beta$	Angle between the relative and peripheral velocity	[deg]
$\beta_b$	Blade angle	[deg]
$\eta$	Efficiency	[-]
$\Omega$	Rotational speed	[1/s]
$\Omega_s$	Specific speed	[-]
$\rho$	Density	[kg/m <sup>3</sup> ]
$B$	Runner outlet width	[m]
$C$	Absolute velocity	[m/s]
$C_m$	Meridional component of C	[m/s]
$C_u$	Peripheral component of C	[m/s]
$D$	Runner diameter	[m]
$D_s$	Specific diameter	[-]
$g$	Gravitational constant	[m/s <sup>2</sup> ]
$H$	Head	[m]
$H_S$	Suction Head	[m]
$h_s$	Barometric head	[m]
$n$	Rotational speed	[rpm]
$NPSH$	Net Positive Suction Head	[m]
$P$	Power	[W]
$p_{amb}$	Ambient pressure	[Pa]
$p_v$	Vapour pressure	[Pa]
$Q$	Discharge	[m <sup>3</sup> /s]

---

$r$	Runner radius	[m]
$T$	Torque	[Nm]
$U$	Peripheral velocity	[m/s]
$W$	Relative velocity	[m/s]

## Subscripts

$1$	Pressure side of impeller
$2$	Suction side of impeller
$m$	Meridional
$p$	Pump mode
$r$	Radial
$t$	Turbine mode
$u$	Peripheral
$z$	Axial
$exp$	Experiment



# List of Figures

2.1	Globally estimated energy storage capacity from 2010. Collected from [10] . . . . .	9
2.2	Energy losses for a single round-trip pumped storage cycle. Total efficiency typically around 80%. Collected from [10] . . . . .	10
2.3	Comparison of a Francis runner (left) and an RPT (right) from the Waterpower laboratory at NTNU. Collected from [14] . . . . .	10
2.4	Multistage reversible pump turbine. Collected from [18] . . . . .	11
2.5	Difference between the head for turbine and pump mode. Collected from [17] . . . . .	12
2.6	Velocity triangles for an RPT. Collected from [19] . . . . .	12
2.7	Cavitation bubble imploding near a wall. Collected from [13, p. 263] . . . . .	13
2.8	Illustration of the patent which utilizes a booster pump in a separate waterway. Collected from [21] . . . . .	15
3.1	Pump curves for a booster-pump in series with another pump, along with the combined pump curve. Collected and adapted from [13, p. 670] . . . . .	18
3.2	The <i>Cordier</i> diagram. This diagram gives an indication of suitable hydraulic machine based on specific speed and specific diameter. Collected from [25] . . . . .	19
3.3	Illustration of a mixed-flow pump (left) and an axial flow pump (right). Collected and adapted from [13, p. 61] . . . . .	20
3.4	Pump characteristics of a mixed-flow pump with pre-rotation control. Collected from [13, p. 675] . . . . .	21
3.5	Hydraulic losses for a RPT in pump mode at different guide vane openings. (a) 12°guide vane opening, (b) 16°guide vane opening, (c) 20°guide vane opening. Collected from [29] . . . . .	22
4.1	A logarithmic representation of a turbulent boundary layer profile. Collected from [26] . . . . .	27
5.1	The RPT geometry investigated in this thesis . . . . .	32

5.2	Structured surface mesh on impeller blades . . . . .	32
5.3	Structured surface mesh on a few guide vanes . . . . .	33
5.4	Unstructured surface mesh of spiral casing . . . . .	33
5.5	Surface mesh of the spiral casing tongue . . . . .	34
5.6	Surface mesh of draft tube . . . . .	35
5.7	Velocity vector plot showing the circumferential velocity components at the inlet; top-left: 12°, bottom-left: 24°, top-right: -12°, bottom-right: -24° . . . . .	37
5.8	Streamlines in the draft tube showing the path of a fluid particle with zero mass for the different inlet boundary conditions. Results from 1.2BEP with no pre-rotation, 24°PCPR and 24°NPR . . . . .	38
5.9	$\bar{Q} - \bar{H}$ plot with normalized values for different pre-rotation values . . . . .	39
5.10	$\bar{Q} - \bar{\eta}$ plot with normalized values for different pre-rotation values . . . . .	39
5.11	Difference in the $UC_u$ distribution at the impeller inlet with different pre-rotation . . . . .	40
5.12	Secondary flows in draft tube cone at 1.2BEP. The view is from beneath the draft tube, looking up at the runner inlet. The bottom right figure shows the location of the plane in the draft tube cone. The top left figure shows the secondary flows occurring around the x-axis as expected for zero pre-rotation, whereas the secondary flows twist with the pre-rotation for positive pre-rotation (upper right) and negative pre-rotation (lower right) . . . . .	41
5.13	Hydraulic losses in draft tube . . . . .	43
5.14	Difference in hydraulic losses in draft tube from no pre-rotation . . . . .	43
5.15	Hydraulic losses in guide vanes . . . . .	43
5.16	Difference in hydraulic losses in guide vanes from no pre-rotation . . . . .	43
5.17	Hydraulic losses in stay vanes and spiral casing . . . . .	43
5.18	Difference in hydraulic losses in stay vanes and spiral casing from no pre-rotation . . . . .	43
6.1	RPT and booster-pump connected in series with bulb configuration. . . . .	46
6.2	RPT and mixed-flow booster-pump in series with shaft going through the draft tube . . . . .	46
6.3	Mesh of draft tube showing the bulb implementation. Mesh is shown at a plane going through the center of the draft tube . . . . .	47
6.4	Losses in the guide vanes, stay vanes and spiral casing for the RPT for the case of no pre-rotation . . . . .	47
6.5	Design of mixed-flow booster pump with converging nozzle at the inlet. The outlet of the pump has the same diameter as the draft tube gate, but the inlet of the booster-pump is smaller. . . . .	48



6.6	Pump curves for the converging mixed-flow booster-pump . . . . .	48
6.7	Contour plot of turbulent kinetic energy in diffuser channels which shows separation at 0.5 span-wise direction . . . . .	49
6.8	Normalized $NPSH$ for the RPT and booster-pump. $NPSH_A : RPT$ is set such that the RPT can run in turbine mode at 1.25BEP without experiencing cavitation . . . . .	49
6.9	Velocity profiles for the outlet of the booster-pump . . . . .	50
6.10	RPT impeller and converging-nozzle mixed-flow booster-pump running in the <i>opposite</i> direction in series . . . . .	51
6.11	Pump curves for the booster-pump and the RPT connected in series with <i>opposite</i> rotational direction. $\eta_{RPT}^{ref}$ refers to the case of no pre-rotation for the RPT . . . . .	51
6.12	Illustration of the trailing wake following the booster-pump at BEP. . . . .	52
6.13	RPT impeller and converging-nozzle mixed-flow booster-pump running in the <i>same</i> direction in series. . . . .	52
6.14	Pump curves for the booster-pump and the RPT connected in series with the <i>same</i> rotational direction. $\eta_{RPT}^{ref}$ refers to the case of no pre-rotation for the RPT . . . . .	52
6.15	Comparison of the combined pump performance curves when having the booster-pump rotating in the same direction or the opposite direction of the RPT . . . . .	53
A.1	Inducer used on the RPT investigated in the paper by <i>Schilling et al.</i> Collected from [38] . . . . .	67
A.2	Illustrative example for calculation of the necessary submergence to avoid cavitation in a pump. Collected from [13, p. 44] . . . . .	68
B.1	Design of an axial flow pump. Here, the inlet and outlet of the booster-pump has the same diameter as the outlet of the draft tube. Rotational speed: $n = 200rpm$ . . . . .	69
B.2	Pump curves for the axial booster-pump . . . . .	69
B.3	Design of mixed-flow booster-pump. Here, the inlet and the outlet of the booster-pump has the same diameter as the outlet of the draft tube. Rotational speed: $n = 150rpm$ . . . . .	70
B.4	Pump curves for the large mixed-flow booster-pump . . . . .	70

# List of Tables

2.1	Empirical values used for the submergence of pumps and turbines [17] . . . . .	14
5.1	Mesh independence study at best efficiency point . . . . .	35

# Part I

## Introduction



# Chapter 1

## Introduction

### 1.1 Motivation

On the 8th of December 2018, wind power generated one-third of Europe's energy need. The next few days, the output from wind power dropped from  $98GW$  to below  $30GW$  [3]. This vast discrepancy emphasizes the fact that wind power is inherently weather dependent. Today, the European electricity grid is receiving more and more energy from unsteady wind energy as the prices for building wind capacity are rapidly decreasing [3],[4]. As a consequence, the need for balancing power capabilities is growing proportionately.

Hydropower is the world's largest source of renewable energy production, and it has been for a long time [5]. In 2018, Europe installed  $11.7GW$  of new wind capacity, which accounts for 48% of the total installed power capacity that year [3]. As the magnitude of wind power is rapidly increasing, enabling efficient collaboration between hydropower and wind power is increasingly crucial. *REN21 (Renewables Global Status Report)* emphasizes the need for balancing energy production from different renewable energy resources [4]. That is, to utilize the excess energy when production is higher than demand, and to store energy for times when energy production is too low.

The most promising tool for meeting this emerging power and capacity demand is pumped hydropower storage [6]. By 2050, an estimated hourly power balancing need of about  $200 - 300GW$  is needed only in West-Central Europe [7]. By mid-2017, globally installed power storage capacity was only  $176GW$  [8]. Therefore, to cope with the increase in unsteady renewable energy resources, more pumped hydro power plants are needed.

Norway has a staggering 50% of Europe's hydropower reservoir capacity [1]. According to studies performed by *NVE*, much of this capacity is suitable for retrofitting of pumping capabilities [2]. With all this storage potential, Norway could act as a battery for the European power system, effectively balancing the grid [7]. To become Europe's new, green battery, retrofitting of pumping capabilities is a task that needs to be accomplished. Many of the hydropower plants suitable for this retrofitting use Francis turbines and, consequently, replacing Francis turbines with Reversible Pump Turbines (RPTs) is a task that is being reviewed by *HydroCen* [9].

When replacing Francis turbines with RPTs, the problem of cavitation in pump mode needs to be solved. In pump mode, pressure zones below vapor pressure generate cavitation when the impeller is submerged to a turbine level of submergence. To avoid cavitation in pump mode, the RPT would typically have had to be submerged further down. The extra submersion would lead to new waterways and, according to another study performed by *NVE*, this implies that the project of replacing Francis turbines with RPTs would not

be profitable [2].

A proposed solution, which sidesteps the expensive procedure of digging new waterways, is to install a booster-pump in front of the RPT. In particular, a booster-pump near the draft tube gate. A booster-pump would increase the static pressure at the inlet of the RPT, solve the cavitation problem, and thereby avoiding the need for extra submergence. This solution will hopefully provide cost savings notable enough to make the project profitable.

Installing a booster-pump in front of an RPT is a mammoth task that involves several different aspects. One of these aspects is the interaction between the booster-pump and the RPT. In particular, how the flow following the booster-pump affects the pumping characteristics of the RPT. The flow following the booster-pump could involve a rotational component, and how this rotational component affects the RPT will be studied in detail in this thesis.

## 1.2 Previous Work and Hypothesis

If there is a rotational component following the booster-pump, this rotational component will act as pre-rotation for the RPT. Previously, a study regarding pre-rotation in an RPT in pump mode was conducted by *Martin* [10]. Martin investigated whether an induced pre-whirl could benefit the off-design pump operation of an RPT. The pre-rotation was here induced by blowing water through slits in the draft tube cone. The results of this work remain inconclusive as the blowing intensity of the jets proved too weak. However, research regarding pre-rotation in both centrifugal and mixed-flow pump has shown that pre-rotation can alter the characteristics of the machine significantly and even increase the efficiency [11], [12], [13, p. 675]. The studies mentioned above impose the pre-rotation with the help of inlet guide vanes in a straight suction pipe.

In this thesis, the working hypothesis is that pre-rotation will alter the pumping characteristics of an RPT. Here, pre-rotation will be imposed from the outlet of a booster-pump, at the inlet of the draft tube - near the draft tube gate. This location of the booster-pump indicates that the pre-rotation will evolve through the draft tube and the draft tube bend, before reaching the impeller.

## 1.3 Objective and Outline

The objective of this work is to study how the rotational component in the outlet flow of a booster-pump is distributed and evolves towards the RPT. How the rotational component affects the pump performance curves of the RPT are to be investigated in detail. These matters are examined in the following order:

- First, the theory behind pumped hydropower storage is examined. Cavitation and the reasoning for why a pump turbine normally would have to be further submerged than a Francis turbine is explained. Further, pumping theory is considered, and aspects related to running a booster-pump and an RPT in series is discussed. Before diving into the method used in this thesis, some of the theory regarding the numerical tools simulations is presented.
- A numerical model of an existing RPT is created and examined with and without an induced, uniform pre-rotation at the inlet of the draft tube. Here, pump curves are extracted and examined.
- To induce a more realistic pre-rotation for the RPT, a design of a booster-pump is created and simulated together with the RPT. The outlet velocity field of this booster-pump is examined along with the combined pump performance curves for the entire system.

- Finally, conclusions are drawn, and suggestions for further work are established.

## 1.4 Limiting the Scope

The task of replacing Francis turbines with RPTs is an enormous task, and limitations in the research need to be taken to progress. For this work, the economic aspects of the project have been disregarded. Although this is an essential driving force for the project, it is not accounted for in this work. Meaning that, even though the technology of a booster-pump might be more expensive than new waterways, this has not been considered. Moreover, turbine mode has not been investigated, even though the turbine operation is of utmost importance in a project like this. For the idea of installing a booster-pump in series with an RPT, it has not yet been decided whether to utilize the booster-pump in turbine mode or not. To clarify, this work focuses strictly on pumping mode.





## Part II

# Theoretical Background



# Chapter 2

## Pumped Hydropower Storage

---

Pumped hydropower storage is a valuable tool to balance the energy grid and to thoroughly utilize renewable energy resources. This chapter gives a brief overview of the technology and aspects concerning the objective of this thesis.

---

### 2.1 Energy Storage

The nature of renewable energy resources like solar and wind are fluctuating. When utilizing energy resources like these, there can suddenly become differences in supply and demand in the energy grid. Unlike the case of hydropower, the energy from wind and solar is not something that can be controlled by humans. The energy is available when the weather is windy, or the sun is shining. In Norway, it is possible to stabilize the grid by simply shutting down a hydropower plant, but in other places where the energy production comes from less flexible power sources, energy storage is of more importance.

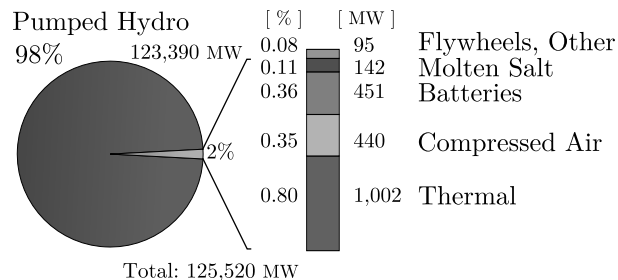


**Figure 2.1:** Globally estimated energy storage capacity from 2010. Collected from [10]

There are several ways of storing energy, but pumped hydropower storage is by far the most common. As seen in Fig. 2.1, pumped hydro storage have the vast majority of energy storage worldwide. Batteries, compressed air, thermal energy storage, and molten salt has a small percentage, but as of today pumped hydro storage remains as the most used source of energy storage. A reason for this is the sheer amount of energy that can be stored in elevated water.

Whereas the technology regarding batteries is today rapidly improving, pumped storage has been around for decades and is considered by many as a mature technology [10]. The technology is equipped for meeting the growing demand for electrical power consumption, by absorbing vast quantities of excess energy. However, pumped hydropower storage is not perfect. For a single round trip for the water in a pumped hydropower plant, meaning from the lower reservoir to the upper and back down again, a typical efficiency lies between 76% to 85% [10]. The losses of energy come from different sources, as can be seen in Fig. 2.2.

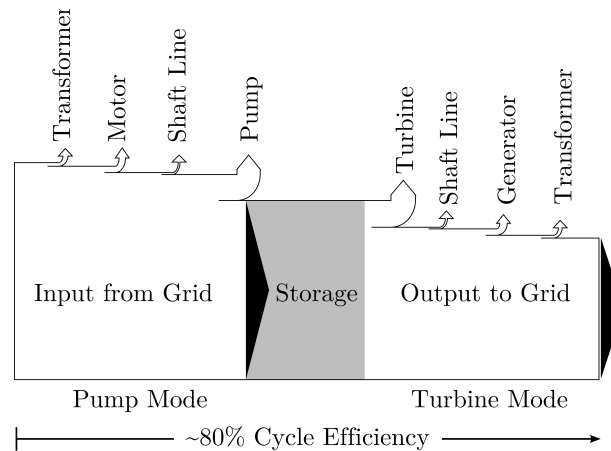


**Figure 2.2:** Energy losses for a single round-trip pumped storage cycle. Total efficiency typically around 80%. Collected from [10]

## 2.2 Francis Reversible Pump Turbine

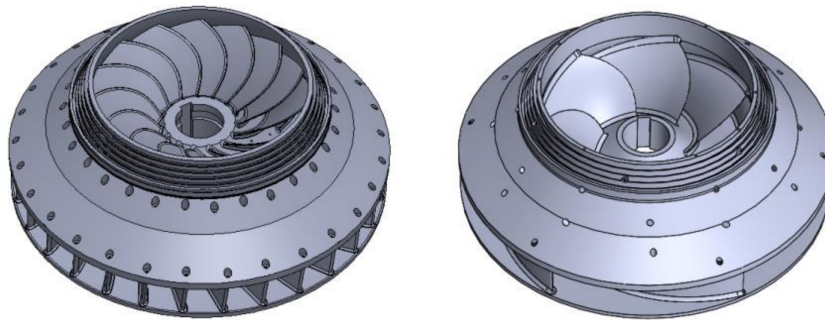


**Figure 2.3:** Comparison of a Francis runner (left) and an RPT (right) from the Waterpower laboratory at NTNU. Collected from [14]

A Francis type RPT is basically a centrifugal pump with guide vanes, that works as a turbine in one rotational direction and as a pump in the opposite direction [15]. The RPT separates itself from the typical Francis turbine by having fewer blades, among other design factors that are important for pumping mode. Because of losses in the waterways, the operating head is different for turbine mode than it is for pumping mode. In Fig. 2.3, we can see two runners that are used at *NTNU's* water power laboratory. Here the inlet and outlet diameters are roughly the same, but the RPT has fewer blades than the Francis runner. The peak efficiency of the Francis runner in turbine mode is  $\eta_h = 92.6\%$  while for the RPT the peak efficiency is  $\eta_h = 89.6\%$  in turbine mode [14].

## 2.3 Multistage Reversible Pump Turbine

A limit for operating head on a single-stage RPT in pump mode is around  $900m$ . This number is found when considering the strength of a runner and the forces working on the impeller during such large pressure gradients [16]. In the case of higher elation gain than  $900m$ , or situations where less submergence than for what is optimal for a single stage RPT is needed, multistage RPTs is often a viable option. When the unit's capacity is small, multistage units may be applied simply for the reduction in operating speed [16]. By utilizing several stages, one can run the pump at a lower rotational speed than a single stage pump but yet receive the same head. The reduced rotational speed is advantageous with regards to cavitation, as is discussed later.

The number of stages on a multistage RPT ranges between two to six and the complexity of the design and flow increases with each stage. The RPTs can typically be divided into two groups; RPTs with movable guide vanes for each stage and those with movable guide vanes for only the last stage. For RPTs with three or more stages, movable guide vanes are typically not used for any of the stages [16]. An advantage of multistage RPT is a more compact machine compared to a single stage RPT, as well as lower velocities at the outlet of the pump. The lower velocities give less wear, causes less vibration and less noise in pumping mode [17]. A typical multistage RPT can be seen in Fig. 2.4. The use of a booster-pump is essentially the same as a multistage pump turbine, only that the stages are placed further apart from each other.

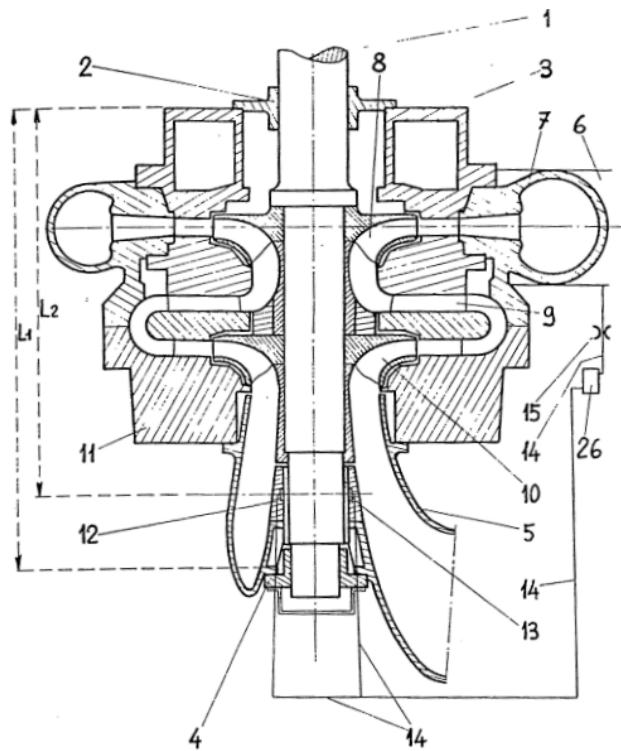


Figure 2.4: Multistage reversible pump turbine. Collected from [18]

## 2.4 Difference between Turbine Mode and Pump Mode

The head of an RPT needs to be higher in pumping mode than in turbine mode because of the hydraulic losses in the waterway. When the RPT is running in turbine mode, frictional forces work against the water

from the upper reservoir to the runner, giving less actual energy on the impeller. For the opposite direction; when the RPT is running in pump mode, the frictional forces work against the water from the runner to the upper reservoir. The difference in head is illustrated in Fig. 2.5. Here,  $H_{st}$  represents the height between the upper and the lower reservoir.  $H_{sp}$  and  $H_{st}$  represents the same height but accounts for frictional losses in respectively pumping mode and turbine mode. If the hydraulic losses in the waterways from the upper reservoir to the turbine are  $H_l = 5m$ , then the pump turbine would have to operate at the same head as the turbine plus two times the losses in the waterways. For the example mentioned above, this gives a difference in the operational head of  $10m$ . As the flow field in turbines and pumps are heavily influenced by what head the runner is operating with, the differences in head need to be accounted for when retrofitting a Francis turbine with an RPT.

To further understand this difference in the operating head, it is interesting to investigate some analytic equations regarding the performance of the impeller. To do so, one must first investigate the velocity diagram of the impeller. It is useful to get a grasp of the one-dimensional flow theory of impellers and diffusers to understand the flow in any hydraulic machine. With the help of velocity triangles, one can decide the main dimensions and angles of the impeller and diffuser. To do so, one needs to know the head, flow, and rotational speed of the runner. The velocity diagram of a pump turbine can be seen in Fig. 2.6. With the help of the velocity diagram, Euler's turbomachinery equation defines the theoretical head  $H_p$  in a pump as:

$$gH_p = \eta_p(U_2C_{u2p} - U_1C_{u1p}) \quad (2.4.1)$$

where  $U$  is the peripheral velocity of the runner,  $C$  is the absolute velocity,  $g$  is the gravitational constant, and the subscript  $_1$  and  $_2$  refers to respectively suction side and pressure side of the impeller. Subscript  $_p$  refers to pump mode and  $_t$  refers to turbine mode. If we look at the Euler equation for turbine mode, we get the theoretical head  $H_t$  in turbine mode:

$$gH_t\eta_t = U_{2t}C_{u2t} - U_{1t}C_{u1t} \quad (2.4.2)$$

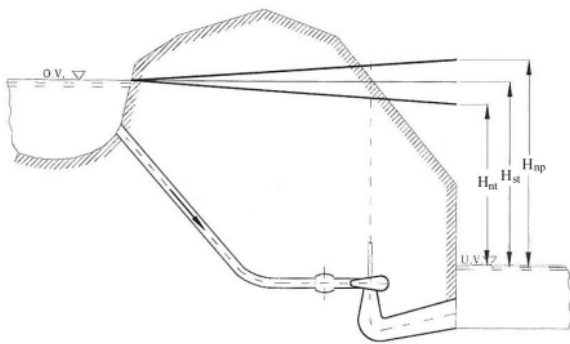


**Figure 2.5:** Difference between the head for turbine and pump mode. Collected from [17]

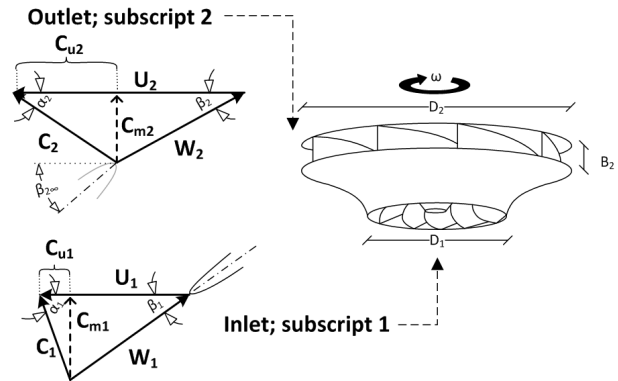


**Figure 2.6:** Velocity triangles for an RPT. Collected from [19]

## 2.5 Cavitation

Cavitation is a potential destroyer of hydraulic machinery and an essential obstacle when replacing Francis turbines with RPTs. It is, therefore, necessary to have an understanding of what cavitation is and why we want to avoid it. Cavitation occurs in hydraulic machines if the local velocities become large enough so that

the pressure of the fluid becomes lower than the vapor pressure,  $p_v$  [15]. Thus, cavitation is evaporation of water, or in other words, boiling water. If the pressure drops below vapor pressure in a fluid flow, vapor bubbles forms. These bubbles are called voids, or cavities [15]. Water in vapor form is considerably larger than water in liquid form. The vapor bubbles change the area the water flows through and thus reduce the efficiency of a runner when cavitation is developed.

Another important aspect of cavitation is what happens when the vapor bubbles enter a zone with higher pressure. When entering these zones, the cavitation bubbles collapse [20, p. 772]. The collapsing happens fast, creating a powerful local shock. If there is cavitation in an impeller during operation, this can be heard like a crackling noise. The noise is the sound of cavitation bubbles collapsing. If the collapsing of the bubbles happens near a solid surface, this erodes on the material of the runner. This eroding is called cavitation eroding and is preferable to avoid as it can eventually destroy the runner [15]. The process of a cavitation bubble collapsing on a solid surface and the local shock it creates is demonstrated in Fig. 2.7.

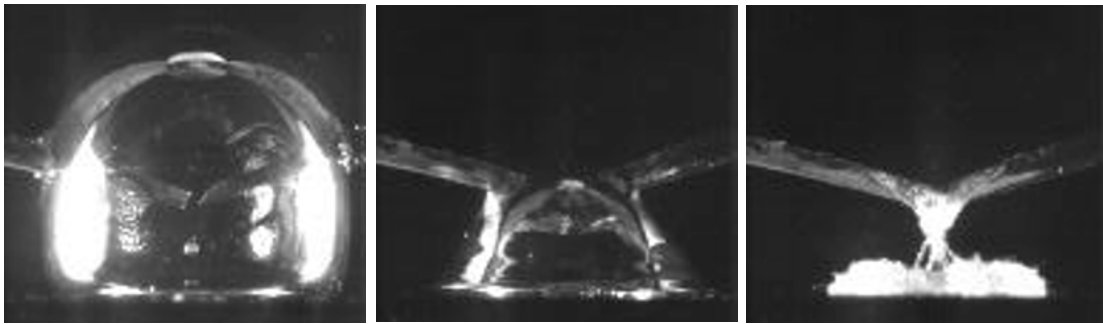


**Figure 2.7:** Cavitation bubble imploding near a wall. Collected from [13, p. 263]

## 2.6 Net Positive Suction Head and Submergence

The risk of cavitation is highest at the suction side of the impeller. The suction side is the inlet in pump mode and outlet in turbine mode. Pressure and velocities need to be controlled to avoid getting pressure zones below vapor pressure ( $p_v$ ). One way to control this is to submerge the runner below the lower reservoir. Additional submergence increases the static pressure at the suction side of the runner and hence reduces the risk of cavitation. The minimum local static pressure at the pump inlet determines the extent and occurrence of cavitation in a pump [13]. When installing a pump, the submergence of the machine is decided by a few basic principles. The Net Positive Suction Head,  $NPSH$ , is defined as the absolute pressure at the suction side of the impeller minus the vapor pressure:

$$NPSH = H_S + \frac{p_{amb} - p_v}{\rho g} \quad (2.6.1)$$

Here,  $H_S$  is the head at the suction side of the pump,  $p_{amb}$  is the ambient pressure and  $p_v$  is the vapor pressure of the fluid. There are two different  $NPSH$  and one demand that needs to be fulfilled to avoid cavitation:

$$NPSH_A > NPSH_R \quad (2.6.2)$$

$NPSH_A$  (A = available) is dependent on the plant and where the impeller is installed.  $NPSH_R$  (R = required) is impeller data and indicates what is required to avoid cavitation on the impeller. The lowest

pressure at the impeller inlet results from the acceleration of the main flow and the hydraulic loss at the inlet together with the local excess velocities created by the flow near the leading edge of the blade [13]. Thus an expression  $NPSH_R$  can be calculated from:

$$NPSH_R = a \frac{C_{m1}^2}{2g} + b \frac{U_1^2}{2g} \quad (2.6.3)$$

Where  $a$  and  $b$  are extracted from empirical data from Table 2.1.  $NPSH_R$  is normally given by the pump manufacturer and is found by running experiments on the pump. The testing is done by gradually decreasing the static pressure at the inlet of the pump and report the static pressure where cavitation occurs. When  $NPSH_R$  is known, the customer knows how much submergence the pump needs by using Bernoulli's equation on the system. When studying Table 2.1 and Eq. (2.6.3), it is apparent that the submergence needed to avoid cavitation is more significant when the RPT is running in pump mode than in turbine mode. Thus, when replacing Francis turbines with RPTs, there is a need for additional submergence.

**Table 2.1:** Empirical values used for the submergence of pumps and turbines [17]

Parameter	Turbines	Pumps
a	$1.05 < a < 1.15$	$1.60 < a < 2.00$
b	$0.05 < b < 0.15$	$0.20 < b < 0.25$

## 2.7 Booster Pump in Series with RPT

An invention for overcoming the differences in the operating head for pumping and turbine mode for RPTs was patented in 1982. The idea is to use a booster pump for running in pump mode and a separate waterway, avoiding the booster-pump, when running in turbine mode. The invention does not only overcome the differences in the operating head but also accounts for the further submergence needed in pumping mode. The extra submergence needed is accounted for by increasing the pressure in front of the RPT with a booster-pump. The main components of the invention can be seen in Fig. 2.8. The invention claims to increase the pressure at the inlet of the RPT in pump mode and thereby avoid cavitation problems. By using a separate waterway for turbine/pump mode, it is possible to operate the RPT at different operational heads than what would be the case if the booster-pump had affected the flow in both directions.

Installing a booster-pump near the draft tube gate has been suggested. For such a device, one would have to have a rather big booster-pump as the draft tube is expanding towards the gate. An advantage of putting the booster-pump here is that one would get some extra submergence compared to the RPT and hence reduce the risk of cavitation at the booster-pump. If one were to install a booster-pump which itself experience cavitation the problem is only shifted, not solved. With this in mind, one can set out to design the booster-pump. A proposed procedure of replacing a Francis turbine with an RPT with the use of a booster-pump is given below:

- The RPT runner should have the same dimensions as the existing Francis runner. This is to be able to reuse as much as possible of the structure from the old Francis turbine. The old structure includes the guide vane bearings, spiral casing, stay vanes, shaft, generator and otherwise as much as possible. The guide vanes should be replaced with guide vanes suitable for running in pump mode, but the diameter of the guide vane ring should be as on the old Francis turbine, if possible. Guide vanes suitable for pump mode has a rounder trailing edge than guide vanes used in Francis turbines [16, p. 161]. The purpose of the round trailing edge is for generating a smoother flow in pump mode. The guide vanes should also be made stronger, to account for the severe vibrations that can occur in pumping mode [16, p. 161].



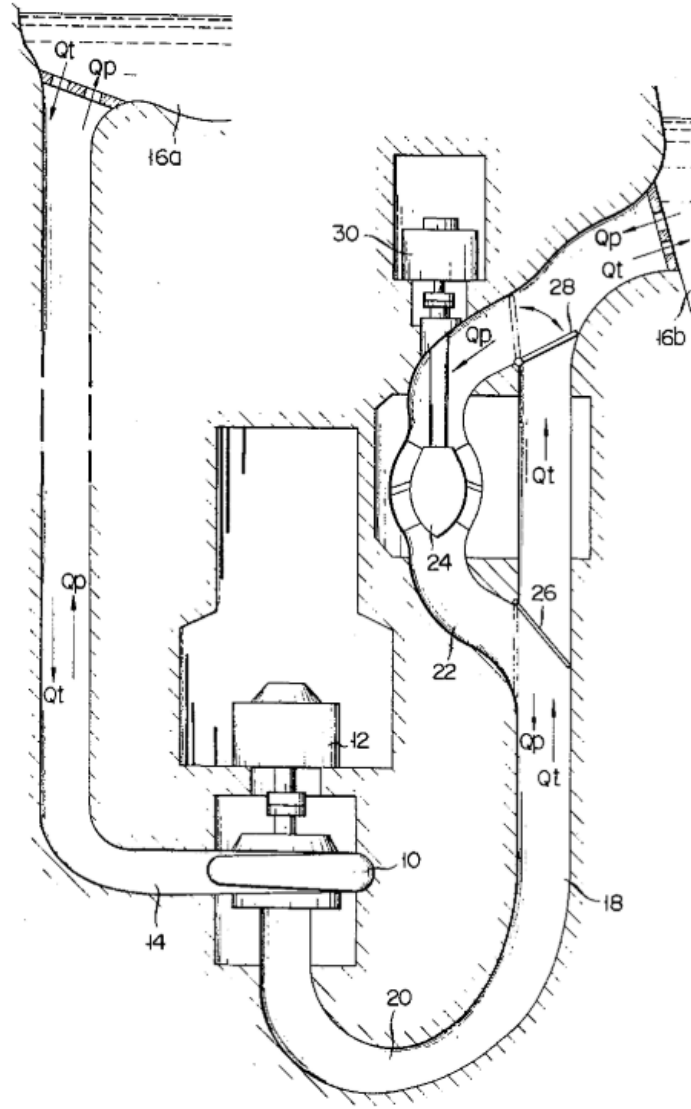


**Figure 2.8:** Illustration of the patent which utilizes a booster pump in a separate waterway. Collected from [21]

- The RPT should be designed with the dimensions given and tested numerically with the generator that is in place. If it is possible to reuse the old generator, considerable savings could be likely. On this basis, it is possible to see what kind of head the runner can produce. Based on the results of the simulations, an estimation of the needed head from the booster-pump can be acquired.
- When the required head is found, one can design the booster-pump based on the needed head and mass flow. The rotational velocity can be chosen based on the generator choice, but cavitation and the submergence of the booster-pump sets a limit for the rotational speed.
- A choice should be taken between utilizing an axial pump, a multistage axial pump or a mixed-flow pump. This choice can be taken based on the specific speed. If the required head is small enough - an axial pump can be utilized. If the head required is larger, a mixed flow pump might be a better option. If the required additional head is large, maybe a multi-stage RPT is the way to go.

### 2.7.1 Booster-Pump at Roskrepp Hydropower Station

*Sira Kvina* has disposed *Roskrepp* hydropower station as a project for retrofitting the existing Francis turbine with an RPT in series with a booster pump. *Roskrepp* hydropower station was finished in 1979 and consist of a single  $50MW$  Francis turbine which has a maximum capacity of  $70m^3/s$  [22]. The power plant operates with a head of  $83m$  in turbine mode as of today. *Rainpower* has conducted a preliminary analysis of how to retrofit this power plant with pumping capabilities. Based on their calculations, an RPT with the same dimensions as the existing Francis turbine would need an additional  $20m$  head for the water to reach the upper reservoir. That is when running at a capacity of  $Q = 50m^3/s$  and a rotational speed of  $250rpm$ . The assumption of running the RPT at this rotational speed comes from the basis of using the old generator. Using the old generator at the new RPT means that the booster-pump at *Roskrepp* would have to supply around 25% of the total head of the combined system.

# Chapter 3

## Pump Theory

---

When reviewing the task of using a booster-pump in front of an RPT, the theory behind pumps needs to be appreciated. This chapter goes through some fundamental aspects of pumps and their operation.

---

### 3.1 Pump Performance Curves

A pump is a machine that moves fluid by mechanical action. Pumps are well known and used in many aspects of modern life, in one way or another. Pump performance curves, typically labeled  $H - Q$  curves, are a useful way of understanding the pump's performance during different points of operation. During operation, a pump operates at different volume flows and heads depending on the fluid level in the different reservoirs, the rotational speed, and the power supply. The maximum flow rate through a pump occurs when the net head is equal to zero and is called the pump's free delivery. At the other end of the scale, the pump's maximum head is achieved when there is no flow running through the pump. The head at no flow is called the shutoff head. All operating points between these extremes are called the performance curve of the pump and can vary greatly depending on the pump's size, rotational velocity, and geometry.

Along the performance curve, every pump also has a curve for its efficiency. The Best Efficiency Point (BEP) is where one would want to operate the pump as it is most economical and produces less wear on the runner. Knowing the performance and efficiency curves for a pump is therefore important knowledge before installation. Examples of pump curves for a pump in series with a booster-pump is given in Fig. 3.1.

When arranging pumps in either parallel or series, there are certain aspects to keep in mind. While parallel or series arrangements are often a good choice for an application, it could lead to problems when one pump is much larger than the other [23]. Arranging pumps in series may cause problems because the volume flow through each pump is the same, but the pressure rise for the overall system is the pressure rise from one pump plus the other. In terms of arithmetic; the net head for  $n$  pumps in series is given as:

$$H_{combined} = \sum_{i=1}^n H_i \tag{3.1.1}$$

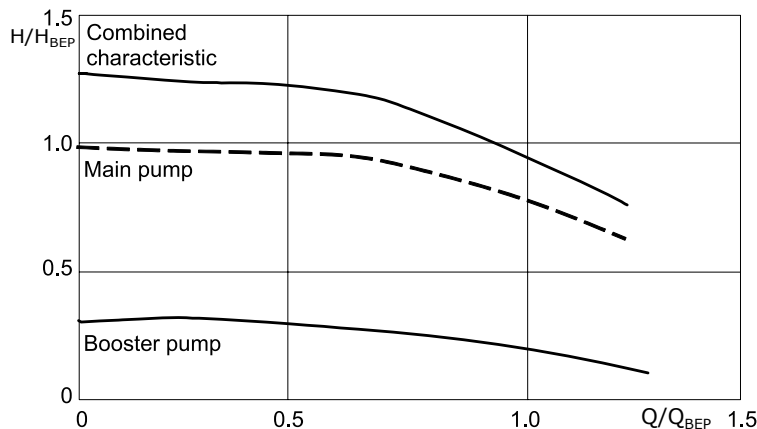


**Figure 3.1:** Pump curves for a booster-pump in series with another pump, along with the combined pump curve. Collected and adapted from [13, p. 670]

If the pumps have widely different pump performance curves, this may lead to one pump operating at a point above its free delivery rate. Instead of working as a pump, the pump then instead acts as a head loss. In light of this, it is vital to know each pumps energy-discharge characteristic before operating them either in parallel or series. For the task of arranging a booster-pump together with an RPT in series, one would achieve an application where one pump is larger than the other. For this application, it is necessary to make sure that both the booster-pump and the RPT has BEP at around the same mass flow, and that the range of the two pump characteristics have a similar extent.

### 3.2 Specific Speed and the Cordier Diagram

All pumps are characterized by the flow rate  $Q$ , the lifting head  $H$  and the rotational speed  $n$ . By defining certain ratios, we can derive the specific speed  $\Omega_s$  and specific diameter  $D_s$  for any given hydraulic machine. Based on experience from previous, well-designed pumps, we can then decide what kind of hydraulic machine that is most applicable to any situation. The ratios are defined as:

$$\Omega_s = \frac{\Omega\sqrt{Q}}{(gH)^{3/4}} \quad (3.2.1)$$

$$D_s = \frac{D(gH)^{1/4}}{\sqrt{Q}} \quad (3.2.2)$$

The value of the specific speed indicates what kind of machine that is most suitable for an application based on previous successful designs. By using this resemblance, it is possible to estimate the characteristics of machines with different sizes and speeds [24]. In 1953, a rough, but helpful diagram named the *Cordier* diagram was proposed. The line in the diagram is based upon results from a large number of machines and indicates both the specific size and specific speed of a machine for any given application. The diagram is shown in Fig. 3.2. It should be noted that the line in the Cordier diagram has a fairly broad specter of results around either side of the line, so one could have a well performing hydraulic machine and not strictly follow the Cordier diagram, but for the initial selection process, the diagram can be a helpful indicator. Below is a brief description of the different machines mentioned in the Cordier diagram.

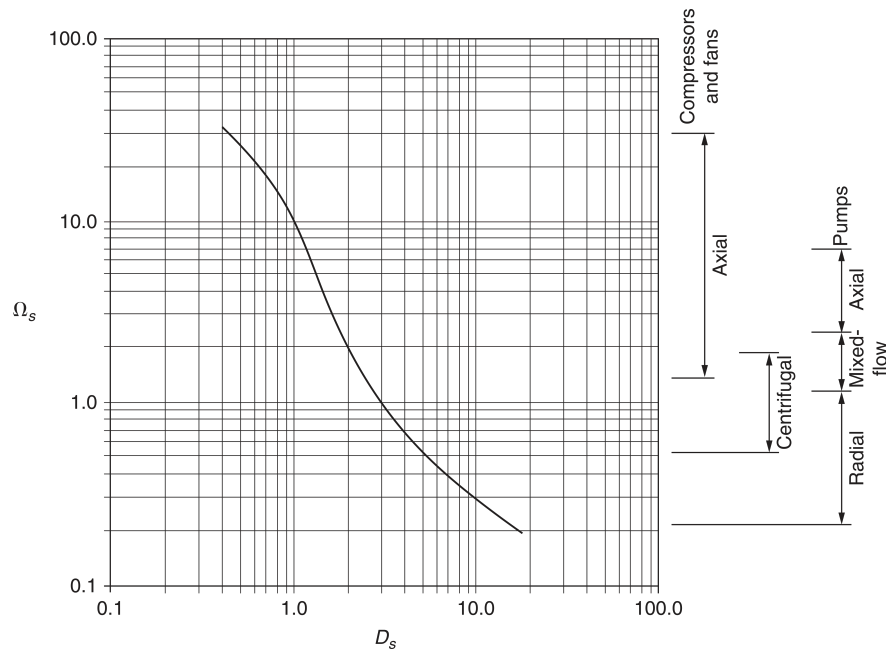


**Figure 3.2:** The *Cordier* diagram. This diagram gives an indication of suitable hydraulic machine based on specific speed and specific diameter. Collected from [25]

### 3.3 Pump Types

**Centrifugal pumps** are machines that convert mechanical power into hydraulic power by utilizing centrifugal forces [26]. When running a Francis type RPT in pump mode, the RPT can be viewed as a centrifugal pump. The working principle of a centrifugal pump is to transfer angular momentum from the rotating impeller to the flow through the pump. Centrifugal pumps are machines that are a key component of numerous technical processes, and the working principles of this incredible machine have been studied in detail for decades. The flow can vary from a few liters per minute for the smallest pumps to several hundred cubic meters per second for the most massive water storage pumps [13]. The head of a centrifugal pump can vary from 1 – 5000m and rotational speeds can range from a few hundred revolutions per minute to over 30000 revolutions per minute [13]. The design of the centrifugal pump varies from one application to another, but a standard feature for this type of pump is the volute. The volute is the most common type of diffusing element in centrifugal pumps [13, p. 36], and this element separates the centrifugal pump from the axial pump.

**Axial pumps** are generally pumps that are used for generating large flows at relatively low heads. The blades can be either fixed or variable-pitched. Variable-pitched blades give the machine a wider operating range [27]. Axial pumps do not utilize centrifugal forces. Instead, the impeller blades act like wings on an airplane and generate lift as they rotate. The lift force is generated from pressure differences from the bottom side and top side of the blade. Depending on the blade profile and angle of attack, the lift can be highly varying from one pump to another. Typical usage of axial pumps is cooling water pumps, irrigation, sewage treatments plants and drainage systems [13]. Axial pumps are employed for applications where high specific speeds are involved. Although axial pumps can be designed for lower specific speeds than what is suggested in the Cordier diagram, mixed-flow pumps are used unless the plant requires purely axial design because of geometrical constraints [13]. An axial flow machine, together with a mixed-flow machine, can be seen in Fig. 3.3.

**Mixed-flow pumps** are pumps that are a combination of axial flow and radial flow machines. They are compact as they do not use a volute. Mixed-flow pumps can operate under a wide variety of head but

typically gives more head than the axial pump and less head than the radial pump. Mixed-flow pumps are used for transporting drinking and cooling water and for irrigation and drainage purposes. Other usages can be inboard thrust motors for boats and ships. Mixed flow pumps have been studied in turbine mode as a PAT (Pump as Turbine), with fair results. The results of one paper concluded with around the same efficiency for turbine mode as for pump mode, but with another specific speed [28].

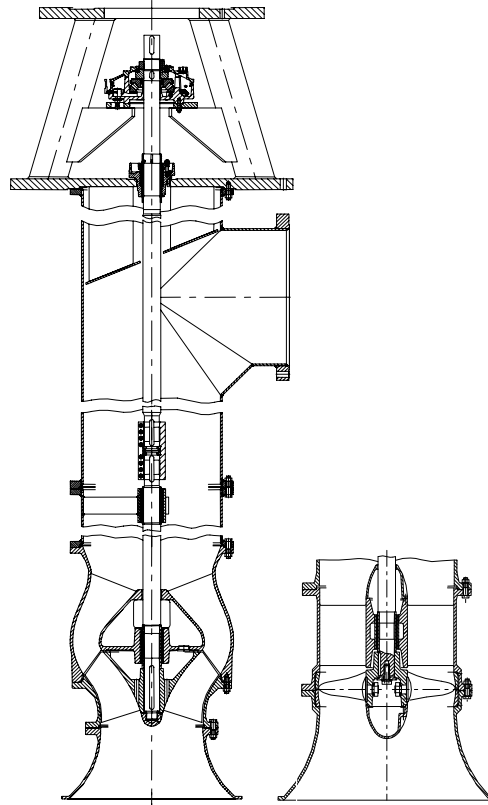


**Figure 3.3:** Illustration of a mixed-flow pump (left) and an axial flow pump (right). Collected and adapted from [13, p. 61]

### 3.4 Impeller Approach and Pre-Rotation

When designing a pump, a general approach is to assume zero pre-rotation at the inlet ( $C_{u1} = 0$ ). As the flow varies along the pump curve, correct inflow angle cannot be achieved for all operating points as the angle of the impeller blades does not vary. Because of this, regulation of the inlet flow angle could be a suitable measure for optimizing the flow conditions. According to the Euler equation Eq. (2.4.1), *pre-rotation reduces* the head while *counter pre-rotation increases* the head. The effect of pre-rotation control increases for pumps along with the ratio of the diameter of the inlet over the diameter at the outlet,  $D1/D2$  [13, p. 675]. In effect, this means that pre-rotation is more effective for pumps with a high specific speed, such as axial flow impellers and mixed-flow impellers. However, pre-rotation regulation with inlet guide vanes (IGVs) has been investigated on a centrifugal impeller by *Liu et al.* [11] and *Ahmed et al.* [12]. The reports show that pre-whirl with IGVs can increase the efficiency curve of a centrifugal pump in a wide region.

Pre-rotation regulation has also been investigated on a mixed-flow pump, and the results can be seen in Fig. 3.4. Here, it can be observed that the total head produced by the pump increases with counter pre-rotation, while the head decreases rapidly for pre-rotation in the same direction as the impeller rotation.

The same goes for efficiency. For pre-rotation, the efficiency decreases, but for counter pre-rotation, the efficiency increase slightly at BEP.

For  $NPSH$ , the behavior is different. In and around BEP,  $NPSH$  do not change much with pre-rotation. But for lower flow-rates,  $NPSH$  increases dramatically. Fig. 3.4 reveals that the range available for controlling the flow rate is large if the system characteristic is flat ( $H_{A,1}$ ) compared to if the system characteristic is steep ( $H_{A,2}$ ) [13, p. 675]. In effect, this means that pre-rotation control is more advantageous for applications where a large range of flow rates is required at a constant head.

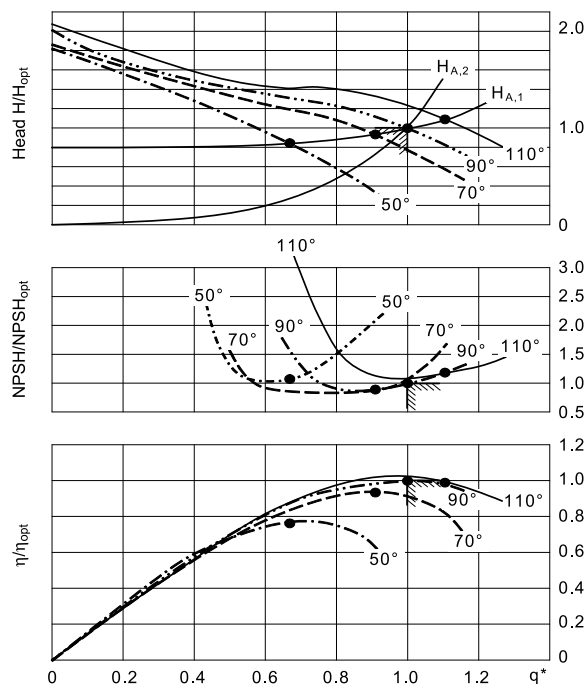


Figure 3.4: Pump characteristics of a mixed-flow pump with pre-rotation control. Collected from [13, p. 675]

### 3.5 Diffusers and Guide Vanes

The diffusers in a pump are used for decelerating the flow and consequently, convert kinetic energy into potential energy [13, p. 27]. While potential energy can be converted into kinetic energy without major losses, the process of doing the opposite involves far greater losses. The reason for this is that the distortion in the flow upon deceleration is greater than what it is for accelerating flows. At the outlet of a rotating impeller the circumferential velocity is  $C_{u2} = C_2 \cos(\alpha_2)$  as described in Fig. 2.6. The specific energy of the rotation component is  $E_{kin} = 1/2 C_2^2$ . This kinetic energy has to be effectively decelerated by the diffusing elements in the pump to achieve acceptable efficiency [13, p. 102]. To effectively decelerate the flow, the angle of the diffusers needs to be given the correct angle. Axial diffusers need to reduce the circumferential velocity component, of the outlet of an axial pump, to a value as close as possible to zero, as any swirl of the outlet of the pump would imply additional losses [13, p. 400]. This means that to have a well-designed booster-pump, there should *not* be a swirl at the outlet of the pump, as this indicates that the diffusers have not been able to convert the kinetic energy into pressure.

As different mass flows and pressure gradients in pumps create various outlet velocity fields; it is useful to make the diffusers adjustable. In RPTs, adjustable diffusers are the equivalent of guide vanes. Selecting optimal angles for the guide vanes have a significant effect on the pump curves and the hydraulic losses in

the machine. In 2017, a study regarding the impact of guide vane opening for an RPT in pumping mode was conducted by *Zhu et al.* [29]. The hydraulic losses for the different domains in the pump turbine at different guide vane openings are plotted in Fig. 3.5. Here, the flow rate and head loss are normalized according to:

$$C_\varphi = \frac{Q}{\pi r_\omega \rho R_2^3} \quad (3.5.1)$$

$$C_\psi = \frac{2gH}{r_\omega^2 R_2^2} \quad (3.5.2)$$

$$C_{\psi_{loss}} = \frac{2gH_{loss}}{r_\omega^2 R_2^2} \quad (3.5.3)$$

Fig. 3.5 shows that the hydraulic losses rely heavily on the guide vane opening. The study concludes that when the flow direction is not consistent with the guide vane opening angle, the flow separates and creates complex vortices. The vortices then block the stay vane passages, and the hydraulic losses increase. In addition, Fig. 3.5 shows that for the low flow rate regime, the head loss in the draft tube increases.

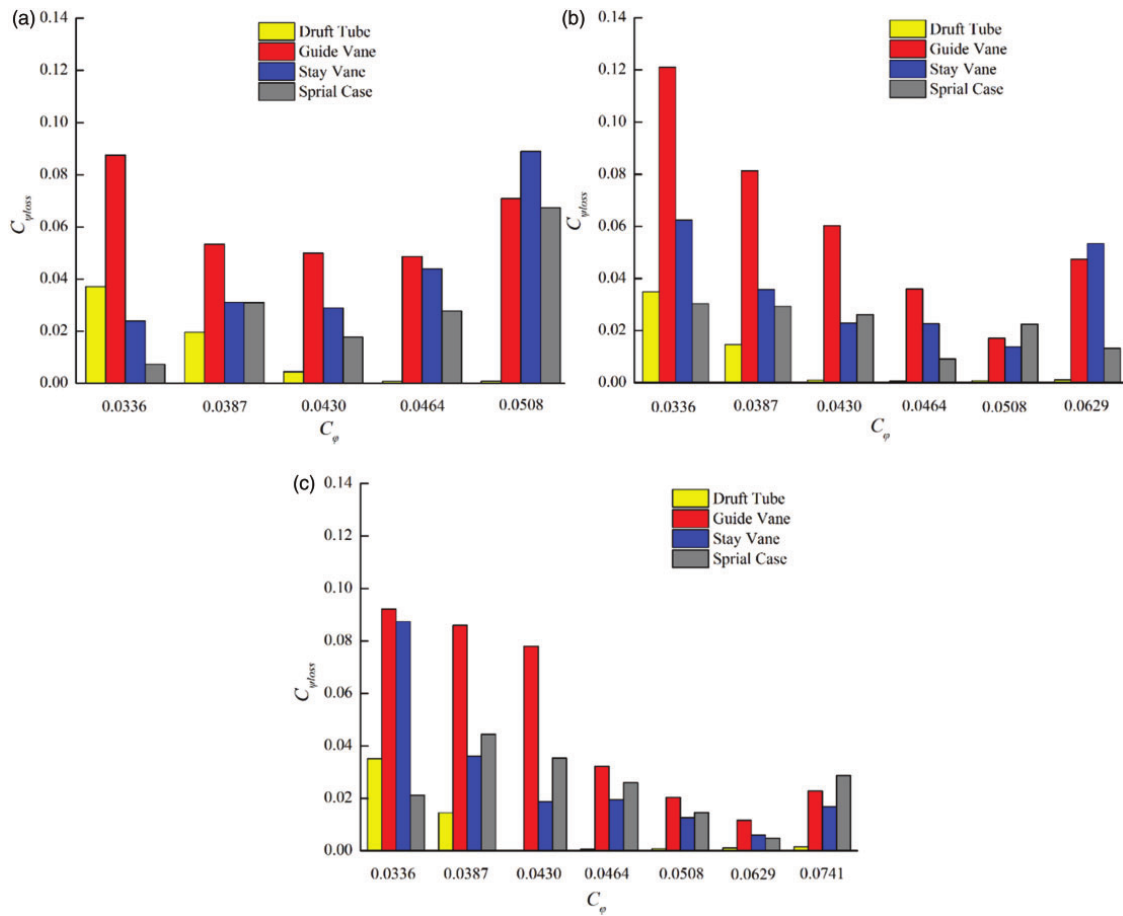


**Figure 3.5:** Hydraulic losses for a RPT in pump mode at different guide vane openings. (a) 12° guide vane opening, (b) 16° guide vane opening, (c) 20° guide vane opening. Collected from [29]



# Chapter 4

## Numerical Theory

---

Computational Fluid Dynamics (CFD) is the analysis of fluid flow using computer-aided simulations. This chapter will give a brief overview of some of the theory used for the simulations in this thesis. *Braun's* Ph.D. regarding CFD simulations for part load in centrifugal pumps has been used for reference throughout this chapter [26].

---

### 4.1 The Incompressible Navier-Stokes Equations

Fluid motion is governed by the conservation laws of momentum and mass [26]. In hydraulic machinery, one can assume that the fluid is incompressible, at least for the present study. Considering time-dependent, three-dimensional fluid flow in an inertial frame of reference, one can deduce the incompressible Navier-Stokes equations. The equations form four nonlinear partial differential equations which can be used to predict fluid flow [30]. The momentum equations using Einstein notation follows as:

$$\frac{\partial C_i}{\partial t} + C_j \frac{\partial C_i}{\partial x_j} = \frac{1}{\rho} \left( \frac{\partial \tau_{ij}}{\partial x_j} - \frac{\partial p}{\partial x_i} \right) + f_i \quad (4.1.1)$$

The conservation of mass is given by:

$$\frac{\partial C_i}{\partial x_i} = 0 \quad (4.1.2)$$

These equations poses as the basis for CFD and can, with a few tweaks, be used to model complex fluid flow. Further tweaking of the momentum equations and the mass conservation equations follows. Water is considered a Newtonian fluid and the shear stress  $\tau$  is determined by the dynamic viscosity  $\mu$  and the strain tensor  $D_{ij}$ :

$$\tau_{ij} = 2\mu D_{ij}, \quad D_{ij} = \frac{1}{2} \left( \frac{\partial C_i}{\partial x_j} + \frac{\partial C_j}{\partial x_i} \right) \quad (4.1.3)$$

Summing these equations together we end up with the incompressible Navier-Stokes equations:

$$\frac{\partial C_i}{\partial t} + C_j \frac{\partial C_i}{\partial x_j} = \frac{1}{\rho} \left( \mu \frac{\partial^2 C_i}{\partial x_i \partial x_j} - \frac{\partial p}{\partial x_i} \right) + f_i \quad (4.1.4)$$

Albeit, the Navier-Stokes equations were first deduced in the 19th century, our physical understanding of these powerful equations remains incomplete. Proof of the existence of a smooth solution in the three-dimensional space is still left to be shown. *Clay Mathematics Institute* has stated this as one of the seven *Millenium Problems* and offers a price of one million dollars to any man or woman who can prove the existence of a smooth solution to the Navier-Stokes equations in space [31]. Even though this has not been established yet, the power of the Navier-Stokes equations remains, and the usage of the equations expands several different fields of interest and poses as vital in our understanding of the fluid flows of the world.

## 4.2 Rotating Frame of Reference

When considering rotating machinery in CFD, a straight forward approach is to use a reference frame moving together with the solid wall boundary geometry [26]. The momentum and flow velocities are considered with respect to the moving frame of reference, adding a contribution to the Navier-Stokes equations. By using this, the Navier-Stokes equation in a rotating frame of reference with constant rotation  $\omega$  can be written as:

$$\frac{\partial W_i}{\partial t} + W_j \frac{\partial W_i}{\partial x_j} = \frac{1}{\rho} \left( \mu \frac{\partial^2 W_i}{\partial x_i \partial x_j} - \frac{\partial p}{\partial x_i} \right) + f_i + f_{r,i} \quad (4.2.1)$$

## 4.3 Turbulent and Laminar Flow

The Navier-Stokes equations can be presented in a dimensionless form by introducing a characteristic length scale  $L_0$ , a characteristic velocity  $v_0$  and a characteristic timescale  $t_0$  and normalizing the rest of the parameters in Eq. (4.1.4). The dimensionless form of the Navier-Stokes equations is given by:

$$St \frac{\partial C_i^*}{\partial t^*} + C_j^* \frac{\partial C_i^*}{\partial x_j^*} = \frac{1}{Re} \frac{\partial^2 C_i^*}{\partial x_i^* \partial x_j^*} - \frac{\partial p^*}{\partial x_i^*} + \frac{1}{Fr^2} \gamma_i \quad (4.3.1)$$

Where the *Strouhal* number  $St$ , *Reynolds* number  $Re$  and *Froudes* number  $Fr$  are given by:

$$St = \frac{L_0}{C_0 t_0} L_0 \quad Re = \frac{\rho C_0 L_0}{\mu} \quad Fr = \frac{C_0}{\sqrt{g L_0}}$$

The remaining variables in Eq. (4.3.1) are made dimensionless by:

$$C_i^* = \frac{C_i t_0}{L_o} \quad x_i^* = \frac{x_i}{L_o} \quad \rho o^* = \frac{p}{\rho C_0^2} \quad t^* = \frac{t}{t_o} \quad \gamma_i = \frac{f_i}{g}$$

Fluid flow can be separated into two different flow regimes with regards to physics — laminar and turbulent flow. Laminar flow occurs at low Reynolds numbers, while turbulent flow occurs in regions of flow with high Reynolds number. The Reynolds number is a dimensionless number defined as the ratio between inertial forces and viscous forces. In hydropower, the Reynolds number is usually large enough for turbulent flow regimes to take place, and there is a need for applying equations which takes turbulent effects into account. Turbulence is inherently chaotic, and the physics involved is yet to be fully understood.

It is, however, still possible to use the Navier-Stokes equations to capture the physics of the flow. Even though the equations have not been proven to have a smooth solution in all three dimensions, there are strong indications that the equations yield physical and accurate results for many applications. To fully capture the smallest turbulent structures in a flow, Direct Numerical Simulation (DNS) needs to be used. This is a numerical method which captures the minor *Kolmogorov* micro-scale turbulent structures. DNS is a highly demanding computational method which requires enormous amounts of computing power and is therefore near impossible to use by today's standards. Large Eddy Simulation (LES) is the next step down the ladder of accuracy. This method can capture the large eddy structures but averages the smaller structures. The Reynolds-Averaged Navies-Stokes (RANS) equations average the Navier-Stokes equations and are, therefore, a relatively cheap numerical method for calculating complex fluid flows.

## 4.4 Reynolds-Averaged Navier-Stokes Equations

Turbulence is inherently chaotic, and there is a need for a way to deal with this chaotic behavior. Reynolds-averaging and modeling of the resulting averages of fluctuating terms make it possible to predict incompressible turbulent flow fields [32]. The Reynolds decomposition of a general flow variable is given as:

$$\phi = \bar{\phi} + \phi' \quad (4.4.1)$$

By following a set of rules given by Reynolds in how to handle the different terms, we end up with the incompressible Reynolds-Averaged Navier-Stokes (RANS) equation:

$$\frac{\partial \bar{C}_i}{\partial t} + \bar{C}_j \frac{\partial \bar{C}_i}{\partial x_j} = \frac{1}{\rho} \left( \mu \frac{\partial^2 \bar{C}_i}{\partial x_j^2} - \frac{\partial \bar{p}}{\partial x_i} \right) - \frac{\partial \overline{C'_i C'_j}}{\partial x_j} + f_i \quad (4.4.2)$$

The terms  $\overline{\rho C'_i C'_j}$  are called the Reynolds stresses and poses as six unknowns in which Eq. (4.1.4) differs from Eq. (4.4.2). The turbulence modeling discussed in the next chapter is in reality about defining laws to predict the Reynolds stresses.

## 4.5 Turbulence Modelling

Since the full Navier-Stokes equations can only be solved by the use of DNS, a turbulence model has to be used. With the turbulence model, we can model the RANS equations, which averages the turbulent structures instead of resolving them.

*The  $k - \epsilon$  turbulence model* is a widely used model which can be used for many applications, often with reliable and with accurate results. The model tends to perform poorly on complex flows involving large pressure gradients, strong streamline curvature, and separation. All of which is believed to be found in the pump mode of an RPT. Despite its severe shortcomings, the  $k - \epsilon$  model is widely used because it is easier to achieve convergence with this model than with other turbulence models [33].

*The RNG  $k - \epsilon$  turbulence model* is a turbulence model that is more suited for complex flow than the standard  $k - \epsilon$  model. It has been shown that this model performs well with flows involving rapid strain, moderate swirl, vortices, and boundary layer separation as well as stall in wide-angle diffusers [34]. In the RNG model, the transport equations are the same as in the standard  $k - \epsilon$  model, only that the model constants differ.

*The SST turbulence model* is often more accurate than the  $k - \epsilon$  models, but it requires a significantly larger mesh to capture the viscous sub-layer. The SST model combines different turbulence models depending on location in the flow. In the core flow, the SST model utilizes the  $k - \epsilon$  model, while on adjacent walls and solid surfaces the model employs the  $k - \omega$  model. The  $k - \omega$  model is a model designed for flows with substantial pressure gradients [33]. As the model is slightly more complicated than the  $k - \epsilon$  model, it is also more computational demanding. Exactly which equations that *ANSYS CFX* uses to model the different turbulence models can be found in [34].

There is no definitive, correct answer to which turbulent model to employ for different applications. Some turbulence models perform better on some problems, while others perform poorly. Using a wrong turbulence model to try to capture a specific physical phenomenon in the flow can even lead to severely wrong answers. An important aspect to remember is always to be critical to the results of the simulation and remember that the choice of turbulence model can be a source of errors. A particularly important aspect of turbulence modeling is accurate modeling of boundary layers.

## 4.6 Boundary Layer Modelling

Modeling boundary layers is an essential part of CFD, and it has a significant influence on the density of the mesh needed to capture the physics of the flow. The no-slip condition,  $\mathbf{C} = 0$ , at solid walls leads to a zone of high gradient velocities near walls. The accuracy of a simulation relies on the correct prediction of velocity profiles near solid walls. In Fig. 4.1, the shear velocity  $C_\tau$ , the non-dimensional velocity  $C^+$  and the non-dimensional wall distance  $y^+$  are given by the following definitions:

$$C_\tau = \sqrt{\tau_w / \rho} \qquad C^+ = \overline{C_t} / C_\tau \qquad y^+ = \frac{\rho C_\tau y}{\mu}$$

The velocity field close to the wall, where the no-slip condition is applied, is divided into three different zones. The zone closest to the wall is called the viscous sub-layer. The zone furthest away from the wall is called the defect layer and is dominated by a velocity defect due to the wall shear [10]. The central zone is called the logarithmic layer and is characterized by:

$$C^+ = \frac{1}{\kappa} \ln y^+ + B \tag{4.6.1}$$

Where  $\kappa$  is the *von Karmán* constant and  $B$  is an empirical constant.

The  $k - \epsilon$  models make use of the logarithmic layer when wall functions are applied, while the SST turbulence model, models the viscous flow close to the wall. To get accurate results, care should be taken

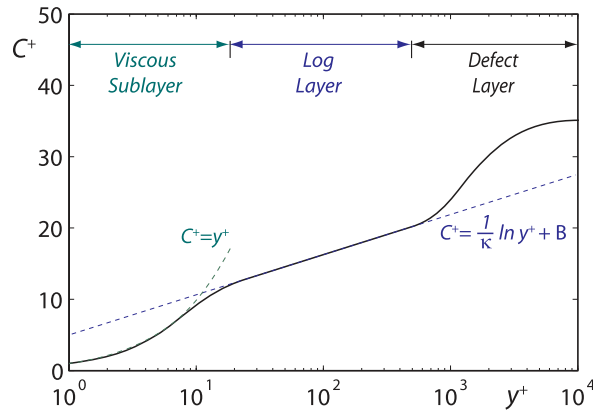


**Figure 4.1:** A logarithmic representation of a turbulent boundary layer profile. Collected from [26]

to have the  $y^+$  value within the ranges that are applicable for the specific turbulence model. If the elements close to the wall are too large when using the SST model, the turbulence model is not able to capture the viscous sublayer. If one uses too large elements in the  $k - \epsilon$  model, the elements closest to the wall is not able to capture the logarithmic layer. For turbulence models where logarithmic wall functions are applicable, like the  $k - \epsilon$  model, the cell sizes near the wall should be selected such that  $30 < y^+ < 100$ . When using the SST model, the cells near the wall should be small enough for  $y^+ < 1$  to hold. For the SST model, at least ten cells should be located between the wall and  $y^+ = 20$  [33]. These criteria are the reason why a much denser mesh is needed when using the SST model, compared to the  $k - \epsilon$  models.

## 4.7 Periodic Boundary Conditions

CFD can be computationally demanding, and every chance for a reduction in computing time for simulation is a possibility worth pursuing. This is especially the case if one is in the early stages of a process and need results quickly to find the right path. Periodic boundary conditions are a good way of saving computation time. If one assumes that the flow is similar across a domain and follows a specific pattern, a periodic boundary condition can be applied. For impellers and diffusers, this is often the case. The periodic boundary condition allows for the computation of only one passage instead of every passage and gives a substantial reduction in the number of elements needed to capture the flow of an entire geometry. The way the boundary condition is used, is by applying a symmetry condition on a symmetric plane, meaning that, for example, the velocity gradients at a symmetry plane are set to zero. Using this, one can repeat one passage flow for all passages instead of calculating all passages. The symmetry condition is a useful tool, but should only be applied where the flow is genuinely symmetric. For example, the flow in a fully developed flow in a straight, vertical pipe can be considered symmetrical, but the flow through a bend would not be symmetrical because of the secondary flows which occur in the bend. Using the same logic, the flow through a rotating impeller can be considered symmetric, but the flow in a volute would not be symmetric, and the symmetric boundary condition should not be utilized.



## Part III

# Method and Results





## Chapter 5

# Reversible Pump Turbine with Uniform Pre-Rotation at Draft Tube Inlet

---

This chapter investigates the effect of pre-rotation on an RPT in pump mode using a uniform circumferential inlet velocity boundary condition and steady-state CFD simulations.

---

### 5.1 Geometry

For investigating the flow field in an RPT, a numerical model was created of an existing geometry of a fully functioning RPT. *Rainpower* provided the model which consists of a geometry of a spiral casing with 28 stay vanes, a set of 28 guide vanes, the runner with 9 blades and a draft tube. The RPT has a specific speed of  $\Omega_s = 0.575$  in pump mode, which categorizes it as a high head machine. At *Roskrepp* the geometry is a low head machine, and thus an entirely different geometry. Experimental performance data for pump mode was also provided for validation purposes. These experimental data consisted of pump curves for all guide vane openings, from shutoff head to the pump's free delivery. The geometry of the RPT can be seen in Fig. 5.1.

### 5.2 Mesh Generation

The software used for the CFD analysis was *ANSYS 19.1*. For the guide vanes and the impeller blades, *TurboGrid* was used for creating a fully structured hexahedral mesh. The input to *TurboGrid* are so-called curve files, which consists of a set of points along curves in the spanwise direction of the blade. In addition to the points for the blades, points for the hub and shroud must also be provided. The hub and shroud files set the limits of the inlet and outlet boundaries of the domains, but can be changed within *TurboGrid* if the accuracy needs improvement. In *TurboGrid*, you need to select a topology for the blade you want to mesh. The topology of the blade tells *TurboGrid* how the blocking of the blade should be performed. *TurboGrid* has several different topologies available. When the topology is selected, there are numerous different options to tweak and adjust the mesh to get the desired output. The quality of the mesh has a direct impact on the accuracy of a CFD simulation. *ANSYS* gives certain guidelines to follow when meshing, to obtain a mesh

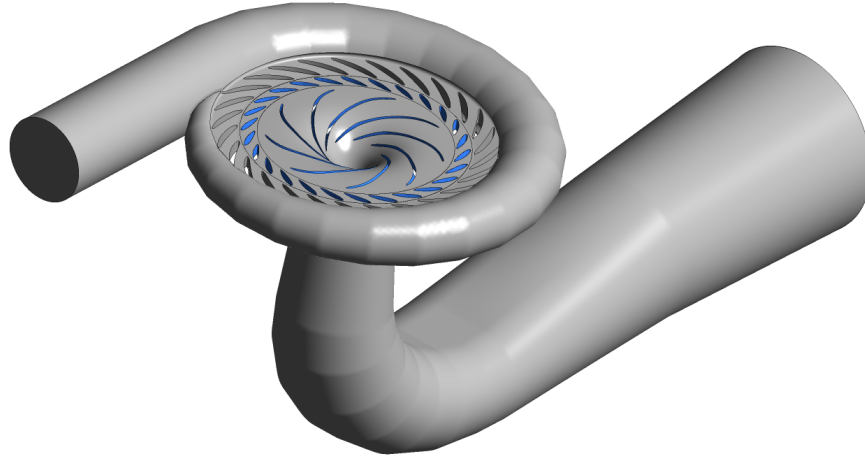


**Figure 5.1:** The RPT geometry investigated in this thesis

with satisfactory performance. For this work, efforts were made to have the absolute best performance on the following three mesh quality criteria:

- Orthogonal angle  $> 20^\circ$
- Aspect ratio  $< 100$
- Expansion factor  $< 20$

By following the guidelines for mesh quality criteria given above, a smooth mesh was produced for the runner and guide vanes. Fig. 5.2 shows the structured surface mesh of the blades of the runner, and how the meshing is inflated in the spanwise direction. The  $y^+$  values can easily be managed in *TurboGrid*, and dependent on the turbulence model you choose, you must also select the corresponding  $y^+$  values. By choosing a  $k - \epsilon$  turbulence model, you can have fewer cells and keep the quality criterion for the expansion factor intact. The RNG  $k - \epsilon$  model was employed in this work, as it has previously performed better on swirling flows than the  $k - \epsilon$  model, and requires a less dense mesh than the SST model, as discussed in Chapter 4.

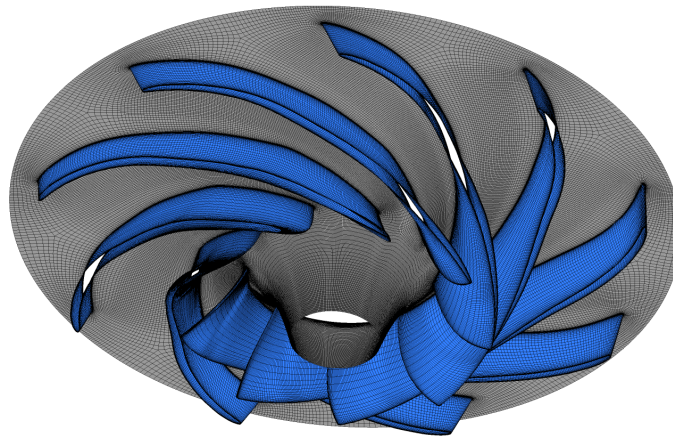


**Figure 5.2:** Structured surface mesh on impeller blades

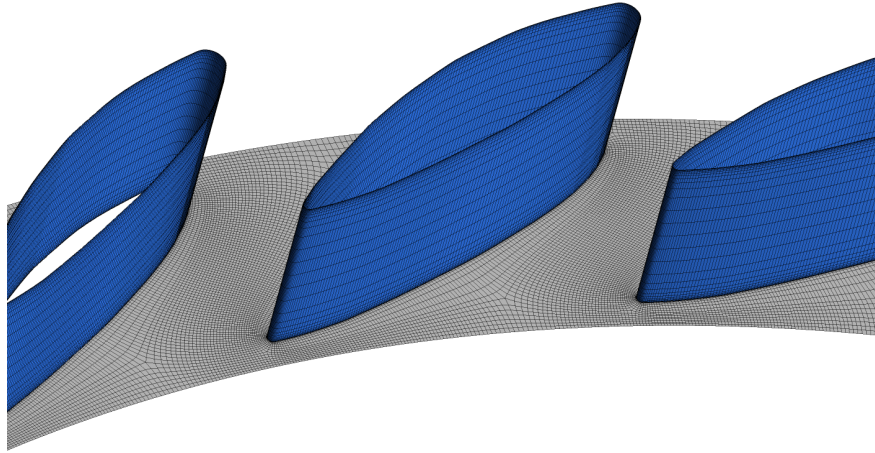


**Figure 5.3:** Structured surface mesh on a few guide vanes

*TurboGrid* creates periodic boundary surfaces for the blades so that the software only needs to mesh one blade passage. The periodic boundaries save computing time and limit the behavior of asymmetry in the flow through the impeller caused by differences in the mesh from one passage to another. The meshing of the guide vanes also utilized this symmetric approach and was meshed with a focus on the same mesh quality criteria as the runner. The angle of the guide vane opening can be changed easily in *TurboGrid* by rotating the guide vane around its rotating axis. For doing this, the rotating axis needs to be known, and in this case, the coordinates for that point was provided along with the curve files from *Rainpower*. When the guide vane angle is changed, the entire mesh needs to be re-meshed, and users should be aware that the mesh parameters set for one guide vane opening, does not necessarily produce a smooth mesh for another guide vane opening. Still, the guide vane opening can be made parametric for performing several simulations on different guide vane openings. A few guide vanes and the structured surface mesh can be viewed in Fig. 5.3.

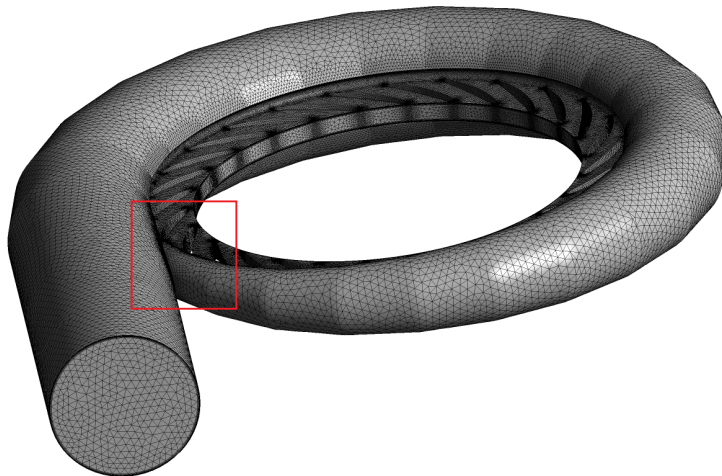


**Figure 5.4:** Unstructured surface mesh of spiral casing

For the meshing of the spiral casing, *ANSYS Meshing* was used to create an unstructured tetrahedral mesh with the help of a patch conforming method. Efforts were made to mesh the stay vanes using *TurboGrid*, but

as the stay vanes are not symmetric around the z-axis, this was deemed inappropriate. It can be observed in Fig. 5.4, that the elements in and around the stay vanes are much smaller than what they are in the rest of the domain. As the stay vanes act as a strong diffuser and the velocities are more significant than in the spiral casing, it was decided to have a finer mesh in stay vane region. In *ANSYS Meshing* one can control the  $y^+$  values by adjusting the size of the elements closest to the wall, but since the geometry is quite complicated in the spiral casing, it proved challenging to obtain a smooth mesh along with the wanted  $y^+$  values in this region. In Fig. 5.5, the strongly imposed sizing function that was utilized at the spiral casing tongue can be seen.

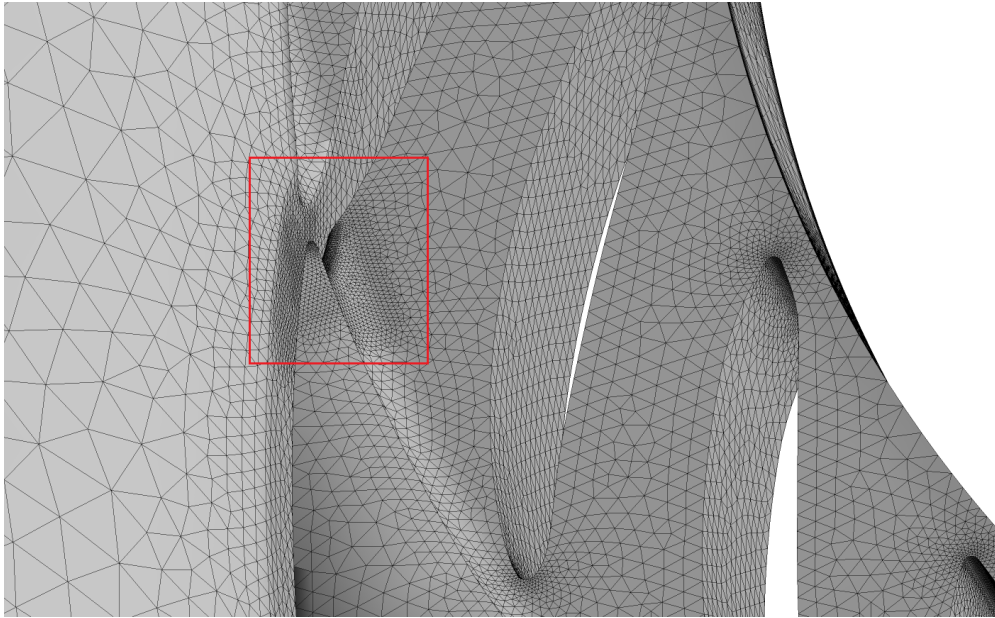


**Figure 5.5:** Surface mesh of the spiral casing tongue

The tongue of the volute is particularly challenging to mesh, as the angle of the tongue is sharp. When trying to impose inflation layers in this region, the orthogonal angle becomes even sharper, and the quality of the mesh declines. By utilizing the stair-stepping function in *ANSYS Meshing*, along with reducing the number of inflation layers and imposing a surface sizing function, the mesh quality was held at a reasonable level. The quality criteria recommended by *ANSYS* for aspect ratio, expansion factor, and orthogonal quality has been upheld for all domains, except for a small percentage of elements containing expansion factor of above 50 at the leading and trailing edge of the stay vanes. Since the portion of these elements is well below 1%, the quality of the mesh was deemed sufficient.

The draft tube consists of a simpler geometry than the spiral casing, and it was therefore decided to use a hexahedral mesh in this region. By the use of a *MultiZone* method in *ANSYS Meshing*, a hexahedral mesh was produced. An illustration of the surface mesh can be viewed in Fig. 5.6. The height of the elements near the wall is set such that the  $y^+$  values fulfill the criteria given in Section 4.6, all the way from the draft tube inlet to outlet. This is done by gradually decreasing the height of the elements closest to the wall, as the velocity increases towards the impeller. Following the same logic, the total size of the elements decreases towards the runner to account for the assumption that the flow is more complex near the bend and impeller. The surface of the bottom of the impeller cone is included in the draft tube cone, and the  $y^+$  values are accounted for in this region by setting a line-size-function at the draft tube cone with decreasing size in elements towards the runner.

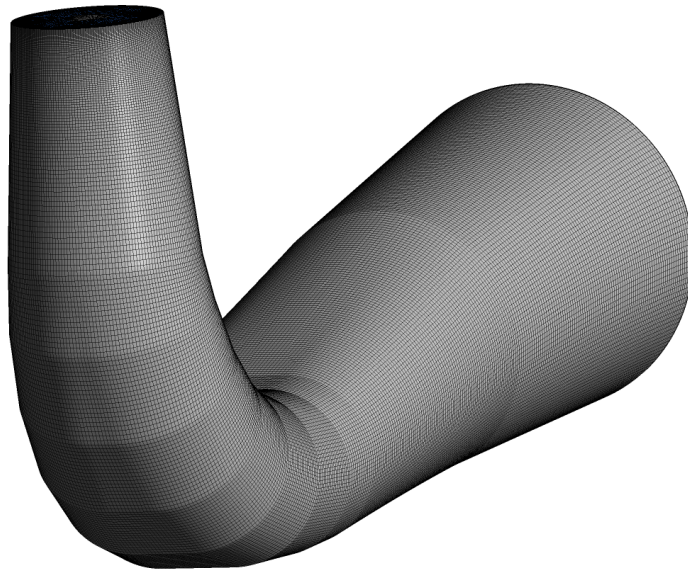


Figure 5.6: Surface mesh of draft tube

### 5.3 Mesh Independence Study

A mesh independence study has been performed to validate the independence of the mesh. The study was performed following the guidelines set by the *Fluids Engineering Division of ASME* [35]. For validation of the independence of mesh density, three sets of meshes with element count from 8 million elements to 30 million elements were examined. Further details can be seen in Table 5.1. For the study, BEP with no pre-rotation was set as a baseline for mesh verification. From the mesh independence study, it was decided that the medium mesh would be sufficient for further calculations. The decision was based on the computational resources available and also the level of accuracy needed for this research.

Table 5.1: Mesh independence study at best efficiency point

Item	Mesh 1	Mesh 2	Mesh 3
Draft Tube	3,738,726	1,926,043	952,666
Runner	9,487,350	4,408,560	2,150,010
Guide Vanes	8,370,648	4,244,604	2,122,302
Spiral Casing and Stay Vanes	9,460,379	4,883,139	2,819,084
Total number of elements	30,712,124	15,462,303	8,044,062
$H/H_3$	0.9935	0.9946	1
$T/T_3$	0.9943	0.9972	1
$H - GCI$	0.57%	2.77%	
$T - GCI$	1.42%	1.43%	

### 5.4 Numerical Setup

In the present work, the computational fluid dynamics software *ANSYS CFX* 19.1, and the RNG  $k - \epsilon$  turbulence model has been applied for steady-state simulations. For the simulations, all 9 blade channels are used as well as all 28 guide and stay vanes. The boundary conditions have been set as a mass flow inlet with



tangential velocity components to induce pre-rotation, and static pressure outlet condition was established at the outlet of the spiral casing. No-slip wall conditions have been employed on all the walls, stationary and rotating. For modeling the interface between the stationary and rotating domains, the frozen rotor interface model has been applied to serve as initial conditions, while the mixing plane interface model has later been applied for precision. The simulations have been conducted in such a way that all operating points have had enough iterations to reach oscillatory convergence with mean root square residuals below  $10^{-4}$ . It should be noted that some oscillatory behavior in the head and efficiency was present at the end of the simulations.

### 5.4.1 Inlet Boundary Conditions

Specification of the correct boundary conditions in a CFD calculation remains as one of the most critical tasks to get tangible results [36]. Therefore, great care was exerted when considering the inlet condition. For inducing pre-rotation, a mass flow inlet boundary condition was employed. The tangential component was set such that the inlet flow would have four different angles;  $-24^\circ$ ,  $-12^\circ$ ,  $12^\circ$  and  $24^\circ$ , in addition to no pre-rotation. This angle refers to the angle between the circumferential velocity component and the axial component at the plane of the draft tube inlet. How the pre-rotation was imposed can be observed in Fig. 5.7. In Fig. 5.7, the circumferential velocity component of the inlet boundary condition is plotted as a vector field. This inlet condition will not accurately model an axial booster pump, nor will it accurately model an inlet flow from IGVs. Still, the inlet condition serves as an approximation of what could be possible for an RPT that experience pre-rotation.

When imposing pre-rotation to the flow, one also adds energy to the flow, compared to what the flow would have without pre-rotation. This should be taken into account when considering the results of the simulation. Positive counter pre-rotation is defined as an angle that adds circumferential velocity in the reverse direction of the runner rotation, while negative pre-rotation would be the opposite. That is if one assumes that the swirl continues in the same direction through the bend in the draft tube. Hence, positive counter pre-rotation adds net-head to the RPT.

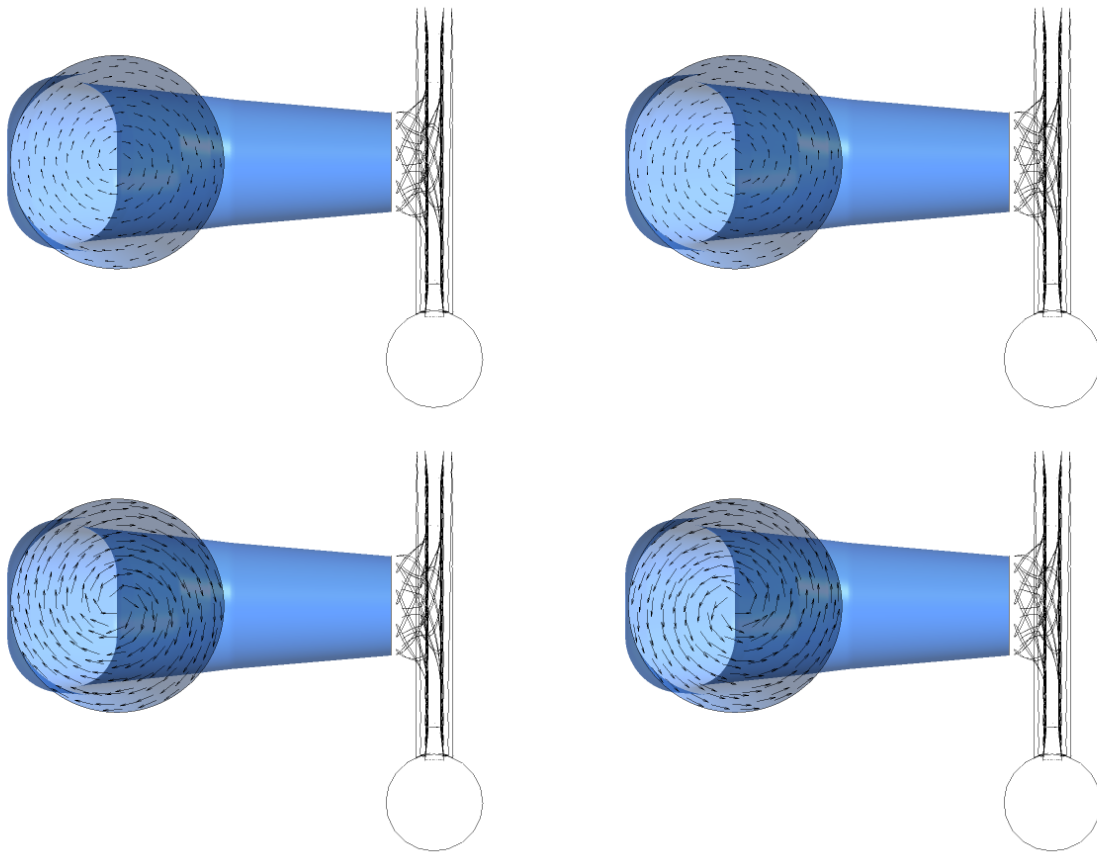


**Figure 5.7:** Velocity vector plot showing the circumferential velocity components at the inlet; top-left:  $12^\circ$ , bottom-left:  $24^\circ$ , top-right:  $-12^\circ$ , bottom-right:  $-24^\circ$

## 5.5 Results

Fifteen different result files were generated. The inlet conditions for these result files separate from one another by having different mass flows and different induced pre-rotation. From these files, it is possible to generate pump performance curves and comparing the effect of pre-rotation with one another. Streamlines are plotted for 1.2 BEP in Fig. 5.8. Fig. 5.8 visualize the path of some of the fluid particles in the draft tube. Here, the streamlines of the case of no pre-rotation can be compared with positive counter pre-rotation and negative pre-rotation. Keep in mind that streamlines show the path of fluid particles with zero mass [34]. No pre-rotation is as mentioned earlier, the assumed case of normal operating. The streamlines visualize that the fluid particles, in some cases, take a longer path through the draft tube, and in other cases, they obtain a shorter path. This increase or decrease in path length could affect the losses in the draft tube.

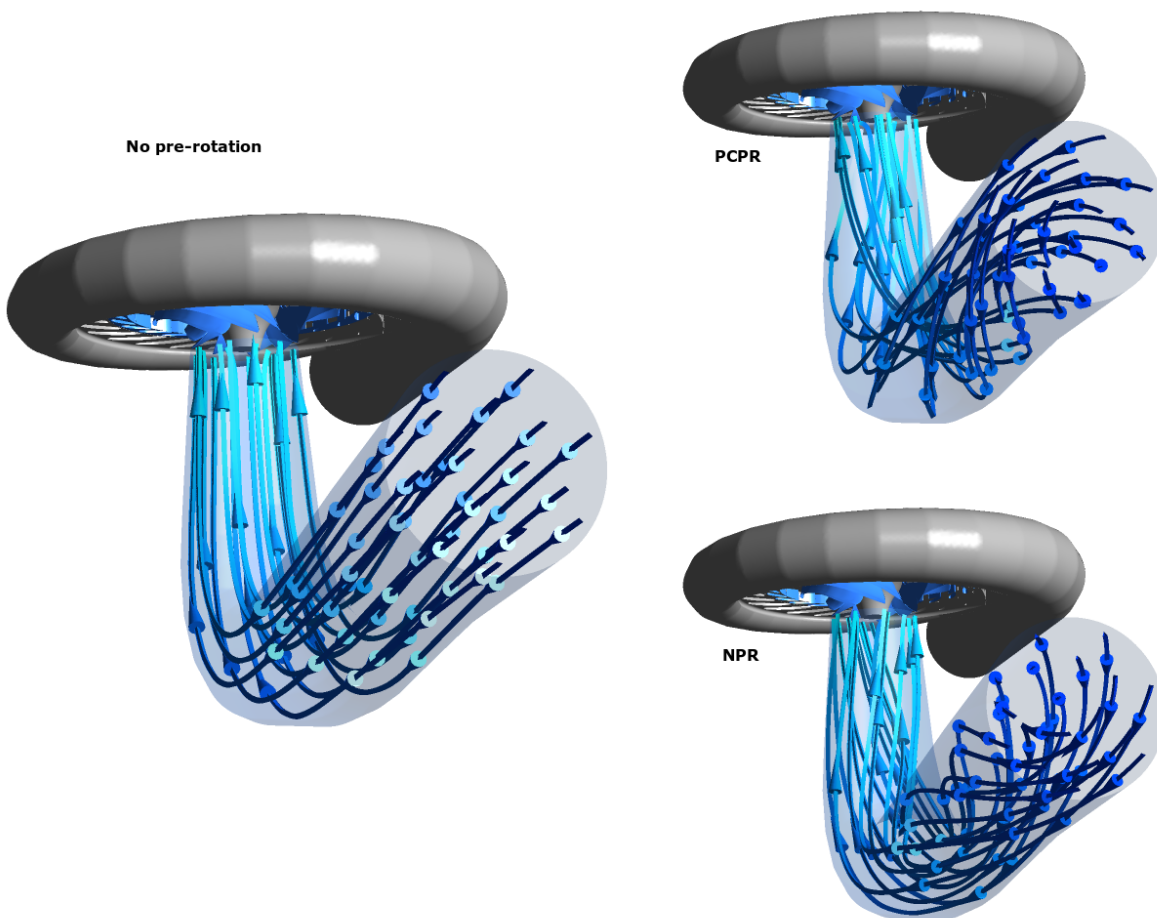


**Figure 5.8:** Streamlines in the draft tube showing the path of a fluid particle with zero mass for the different inlet boundary conditions. Results from 1.2BEP with no pre-rotation, 24°PCPR and 24°NPR

### 5.5.1 Pump Performance Curves

In Fig. 5.9, the head-capacity curves are plotted for both the simulated instances and the experimental data. From Fig. 5.9, we can see that the overall trend seems reasonable compared to experimental data. The simulated curves have a bit lower gradient than the experimental data, meaning that the simulations over-



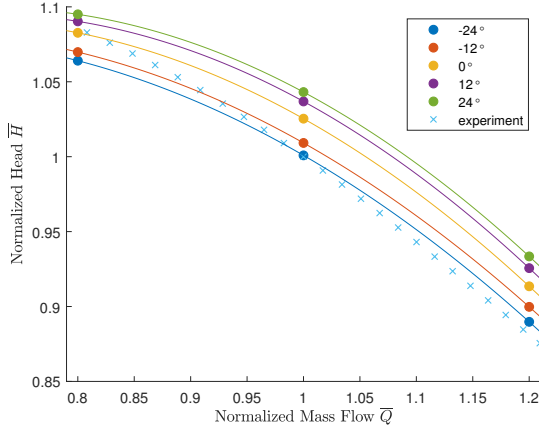


**Figure 5.9:**  $\bar{Q} - \bar{H}$  plot with normalized values for different pre-rotation values

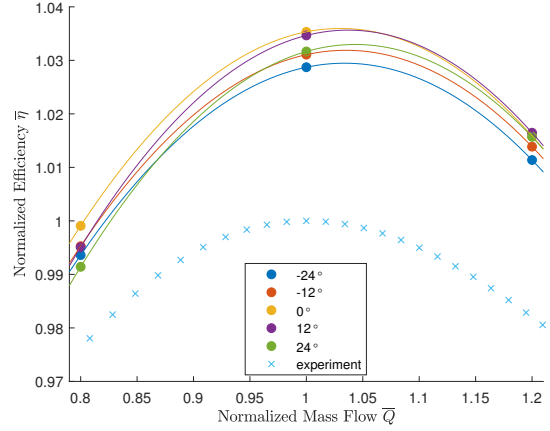


**Figure 5.10:**  $\bar{Q} - \bar{\eta}$  plot with normalized values for different pre-rotation values

predict the simulations at 1.2 BEP and BEP. At 0.8 BEP, the results seem to correlate well. Combined, this results in a lower overall head gradient versus capacity for the simulations than for the experiments. A basic spline function in *MATLAB* has been utilized to smooth the results and visualize the trends. Further, one can see that counter pre-rotation in the opposite direction of the impeller rotation gives an additional head over the whole operating range. This correlation is in accordance with Eq. (2.4.1). However, as mentioned earlier, it is difficult to estimate how much net head that is added to the system by adding pre-rotation, and hence, how this alters the characteristic curve in itself. The head is calculated in *ANSYS CFX* by:

$$H = \frac{p_{s2} - p_{s1}}{\rho g} + \frac{C_2^2 - C_1^2}{2g} \quad (5.5.1)$$

Where  $p_s$  represents the static pressure and  $C$ , represents the absolute velocity. For the measurements of the total head, the inlet has been set as the inlet of the draft tube, and the outlet is the outlet of the spiral casing. This is to account for the losses in the separate domains and to be able to compare the results with the experimental data. Efficiency,  $\eta$ , is given by:

$$\eta = \frac{P_{out}}{P_{in}} = \frac{\rho g H Q}{\Omega T_{shaft}} \quad (5.5.2)$$

Where  $P$  represents power,  $\Omega$  represents the impeller rotational speed,  $\rho$  represents density, and  $T$  represents torque on the impeller [10]. For confidentiality reasons, the head, mass flow, and efficiency are normalized according to:

$$\bar{H} = \frac{H_{CFD}}{H_{exp,BEP}} \quad (5.5.3)$$

$$\bar{Q} = \frac{Q_{CFD}}{Q_{exp,BEP}} \quad (5.5.4)$$

$$\bar{\eta} = \frac{\eta_{CFD}}{\eta_{exp,BEP}} \quad (5.5.5)$$

Here, the subscript  $_{exp,BEP}$  refers to the experimental data at BEP.

By investigating Fig. 5.10, we can see that the added head does not correlate with increased efficiency. The simulations capture the trend of the pump curve, but overprediction of the efficiency is evident for all

operating points. The higher efficiency is expected because the steady-state CFD simulation is not able to predict several of the losses that may occur in the various domains. Therefore, overall efficiency is larger than the experiments for all operating points. However, it is believed that the simulation with no pre-rotation is most similar to the actual experimental data, merely because the pre-rotation is not induced intentionally in the experimental results. Pre-rotation can be present at the inlet of the draft tube. Although, occurring because of bends or other obstacles in the water path before the draft tube. Pre-rotation can also arise from upstream pumps in the laboratory. If one assumes that zero pre-rotation is the most physical, one can see from Fig. 5.10 that efficiency is highest for zero pre-rotation for both 0.8 BEP and BEP. For 1.2 BEP, we can see a slight advantage for  $12^\circ$  counter pre-rotation, but this is only marginal. By this reasoning, one can say that pre-rotation is not advantageous for the efficiency of the pump, at least for the situation investigated here.

## 5.5.2 Velocity Distribution

To further examine why the pump performance curves vary with induced pre-rotation, it is interesting to plot the velocity distribution at the impeller inlet. Euler's equation, Eq. (2.4.1), tells us that the head of a pump is dependent on the circumferential velocity distribution at the impeller inlet, as well as the impeller outlet. When using Euler's equation and referring to the velocity triangles, one looks at one streamline at a time. In *ANSYS CFX*, it is possible to average this value over the entire impeller inlet by taking a mass flow average. By averaging the circumferential velocity distribution on the impeller inlet, we get the results given in Fig. 5.11.

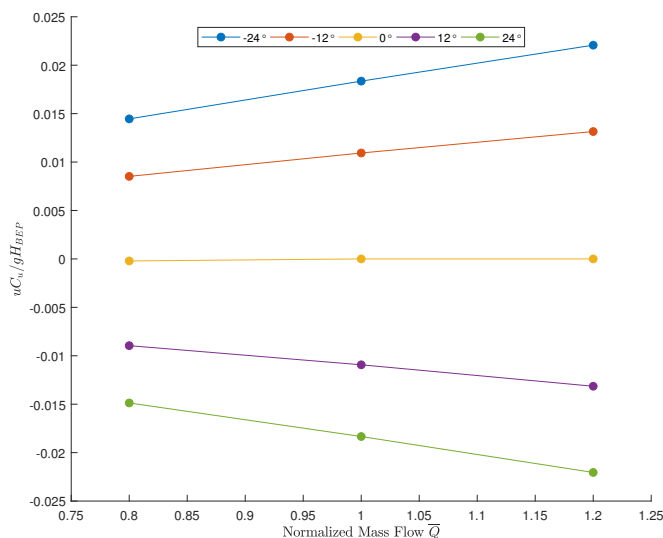


**Figure 5.11:** Difference in the  $UC_u$  distribution at the impeller inlet with different pre-rotation

Fig. 5.11 suggests where the added head in the pump curves originates. The positive counter pre-rotation provides a negative contribution to the Euler equation, thereby increasing the head. For the negative pre-rotation, the opposite happens. The negative pre-rotation provides a positive contribution to the Euler equation, thereby reducing the total head.

When normalizing the value of the  $UC_u$  distribution with the total head, it is understandable why pre-rotation is more effective for pumps with higher specific speed. For a machine with a higher specific speed, the value of  $U$  at the inlet would be relatively much more significant, as the ratio between the inlet and outlet diameter is increased. As the geometry in this thesis is a high head machine, the  $UC_u$  component at

the outlet of the impeller is much higher compared to the  $UC_u$  component at the inlet. For machines with higher specific speeds and smaller outlet diameter, this relation would be smaller, and the  $UC_u$  component at the inlet of the machine would be larger relative to the outlet.

### 5.5.3 Secondary Flows in Draft Tube

In pump mode, secondary flows are expected in the draft tube cone. Bends in pipes produce a more significant head loss than what would occur in a straight pipe. The losses are due to the separated region of the flow near the inside of the bend. Because of an imbalance of the centripetal forces, a separated flow occurs at the inside of the bend. This imbalance is a result of the curvature of the bend and is the origin of the secondary swirling flow [23]. The secondary flow is of significance to the flow in the draft tube and especially at high flow rates when the Reynolds number is higher. When the Reynolds number is big, the separation is believed to happen further upstream. When adding pre-rotation to the flow, this affects the placement and strength of the swirls. The swirls generate a non-uniform inlet velocity field at the inlet of the runner, which could lead to unsteady behavior such as vibrations and pressure fluctuations [37]. How the secondary flows rotate with the induced pre-rotation can be seen in Fig. 5.12.

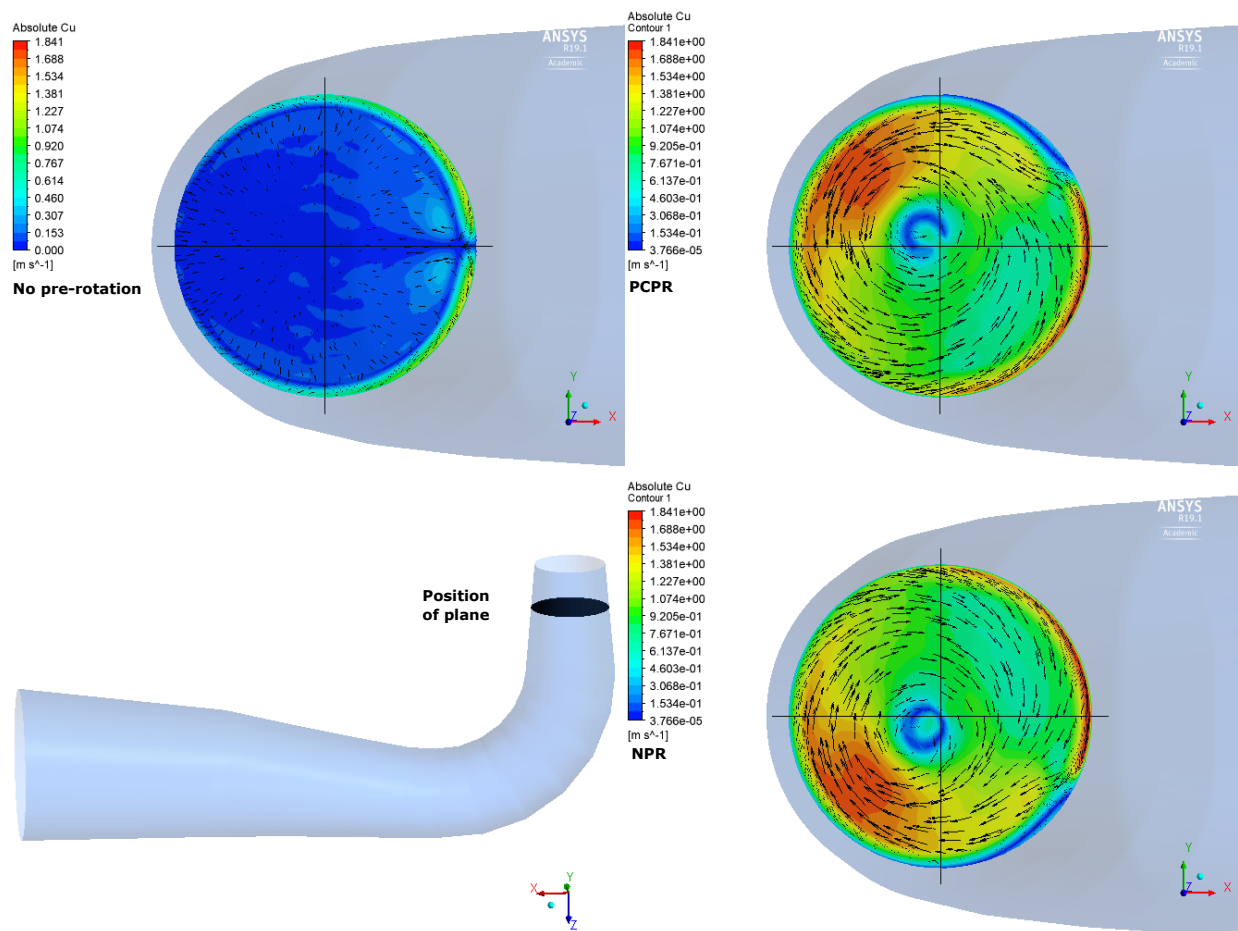


**Figure 5.12:** Secondary flows in draft tube cone at 1.2BEP. The view is from beneath the draft tube, looking up at the runner inlet. The bottom right figure shows the location of the plane in the draft tube cone. The top left figure shows the secondary flows occurring around the x-axis as expected for zero pre-rotation, whereas the secondary flows twist with the pre-rotation for positive pre-rotation (upper right) and negative pre-rotation (lower right)

In Fig. 5.12, the absolute circumferential velocity has been plotted as a contour plot at a plane in the draft tube cone. The vector field is a tangential projection of the velocity and shows the direction of the pre-rotation. The velocity field, along with the contour plot, shows that the bulk swirl does not match the center of the runner inlet. In both cases of pre-rotation, the bulk swirl is pushed towards the outside of the bend. Along with a move of the center swirl in the same direction as the pre-rotation, this calls for a non-symmetric inlet velocity field at the runner inlet compared to the case of no pre-rotation.

#### 5.5.4 Hydraulic Losses

As seen in Section 3.5, the losses in the different domains of an RPT machine relies heavily on the guide vane opening and mass flow. For this work, only one guide vane opening has been studied. However, it is interesting to see how pre-rotation affects the losses in the separate domains. To start, the losses in the draft tube increase with the rise in mass flow, as seen in Fig. 5.13. This is expected because we assume stronger secondary flows caused by the bend for larger volume flows. However, the losses in this region are small compared to the total head of the system. The losses in this section are plotted as a negative percentage of the head of the RPT at BEP according to:

$$\tilde{H} = \frac{H_{loss}}{H_{exp,BEP}} * 100\% \quad (5.5.6)$$

The difference in percentage from the case of no pre-rotation has been plotted according to:

$$\Delta\tilde{H} = \frac{H_{loss} - H_{loss0^\circ}}{H_{loss0^\circ}} * 100\% \quad (5.5.7)$$

Where  $H_{loss}$  is the hydraulic loss in the domain of interest, and  $H_{loss0^\circ}$  is the hydraulic loss in the domain of interest with no induced pre-rotation.

Further, we can see in Fig. 5.14 that the hydraulic losses in the draft tube increase both for positive counter pre-rotation and negative pre-rotation. In fact, they increase by five percent in both directions and a close to an equal amount for all operating points. This implies that introducing swirl to the draft tube flow increases the hydraulic losses in this region independent of the rotational direction of the swirl. As mentioned earlier, the losses in this region are so small that they do not affect the pump performance curves of the RPT much. However, dependent on the distance from the placement of the booster-pump, this could affect the losses in the draft tube. If the distance from the booster-pump to the RPT is long, and the swirl can induce losses over a considerable distance, this could potentially become an issue.

For the guide vanes, we can see that the losses are more substantial in Fig. 5.15. At 0.8 BEP, the losses account for nearly six percent of the total head, while for the losses reduces for BEP and 1.2 BEP. The losses in the guide vanes show the same trend as the efficiency curve. This trend is expected since the losses are significant in this region and heavily dependent on the right inflow conditions. One would perhaps, expect that the losses do not vary much with induced pre-rotation. In other words, one could assume that the runner would absorb the effect of the pre-rotation. However, there are substantial differences in the losses in the draft tube with different pre-rotations. Especially, for the case of negative pre-rotation of  $24^\circ$ , the difference in losses in the guide vanes are over ten percent as observed in Fig. 5.16.

For the losses in the stay vanes and the spiral casing, the losses diverge even more. Also here, the pattern of the losses show the same trend as for the efficiency curve seen in Fig. 5.17. We can see that the losses are largest for 0.8 BEP but varies depending on the pre-rotation. Fig. 5.18 shows that the losses differ with as much as 20% for the case of the most negative pre-rotation at BEP.

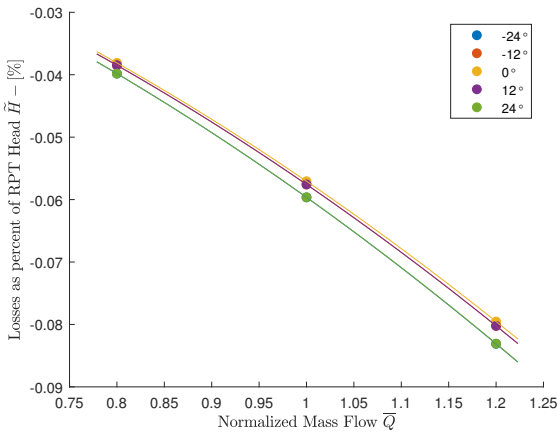


**Figure 5.13:** Hydraulic losses in draft tube

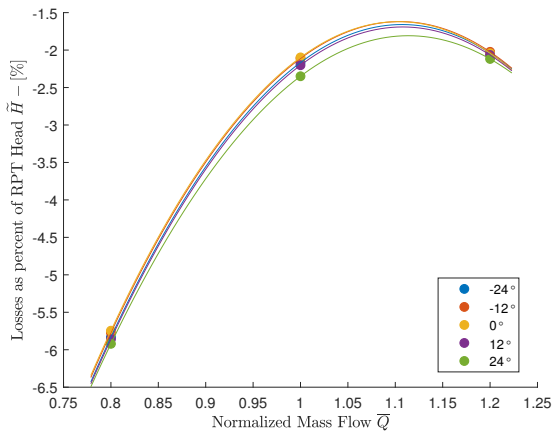


**Figure 5.15:** Hydraulic losses in guide vanes

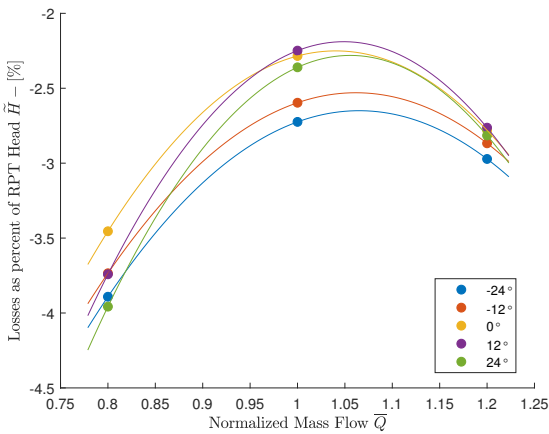


**Figure 5.17:** Hydraulic losses in stay vanes and spiral casing

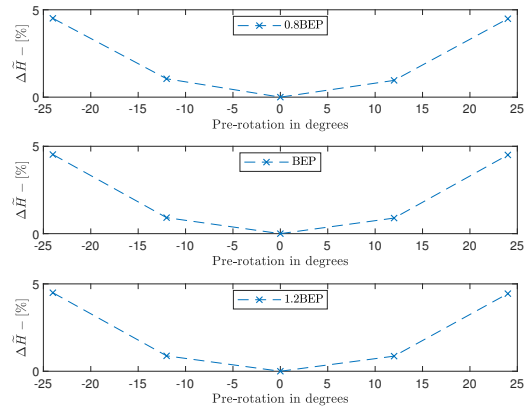


**Figure 5.14:** Difference in hydraulic losses in draft tube from no pre-rotation

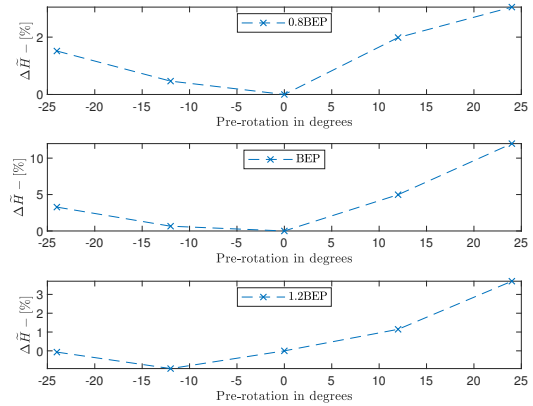


**Figure 5.16:** Difference in hydraulic losses in guide vanes from no pre-rotation

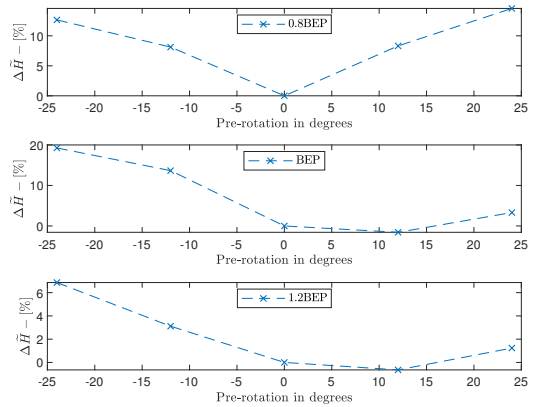


**Figure 5.18:** Difference in hydraulic losses in stay vanes and spiral casing from no pre-rotation



## Chapter 6

# Booster-Pump in Series with Reversible Pump Turbine

---

Using a uniform circumferential velocity field as an imposed pre-rotation can give valuable results when studying the effect it has on the pump performance curves. This simplification can, however, leave out vital features of the flow when the pre-rotation is thought to be coming from the outlet of a booster-pump. These features could have an impact on the research topic of this thesis. Therefore, an attempt to connect an RPT with a booster-pump is examined in this chapter.

---

### 6.1 Booster-Pump Geometry and Placement

When installing a booster-pump in series with an RPT, one must first decide where to place it. The question of where to put the booster-pump is a large one and depends on several different factors. For this thesis, a booster-pump in the same waterway is studied, and the booster-pump is placed at the outlet of the draft tube, i.e., near the draft tube gate, near the outlet surge shaft. It is assumed that the draft tube gate is positioned at the end of the draft tube geometry studied in Chapter 5. Whether or not the pump will be removed in turbine mode is not decided. It is, of course, debatable if this location is a suitable position for a booster-pump, but it is nevertheless the position investigated in this work.

Independent of the placement of the booster-pump, the pump will have an outlet. If this pump has a hub, the outlet of the pump could potentially become a severe diffuser which in turn can create a poor and unsteady flow regime. Moreover, the pump needs to gain its power from a source. There are several options for how to achieve this. Below are some aspects to consider, regarding these matters.

- The pump could be driven by a shaft running through the draft tube. The generator would then be located next to the draft tube bend. The shaft would run through the draft tube, and the diffusing problem mentioned, would be avoided. A shaft through the draft tube bend would pose as an obstacle if one wanted to remove the booster-pump during turbine operation. A possible solution to having a shaft through the draft tube can be viewed in Fig. 6.2. In Fig. 6.2, a mixed-flow pump which can be seen in the appendices, has been used for visualization. For this configuration, the shaft would be quite long. At *Roskrepp* the shaft would have been 25m long, which may seem excessive. Next, the motor

for the booster-pump would be mounted into the concrete. However, this design poses as one possible solution for early phase installing of a booster-pump and points to some of the challenges regarding the matter.

- The pump could be rim-driven like the *Straflo* turbine. Being rim-driven is especially applicable for an axial booster pump. The outlet of the pump would then have a sort of bulb, and the diffusing effect would be present. For a mixed-flow pump, there could be an engine inside the diffuser, as the generator inside a bulb turbine. For this arrangement, the outlet of the machine would become diffusive, and there is a need for an outlet bulb. A proposed design is presented in Fig. 6.1. Here, the proposed bulb is a sphere cut in half. This arrangement is chosen for further investigation.

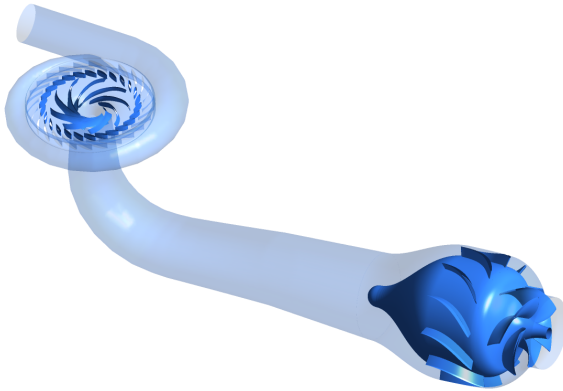


**Figure 6.1:** RPT and booster-pump connected in series with bulb configuration.

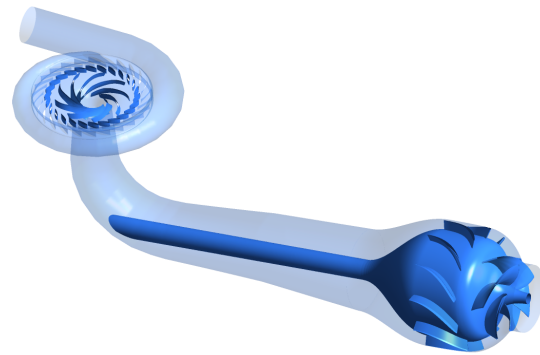


**Figure 6.2:** RPT and mixed-flow booster-pump in series with shaft going through the draft tube

To investigate the effect of pre-rotation, a booster-pump is created and simulated in series with the RPT. Moreover, the choice of not using a shaft through the draft tube is accepted. Henceforth, the draft tube had to be re-meshed to account for the bulb at the outlet of the booster-pump. How the meshing was done around the outlet bulb can be seen in Fig. 6.3.

For simulating the two pumps in series, some simplifications were done to reduce computing time. These simplifications involve using only one passage for the RPT runner, one passage for the booster-pump runner and one passage for the diffusing vanes in the booster-pump. Further, the guide vanes, stay vanes, and spiral casing of the RPT was left out of the simulation. The losses from the guide vanes, stay vanes, and the spiral casing was added after the simulations, as a function of the losses found in Chapter 5. It was shown in Chapter 5, that these losses vary with pre-rotation, but that the mass flow has the largest influence on the losses. Therefore, the losses for the case of no pre-rotation is used for the calculation of the losses in this chapter. The losses can be viewed in Fig. 6.4. As we have seen from Section 3.5, the guide vane opening, and the mass flow have a major impact on the hydraulic losses in an RPT running in pump mode. The losses are large in this region and are a particularly difficult region to simulate because of the diffusing effects the guide and stay vanes have on the water flow. By leaving these regions out of the computational domains, large savings in computational time is achieved.

## 6.2 Selection of Booster-Pump and Rapid Prototyping

The selection of the type of booster-pump should be based on the required head to avoid cavitation at the inlet of the RPT, together with supplying enough head for the given application. For this work, it



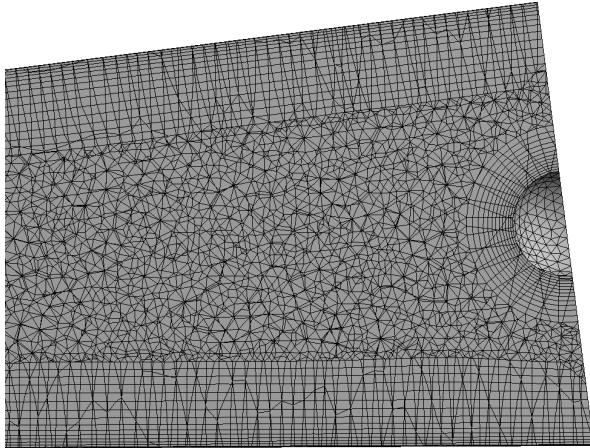


**Figure 6.3:** Mesh of draft tube showing the bulb implementation. Mesh is shown at a plane going through the center of the draft tube

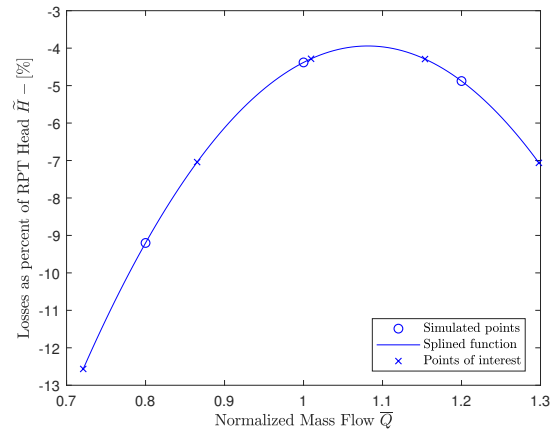


**Figure 6.4:** Losses in the guide vanes, stay vanes and spiral casing for the RPT for the case of no pre-rotation

is assumed that the booster-pump will have to generate at least 25% of the RPT head. Depending on the required head of the booster-pump, the geometry and outline of the machine will look different. The geometry for the booster-pump used in this work is a pump generated from a program called *BladeGen*. *BladeGen* is a turbomachinery design program which follows with the *ANSYS* package. The program is easy to use and allows for rapid prototyping of axial pumps, mixed-flow pumps, centrifugal pumps, inducers, and other turbomachinery components. *BladeGen* allows for giving the blades the correct angles according to the velocity triangles. One also has the option to choose the solidity and thickness profiles of the blades among many other options. *BladeGen* generates geometries that can be used for CFD calculations and to visualize and explore problems related to the matter at hand.

In this work, the rotational speed of the runner was set such that the flow would have correct inflow angle at the midsection of the leading edge of the runner for the same flow rate as for BEP at the RPT. For meshing, *TurboGrid* was used, and the setup in *ANSYS CFX* consisted of one blade for the runner and diffuser with periodic boundary conditions, mixing-plane interface,  $k-\epsilon$  turbulence model, an inlet mass-flow boundary-condition as well as a static pressure outlet condition. The simulations were considered converged when the mean square residuals reached  $10^{-4}$ .

## 6.3 Results

Three fundamentally different designs were investigated, but only one of the models generated enough head to be suitable for a booster-pump connected with the geometry studied in Chapter 5. The other two designs, along with their pump curves, can be seen in the appendices. Because the author was unable to generate a strictly axial pump with sufficient head, it was decided to move forward with a mixed-flow machine.

For fitting the pump near the draft tube gate, one must decide on a couple of crucial factors. Since mixed-flow pumps rely on centrifugal forces to generate pressure, there must be a difference in the diameter of the impeller to achieve that. The width of the impeller outlet needs to be bigger than the impeller inlet, ( $D_2 > D_1$ ). Since the draft tube is designed as a diffuser for the RPT in turbine mode, the diameter of the draft tube near the draft tube gate will be quite large. To utilize centrifugal forces, one must choose to either make the pump larger or smaller than the diameter near the draft tube gate.

### 6.3.1 Converging Nozzle Mixed-Flow Booster-Pump

For this design, the inlet diameter was chosen to be smaller than the diameter of the draft tube near the draft tube gate. By doing this, a relatively small machine is acquired. The centrifugal forces make it possible to achieve greater heads than an axial machine, but by having the impeller inlet smaller than the draft tube diameter, one has to create a converging nozzle in front of the impeller. This nozzle guides all of the flow towards the impeller and increases the axial velocity of the water as more water needs to flow through a smaller area, according to the mass conservation law Eq. (4.1.2). These higher velocities do affect the cavitation properties of the unit, according to Eq. (2.6.2). The proposed design of the booster-pump can be seen in Fig. 6.5.

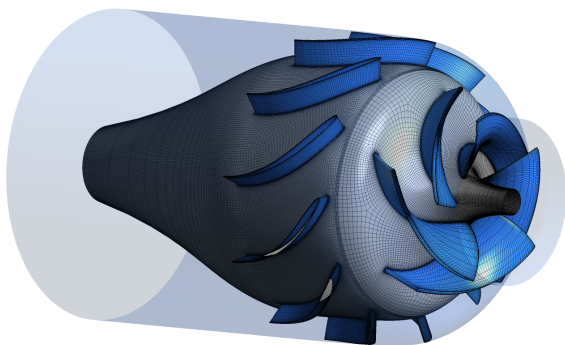


**Figure 6.5:** Design of mixed-flow booster pump with converging nozzle at the inlet. The outlet of the pump has the same diameter as the draft tube gate, but the inlet of the booster-pump is smaller.

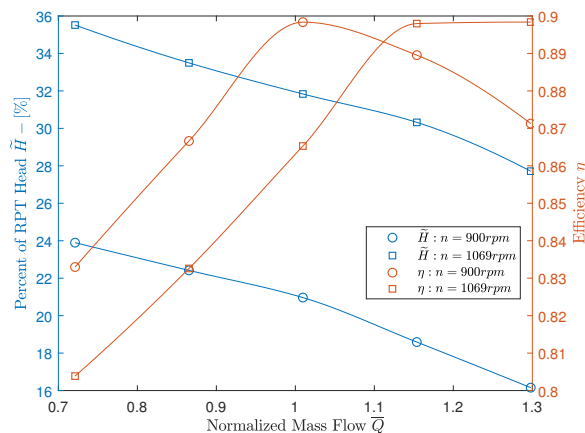


**Figure 6.6:** Pump curves for the converging mixed-flow booster-pump

The design in Fig. 6.5 is a version of the mixed-flow pump example given with the *BladeGen* package. An adjustment that has been done to this geometry is scaling. The scaling was done so that the diffuser outlet would be the same size as the draft tube near the draft tube gate. Further, the trailing edge of the impeller has been modified from a cut-off edge to a rounded trailing edge. The diffuser has been extended so that the shroud at the outlet has the same diameter as the draft tube near the draft tube gate. The hub size at the outlet was set so that  $D_{hub}/D_{shroud} = 0.25$ . *Bezier* curves were used to generate the shape of the diffuser shroud and hub profiles. Efforts were made to have a gradual increase in area to account for a smooth diffusive gradient. To do so, the diffusing elements were also made longer.

The pump curves of the mixed-flow booster-pump with a converging nozzle is given in Fig. 6.6. As can be seen, the optimal mass flow for this pump is larger than what it is for the RPT. That is when running the pump at a rotational velocity that fits with the inlet velocity diagram at the mid-span of the impeller. The mixed-flow machine has been designed with an inlet angle  $\beta_1 = 22.5^\circ$  at the mid-span of the impeller inlet. For a rotational speed of  $n = 900$  rpm, BEP is at the same point as the RPT. However, the head produced is reduced by roughly 10%. Because it is assumed that the booster-pump needs to produce around 25% of the RPT head, it was decided to move forward with the pump curve that is calculated for  $n = 1069$  rpm. For this rotational speed, the machine has a specific speed  $\Omega_s$  ranging from 0.88 to 1.43, and a specific diameter  $D_s$  ranging from 1.57 to 2.23. These parameters place the machine just to the left of the Cordier line within the mixed flow range in the Cordier diagram shown in Fig. 3.2. Thus we can assume that the machine is similar to what has been used in other, similar, and successful applications.

The suction head criterion was calculated from the equations given in Section 2.6. For this work, we can assume that the RPT is submerged according to what it would have been if it was a Francis turbine working strictly in turbine mode. Here, Eq. (2.6.3) has been used.  $NPSH_R$  for the RPT would then have been as seen in Fig 6.8 for turbine mode. We can assume that the RPT would have been submerged to this level

according to  $NPSH_R = NPSH_A$  when  $Q = 1.25BEP$  for turbine mode.  $NPSH_A : RPT$  states that the RPT is submerged to such a level that it can operate at a capacity of  $1.25BEP$  in turbine mode, without experiencing cavitation. If we are to run the RPT in pump mode at this submergence, we can see from Fig. 6.8 that the machine would experience cavitation as  $NPSH_R > NPSH_A$  for most of the desired operating range. Henceforth, we decide to install a booster-pump.

When installing the booster pump, the pressure at the RPT suction side is increased, effectively reducing the need for submergence. However, we must also ensure that the booster-pump do not experience cavitation. Since the booster-pump is placed below the RPT, we get some further submergence. Therefore,  $NPSH_{A-BP}$  is a bit higher than  $NPSH_{A-RPT}$ . Now, to avoid cavitation for the booster-pump,  $NPSH_R < NPSH_{A-BP}$  needs to be fulfilled for the booster-pump in pump mode. As seen in Fig. 6.8, this criterion holds up until around  $1.25BEP$ , and we can assume that the booster-pump can run without cavitation in pump mode. In these calculations, the most conservative values, meaning the largest values, from Table 2.1 have been used for the calculations of the suction head. The experimental head at BEP for the RPT has been used for normalization.

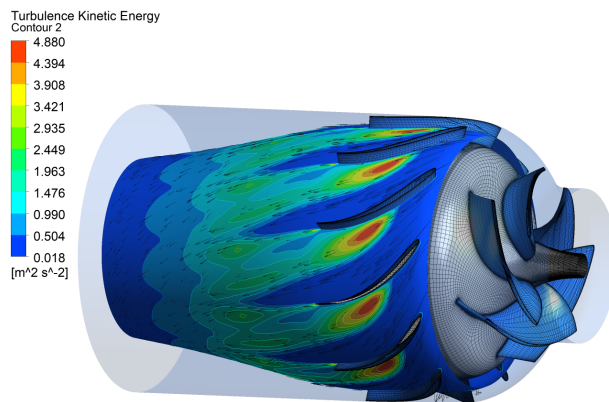


**Figure 6.7:** Contour plot of turbulent kinetic energy in diffuser channels which shows separation at 0.5 span-wise direction

The design of the diffusing channels of the booster-pump proved troublesome. In Fig. 6.7 the separation in the diffuser vanes are shown by a contour plot of the turbulent kinetic energy at BEP load. In the diffusing channels, separation occurs and creates turbulent eddies, which disrupts the flow field. To improve efficiency, the generation of these turbulent structures should be minimized. Fig. 6.7 shows a vector field on the same span-wise plane. Here the diffusers do not manage to convert the kinetic energy in the swirling component into pressure. However, this swirling component can benefit the RPT if the rotation is induced as a counter pre-rotation, as shown in Chapter 5.

As mentioned, using a uniform velocity field as an approximation of an outlet velocity field could leave out essential aspects of the flow regime. In Fig. 6.9, the axial, radial, and circumferential velocity components at the outlet of the booster-pump are plotted. The profiles show the spanwise distribution of the velocity from hub to shroud at the outlet of the booster-pump and visualize that the velocity field from this booster-pump is far from uniform. To start with, the axial velocity profiles show that for capacities at BEP and above, the axial velocity near the hub is negative. In other words, the flow is reversed near the hub.

Further, we can see that the circumferential velocity distribution is negative for all operating points. In this regard, it means that the flow leaving the booster-pump has a swirl in the same direction as the impeller rotation, emphasizing that the diffusers have not managed to convert the rotational kinetic energy

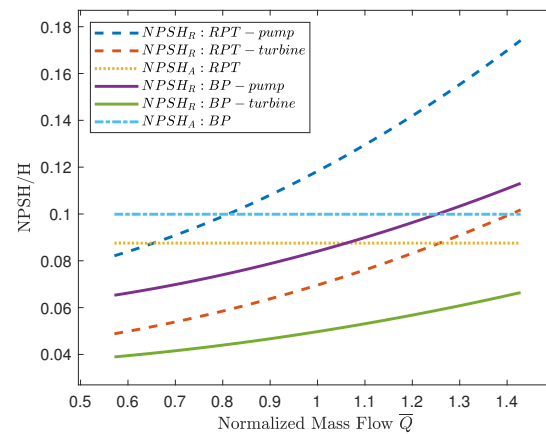


**Figure 6.8:** Normalized  $NPSH$  for the RPT and booster-pump.  $NPSH_A : RPT$  is set such that the RPT can run in turbine mode at  $1.25BEP$  without experiencing cavitation

into pressure. We can see that the circumferential velocity component is in the same direction, meaning negative, for all operating points. Moreover, it can be seen that the radial velocity is mainly positive for the two profiles with the least mass flow. Positive radial velocity means that the water is flowing outwards, corresponding well with the axial velocity. For the three largest mass flows, the radial velocity is positive, meaning that the liquid is flowing towards the hub. All in all, it is clear that the outlet velocity field is far from uniform.

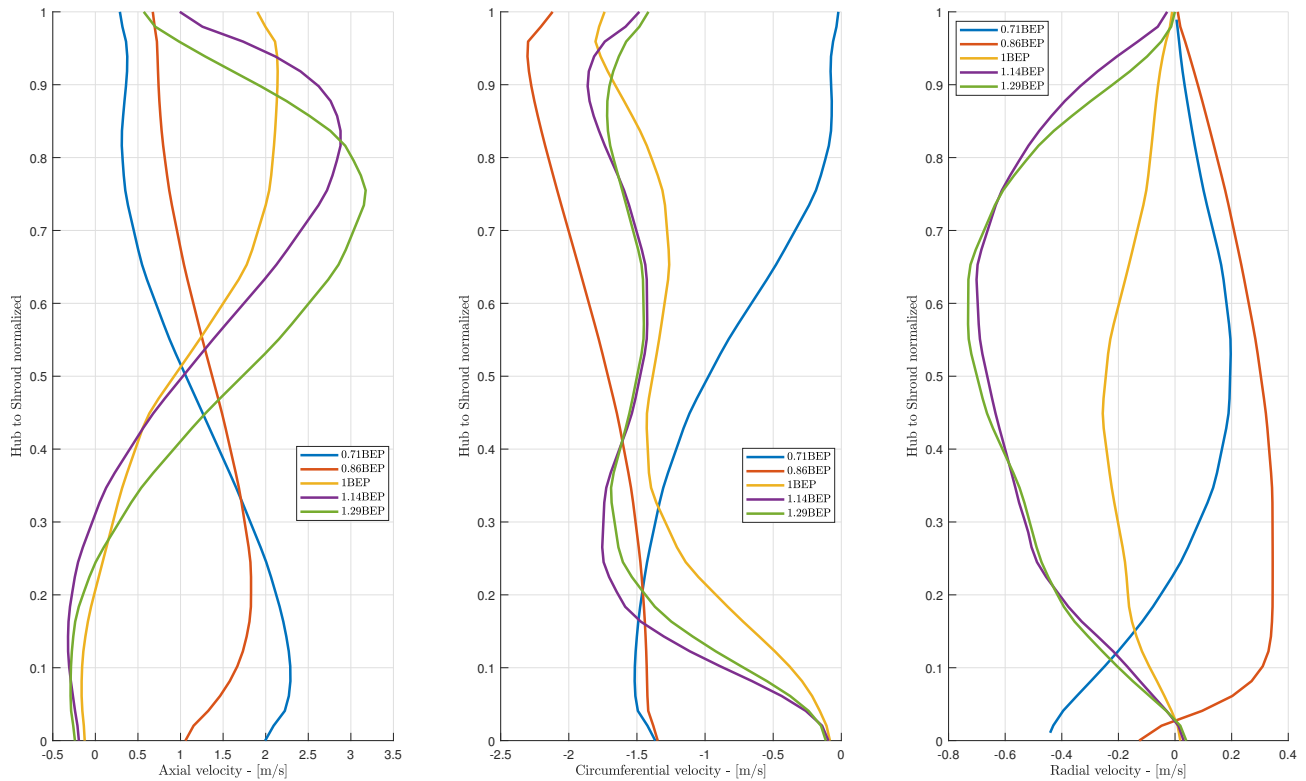


**Figure 6.9:** Velocity profiles for the outlet of the booster-pump

### 6.3.2 Booster-Pump Running in Opposite Direction as RPT

We know from Chapter 5, that pre-rotation affects the pump curves of the RPT. The goal of this chapter is to create a more realistic pre-rotation than that of a uniform velocity field. Even though that the booster-pump implemented here creates pre-rotation that could be more realistic, it should be noted that if the final design of the booster-pump has any alterations from this design, the flow field might look entirely different. Care should, therefore, be taken when extrapolating conclusions from this design to other models. However, it is believed that this design can point to some interesting flow phenomena that might occur when utilizing a booster-pump, as well as showing how a rotational component can influence the RPT. From Section 3.1, we know that the head from two separate pumps can be added together to find the combined head-capacity curve. This assumption does not take into account the effect of pre-rotation. If the two pumps have head-capacity curves that have been obtained separately, then the impact that the booster-pump has on the RPT is neglected.

To investigate how the booster-pump affects the RPT, they are simulated in series. The entire compu-

tational domain can be viewed in Fig. 6.10. Here, the booster-pump has been angled to fit with the top of the draft tube. The angling is done this way because it is assumed that the draft tube will move upwards, towards the lower reservoir. The shift in direction creates a blunt angle at the bottom of the draft tube of  $7.25^\circ$ , which could affect the flow regime. The pump curves for the two pumps in series can be seen in Fig. 6.11. For the combined system, the head is computed from Eq. (3.1.1). The combined efficiency has been calculated according to:

$$\eta_{combined} = \frac{\rho g Q (H_{RPT} + H_{BP})}{P_{RPT} + P_{BP}} \quad (6.3.1)$$

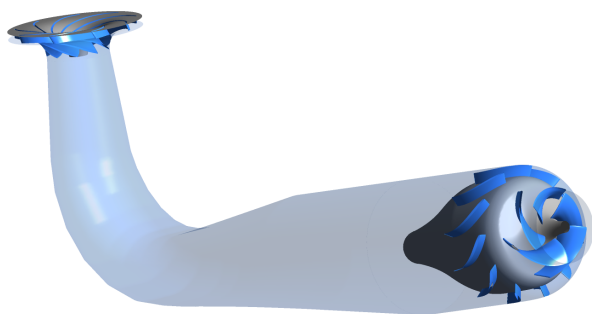


**Figure 6.10:** RPT impeller and converging-nozzle mixed-flow booster-pump running in the *opposite* direction in series

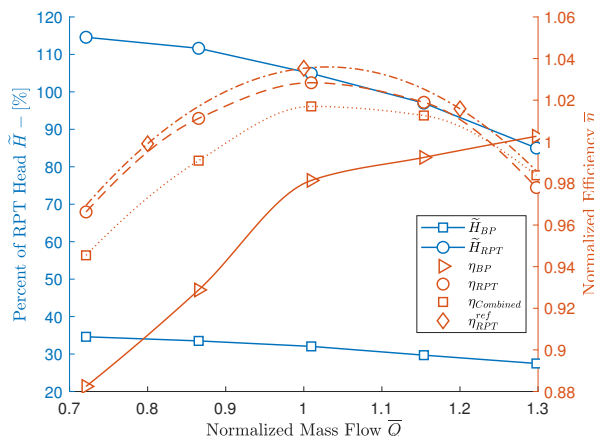


**Figure 6.11:** Pump curves for the booster-pump and the RPT connected in series with *opposite* rotational direction.  $\eta_{RPT}^{ref}$  refers to the case of no pre-rotation for the RPT

The efficiency in Fig. 6.11, can be compared to the reference value of the efficiency,  $\eta_{RPT}^{ref}$ , for the RPT which was calculated in Chapter 5.  $\eta_{RPT}^{ref}$  refers to the calculated efficiency for the case of no pre-rotation calculated in Chapter 5. As we can see, the efficiency of the RPT is lower in this case. However, the simplification with utilizing the losses from the reference case seems to work rather fine, as the trend of the efficiency matches rather well. The efficiency curve of the booster-pump is similar to what was seen when calculating by the booster-pump by itself, but there is a slight increase in the efficiency for the highest capacity. Overall we can see that the combined efficiency is lower than what it was for the RPT alone. However, because the RPT uses much more power than the booster pump, the combined efficiency is still at an acceptable range. As the booster-pump generates more than 25% of the RPT head, we can be fairly confident that the RPT will not experience cavitation if it is submerged according to a turbine level. This statement is at least true for the increased level of the required suction head for pumping mode observed in Fig. 6.8.

Following a mixed-flow pump, there will be a wake. This wake could cause problems during operation. The wake is a source of losses and could be reduced by having a shaft running through the draft tube, as suggested in Fig. 6.2 and which is often used for mixed flow pumps similar to Fig. 3.3. In Fig. 6.12 the wake of the booster-pump is shown as a contour plot on a plane running through the draft tube. As can be seen from the contour plot, the velocities following the outlet bulb of the booster-pump are small compared to the velocities near the wall of the draft tube. A vector plot of the tangential projection of the velocity is plotted on top of the plane. The velocity vectors show some of the turbulent behaviors in the wake, as well as the direction in the flow going towards the RPT.

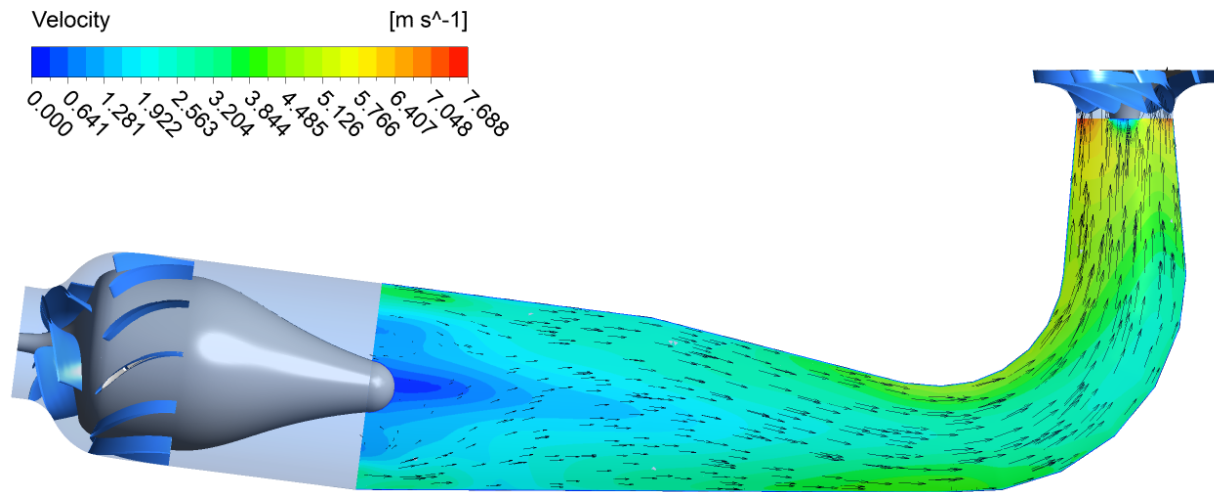


**Figure 6.12:** Illustration of the trailing wake following the booster-pump at BEP.

### 6.3.3 Booster-Pump Running in the Same Direction as RPT

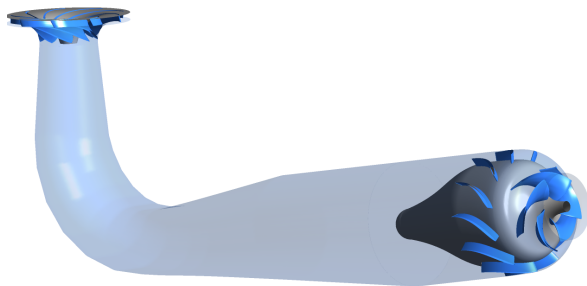


**Figure 6.13:** RPT impeller and converging-nozzle mixed-flow booster-pump running in the *same* direction in series.

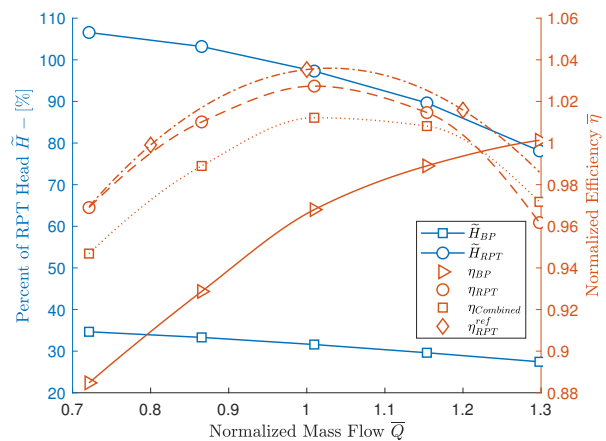


**Figure 6.14:** Pump curves for the booster-pump and the RPT connected in series with the *same* rotational direction.  $\eta_{RPT}^{ref}$  refers to the case of no pre-rotation for the RPT

From Section 3.4, we know that pre-rotation can make a difference in the pump curves. The question then becomes; how does the rotational direction of the booster-pump affect the combined system characteristics? To answer that question, the booster pump has been mirrored around its axis. The reversed pump gives the same pump curve and outlet velocity field, only in the opposite direction. The combined system can be viewed in Fig. 6.13 along with the pump curves in Fig. 6.14. From Chapter 5, we would assume a reduction in the head pump curve for the RPT when applying the booster-pump in the same rotational direction as the RPT. We can see that the same pattern is repeated for the setup when having the pumps in series.

When investigating the pump curves of the combined system, where the rotational direction is the same



for both pumps, we see that the behavior of the system is somewhat similar to before. However, there is a more significant discrepancy between the reference efficiency and the efficiency of the RPT, meaning that the efficiency of this system is lower than the previous. However, both pump's does the job of giving around 30% more head to the system, thereby avoiding cavitation at the RPT suction side.

### 6.3.4 Comparison of Options

A comparison of the alternatives can be examined in Fig. 6.15. The resulting pump curves are consistent with what was found in Chapter 5. Pre-rotation in the opposite direction of the rotation of the RPT is beneficial with regards to increased head. The combined system generates almost 10% more head when the booster pump is rotating in the opposite direction. With regards to efficiency, the same can be said when comparing the two alternatives. However, the combined efficiency would most likely be larger if there were no swirl at the outlet of the diffuser, thereby increasing the efficiency of the booster-pump. Even so, one matter is evident, and that is that positive counter pre-rotation can increase the head-capacity curve, compared to having negative pre-rotation.

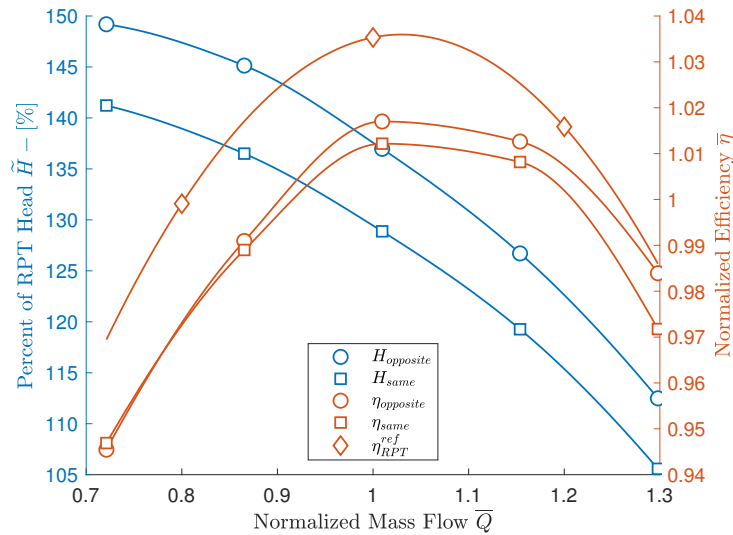


**Figure 6.15:** Comparison of the combined pump performance curves when having the booster-pump rotating in the same direction or the opposite direction of the RPT





## Part IV

# Concluding Remarks



# Chapter 7

## General Discussion

This thesis has investigated pre-rotation for an RPT in pump mode. The project that this research is related to is the project of replacing Francis turbines with RPTs by utilizing a booster-pump. The hydropower plant connected to this research is the *Roskrepp* hydropower station. *Roskrepp* uses a high specific-speed runner, while this work investigates a low specific-speed runner. The geometry studied here is, therefore, inherently different from the *Roskrepp* case. Care should be practiced when extrapolating results from this geometry, onto the case mentioned above. As stated in the section regarding impeller inflow, pre-rotation is more effective as the ratio between the diameter of the inlet and outlet of the pump,  $D_1/D_2$ , increases. Following this argument, pre-rotation could have a stronger influence on high specific-speed machines, as is the case of *Roskrepp*.

The simulation performed in Chapter 5 are validated against a mesh independence study, but only at BEP and with no pre-rotation. As the inlet boundary condition imposed in Chapter 5 is a uniform tangential velocity profile, it was deemed more useful to further investigate the inlet boundary condition of an actual booster-pump, rather than further dwelling on the accuracy of the mesh. For further investigation and more thorough validation of the model, experimental studies with an induced pre-rotation could prove useful.

As shown in Chapter 6, the outlet flow of the booster-pump is not uniform. The outlet velocity field varies greatly, and the circumferential component leaving this booster-pump is presumably more extensive than what it would have been if the diffuser vanes were designed in another manner. However, it is believed that the results show a physical and actual effect regarding pre-rotation. A strong indicator of the validity of the results is that the Euler turbomachinery equation supports them. Moreover, the results are similar to what has been found in previous work regarding pre-rotation in pumps [11], [12], [13, p. 675]. It should be mentioned that the research referred to here applies to pre-rotation that is induced by inlet guide vanes and not by a booster pump. Also, the literature has not imposed pre-rotation before a bend, and thus, the effect of secondary flows are not present in these results.



# Chapter 8

## Conclusion

The present work act as a contribution to the understanding of pre-rotation for RPTs running in pump mode. It also sheds light on some of the issues regarding retrofitting Francis turbines with RPTs. An RPT with a specific speed of  $\Omega_s = 0.58$ , has been investigated numerically in pump mode. The work included steady-state CFD simulations using a uniform inlet circumferential velocity field at the draft tube inlet. Next, to induce a more realistic pre-rotation, the same RPT has been simulated in series with a booster pump. These simulations have been performed with the booster-pump running in the same direction as the RPT and the opposite.

The simulations with a uniform induced pre-rotation imply that for a positive counter pre-rotation, the head of the machine is increased. On the contrary, the head of the pump decreases for negative pre-rotation. This behavior follows the Euler turbomachinery equation, Eq. (2.4.1), as the circumferential velocity component at the inlet of the machine, is either negative or positive. Further, it is revealed that the efficiency curve is highest when there is no pre-rotation. Still, positive counter pre-rotation is more beneficial than the opposite - which is negative pre-rotation.

The results additionally indicate that the secondary swirls occurring downstream of the bend, twist together with the pre-rotation. This twisting affects the inflow characteristics of the runner. Also, it is found that the losses in the separate domains vary with pre-rotation even downstream of the runner. The losses in the draft tube increase together with absolute pre-rotation intensity, while the losses in the guide vanes show a more complex pattern. For all domains, the hydraulic losses increase with pre-rotation.

The booster-pump created and used in this work is a mixed flow machine that produces more than 25% of the RPT head. The efficiency of the pump is decent, but BEP of the booster-pump is at a higher capacity than BEP of the RPT. However, it is shown analytically that the booster-pump can run without cavitation, as well as giving the RPT enough head to run without cavitation in pump mode, at a turbine level submergence.

The diffuser vanes in this booster-pump are not capable of converting all the kinetic energy from the impeller into pressure. Because of this, there is a swirling component at the outlet of the booster pump. Or in other words, pre-rotation for the RPT as intended. When the system is simulated in series, it is evident that there is a powerful wake following the booster-pump. The wake could have an impact on the performance of the system.

Last, the combined pump curves of the system are extracted for when the booster-pump is running in the same direction as the RPT and the opposite. The results show that there is around 10% difference in the head, depending on whether the booster-pump is running in the same direction or the opposite — the latter

giving the highest head. The efficiency of the combined system is higher when running the booster pump in the opposite direction. Nonetheless, the efficiency of the combined system is lower than it is for the RPT alone for both configurations.

Summing-up, pre-rotation affects the performance curves of the RPT. If one were to retrofit a Francis turbine with an RPT with the use of a booster-pump, one should consider how the booster-pump and pre-rotation affect the RPT. Based on the results of this work; counter pre-rotation seems to be more beneficial than pre-rotation in the same direction with regards to head. The efficiency does not increase with pre-rotation, but it appears that counter pre-rotation is more useful than the opposite in this regard as well.

## Chapter 9

# Future Work

An interesting aspect that was not investigated in this research is what happens when the RPT is working in part load. That is below the capacity that has been studied here. In this region of the pump curve, the transient phenomenons are stronger, and the physics involved become more challenging to simulate accurately. Even so, these features should be studied as it necessary for the pump to go through this region during startup. Pre-rotation could affect this region of the pump curve significantly.

Further, more research on how the suction head is affected by pre-rotation would be intriguing. As seen in Section 3.4, this measure varies when imposing pre-rotation on a mixed-flow pump. How the suction head varies with pre-rotation for this geometry has been left for future work. Keep in mind that when doing CFD analysis, *NPSH* is heavily dependent on the meshing.

The design of the diffusers of the booster-pump used here should be improved. As the main interest involved pre-rotation, it was not crucial that the diffusers converted all of the kinetic energy into pressure. For the final design of the booster-pump, the booster-pump should preferably give less swirl than the booster-pump did in this research. That is to achieve an adequate efficiency for the booster-pump and thereby the entire system.

Additionally, it would be interesting to see how the system operates in turbine mode. It could be that the booster-pump has an influencing effect on turbine operation. It could also be that the booster-pump should be removed in turbine mode to achieve higher efficiency for the RPT. The author believes that it would be preferable to have the booster-pump working in both directions. An argument for is that; the mechanism needed for removing the machine would be complicated. Another argument is that; if the booster-pump were to be placed in another channel, like in the patent visualized in Fig. 2.8, the need for an extra and expensive waterway is present. Mixed-flow pumps have been investigated as PATs before, with promising results [28], and it could be that the booster-pump is useful in turbine operation as well.





# Acknowledgments

Petter Østby has guided me with a steady hand throughout this year. He has always been available and ready to answer whatever questions I've had on my mind. He has also been able to guide me in the right direction when I didn't know what to ask. For this, I am deeply grateful. Further, I would like to express my gratitude to Igor Iliev, who has taken so much time out of his Ph.D. work to discuss matters like turbulence models, pre-rotation, and several other issues. Our discussions by the coffemaker have influenced the direction of this thesis heavily. Also, Chirag Trivedi deserves my gratitude for useful tips and helpful talks along the way. Thank you. For providing me with the task and contributing insights throughout the process, I would like to thank Pål-Tore Selbo Storli. Finally, I want to thank my girlfriend Elisa and all of my friends at the Waterpower laboratory for making this year, a great year.



# Bibliography

- [1] A. Harby, J. Sauterleute, Å. Killingtveit *et al.*, ‘Hydropower for Energy Storage and Balancing Renewables’, SINTEF Energy Research, Tech. Rep., 2016.
- [2] H. Hammnaberg and Vattenfall Power Consultant, ‘Pumpekraft i Noreg - Kostnader og utsikter til potensial’, Noregs vassdrags- og energidirektorat, Tech. Rep., 2011, p. 258.
- [3] C. Walsh and I. Pineda, ‘Wind energy in Europe in 2018’, Wind EUROPE, Tech. Rep., 2019, p. 32.
- [4] REN21, ‘Renewables 2018 - Global Status Report’, REN21 Secretariate, Paris, Tech. Rep., 2018, p. 41.
- [5] International Hydropower Association, ‘Hydropower Status Report’, Tech. Rep., 2018, p. 53.
- [6] Å. Killingtveit, ‘Balansekraft og Pumpekraftverk - NTVAs Energistrategi 2013-2017’, Norwegian Academy of Technological Sciences, NTVA, Trondheim, Norway, Tech. Rep., 2013, p. 3.
- [7] J. Charmasson, M. Belsnes, O. Andersen *et al.*, ‘HydroBalance - Roadmap for large-scale balancing and energy storage from Norwegian hydropower’, Sintef Energy, NINA, NTNU, Tech. Rep., 2018.
- [8] IRENA, ‘Electricity storage and renewables: Costs and markets to 2030’, International Renewable Energy Agency, Abu Dhabi, Tech. Rep., 2017.
- [9] Hydrocen, *Pump turbines in existing power plants - <https://www.ntnu.edu/hydrocen/2.3-pump-turbines-in-existing-power-plants>*. NTNU, Hydrocen, 2019.
- [10] Keith A. Martin, ‘Analysis of the Effects of Pre-whirl on the Efficiency and Operating Range of Hydro Pumps used in Pumped Storage Facilities’, *Research Summary*, 2015.
- [11] Y. Liu, L. Tan, M. Liu *et al.*, ‘Influence of prewhirl angle and axial distance on energy performance and pressure fluctuation for a centrifugal pump with inlet guide vanes’, *Energies*, vol. 10, no. 5, p. 695, May 2017.
- [12] S. Amjad Ahmed, A. Muiz, M. Mubashir *et al.*, ‘Efficiency Enhancement of Centrifugal Water Pump by Using Inlet Guided Vanes’, Tech. Rep. 10, 2016, pp. 1–4.
- [13] J. F. Gülich, *Centrifugal pumps*, 2nd ed. Springer, 2014, vol. 9783642401, pp. 1–1116.
- [14] I. Iliev, C. Trivedi and O. G. Dahlhaug, ‘Simplified hydrodynamic analysis on the general shape of the hill charts of Francis turbines using shroud-streamline modeling’, in *Journal of Physics: Conference Series*, vol. 1042, 2018, p. 12 003.
- [15] H. Brekke, *Introduction to hydraulic machinery*. Vannkraftlaboratoriet NTNU, 2000.
- [16] H. Tanaka, ‘Construction of Pump-Turbines’, in *Mechanical Design and Manufacturing of Hydraulic Machinery*, M. Zu-yan, Ed., 1991.
- [17] H. Brekke, *Pumps and Turbines*. Trondheim: Vannkraftlaboratoriet NTNU, 2003.
- [18] J. Rondot, *Turbine-pompe multi-étages de haute chute*. 1983.
- [19] K. M. Torød, ‘Simulation of pre-rotation in the flow at the inlet of a Reversible Pump Turbine’, no. June, 2018.
- [20] Y. A. Cengel and J. M. Cimbala, *Fluid Mechanics - Fundamentals and Applications*, 2nd ed. 2010.

- [21] S. Tsunoda, *Method of pumping up electric power generation and an apparatus therefore*, 1982.
- [22] Roskrepp kraftverk - <https://www.sirakvina.no/roskrepp-kraftverk/roskrepp-kraftverk-article257-921.html>. Sira-Kvina kraftselskap.
- [23] Y. A. Cengel and J. M. Cimbala, 'Turbomachinery', in *Fluid Mechanics - Fundamentals and Application*, 2nd ed., 2010, ch. 14.
- [24] A. Kováts, 'Operation of pumps and compressors', in *Design and performance of centrifugal and axial flow pumps and compressors*, 1964, ch. 2.
- [25] S. L. Dixon and C. A. Hall, 'Dimensional Analysis: Similitude', in *Fluid Mechanics and Thermodynamics of Turbomachinery*, 6th ed., 2010, ch. 2.
- [26] O. Braun, 'Part load flow in radial centrifugal pumps', *A la faculte sciences et techniques de l'ingenieur*, vol. 4422, no. 4422, p. 177, 2009.
- [27] M. Matsumura, 'Construction of Axial-Flow, Mixed-flow and Tubular Pumps', in *Mechanical Design and Manufacturing of Hydraulic Machinery*, M. Zu-yan, Ed., 1991, ch. 13.
- [28] P. Hlbocan and M. Varchola, 'Numerical Simulation on a Mixed flow Pump operating in a Turbine mode', *Engineering Mechanics*, vol. 20, no. 2, pp. 97–105, 2013.
- [29] D. Zhu, R. Xiao, R. Tao *et al.*, 'Impact of guide vane opening angle on the flow stability in a pump-turbine in pump mode', *Proceedings of the Institution of Mechanical Engineers, Part C: Journal of Mechanical Engineering Science*, vol. 231, no. 13, pp. 2484–2492, Jul. 2017.
- [30] O. Braun, J.-L. Kueny and F. Avellan, 'Numerical Analysis of Flow Phenomena Related to the Unstable Energy-Discharge Characteristic of a Pump-Turbine in Pump Mode', in *ASME 2005 Fluids Engineering Division Summer Meeting*, 2008, pp. 1075–1080.
- [31] C. L. Fefferman, 'Existence and smoothness of the Navier-Stokes equation', no. 1, pp. 1–6,
- [32] H. Verkeeg and W. Malalasekera, *An Introduction to Computational Fluid Dynamics - The finite volume method - Second Edition*. 2007, p. 503.
- [33] J. F. Gülich, 'Numerical Flow Calculations', in *Centrifugal Pumps*, Berlin, Heidelberg: Springer Berlin Heidelberg, 2014, pp. 499–574.
- [34] ANSYS, 'ANSYS CFD-Solver Theory Guide. Release 14.0', vol. 15317, no. November, pp. 724–746, 2011.
- [35] ASME, 'Procedure for Estimation and Reporting of Uncertainty Due to Discretization in CFD Applications', *Journal of Fluids Engineering*, vol. 130, no. 7, 2008.
- [36] H. Keck and M. Sick, 'Thirty years of numerical flow simulation in hydraulic turbomachines', *Acta Mechanica*, vol. 201, no. 1-4, pp. 211–229, 2008.
- [37] A. I. Bosioc, S. Muntean, I. Draghici *et al.*, 'Hydrodynamic Analysis of the Flow in an Axial Rotor and Impeller for Large Storage Pump', in *IOP Conference Series: Earth and Environmental Science*, vol. 49, 2016.
- [38] R. Schilling, G. Shober, M. Hutter *et al.*, 'Development of a Radial-Axial Pump-Turbine for Decentralized Small Pumped Storage Power Plants', Tech. Rep., 2015.
- [39] A. Stepanoff, 'Centrifugal and axial flow pumps: theory design and application', pp. 38–42, 1957.

# Appendix A

## Theory

### A.1 Inducers

Cavitation can be a significant problem for pumps. When having cavitation in a pump because of too little submergence, a smart way to reduce cavitation is to install an inducer. The inducer decreases the required  $NPSH_R$  for a pump, and hence, the problem of cavitation is avoided. An inducer typically allows for a reduction in the required  $NPSH_R$  for a pump to up to half of the value without an inducer [33]. This reduction reduces the necessary submergence of the pump significantly.

As a consequence of using an inducer, the pump can run at a higher rotational speed than it can do without and therefore achieve more head. What the inducer does is essentially the same thing as the proposed axial booster pump is supposed to do, but there are several differences between the two solutions. For once, the inducer is fitted to the inlet of a centrifugal pump.

Inducers have been proposed used in RPTs earlier. A study performed in 2015 regarding the hydrodynamics of an axial rotor for a large storage pump was investigated [37]. The study showed that an inducer could help on more than just cavitation. The axial inducer can improve the incidence angle at the impeller inlet [37]. When the flow moves through the draft tube, towards the pump turbine, the secondary flows created in the suction elbow can create a complex flow pattern at the impeller inlet. These complex flow patterns can generate strong, unsteady flow conditions, such as wakes, pressure fluctuations, stall, and other behaviors that reduce the efficiency of the machine. When mounting the inducer, the deviation angle at the inlet of the pump turbine was reduced by 40%. The RPT inducer can be seen in Fig. A.1.

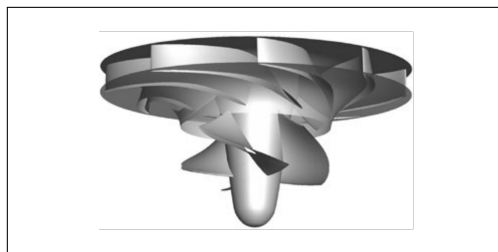


**Figure A.1:** Inducer used on the RPT investigated in the paper by *Schilling et al.* Collected from [38]

### A.2 Submergence

An expression for the necessary submergence of a pump is given in Eq. (A.2.1). Here, all variables are collected from Fig. A.2 and  $H_{V,s}$  refers to the losses in the suction pipe.

$$z_e = NPSH_R + H_{V,S} - \frac{p_{e,abs} - p_v}{\rho g} - \frac{c_e^2}{2g} + a \quad (\text{A.2.1})$$

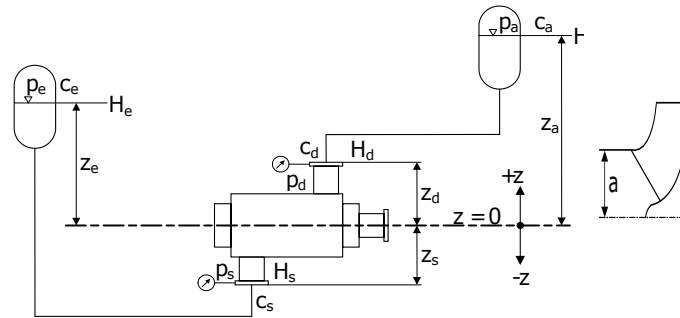


**Figure A.2:** Illustrative example for calculation of the necessary submergence to avoid cavitation in a pump. Collected from [13, p. 44]

# Appendix B

## Rapid Prototyping

### B.1 Axial Booster-Pump

One design of an axial booster-pump is presented in Fig. B.1. When designing the axial booster pump, it became clear, that to design an axial pump with any significant head together with acceptable efficiency would be difficult when using *BladeGen*. Therefore, the goal was to obtain a decent efficiency at the required volume flow. From the literature, ([13], [39]), and according to Section 3.5, it became clear that diffusers need to be added to the pump to generate any head. The diffusers have the task of reducing the rotational component generated by the impeller, converting kinetic energy into potential energy. In Fig. B.2, the pump curves for the axial booster-pump is plotted.

As witnessed in Fig. B.2, BEP of the booster pump does not match the BEP of the RPT. Further, one can observe that the overall efficiency is rather low. It would appear that the efficiency increases for greater mass flows than what has been accounted for here, but then again the head would be even smaller. The head of this design turned out to be less than one percent of the head of the RPT. After many attempts of designing an axial booster-pump, this was the final design, and it was decided that the head produced by this pump was too low to be interesting for further investigation.

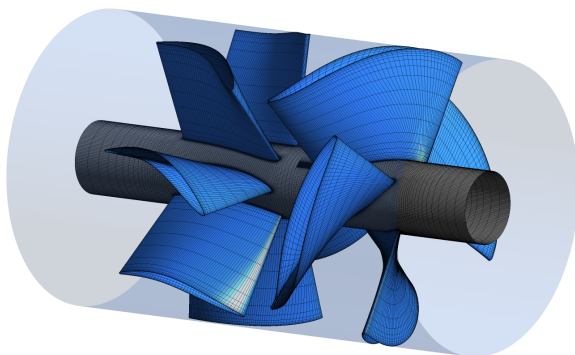


**Figure B.1:** Design of an axial flow pump. Here, the inlet and outlet of the booster-pump has the same diameter as the outlet of the draft tube. Rotational speed:  $n = 200rpm$

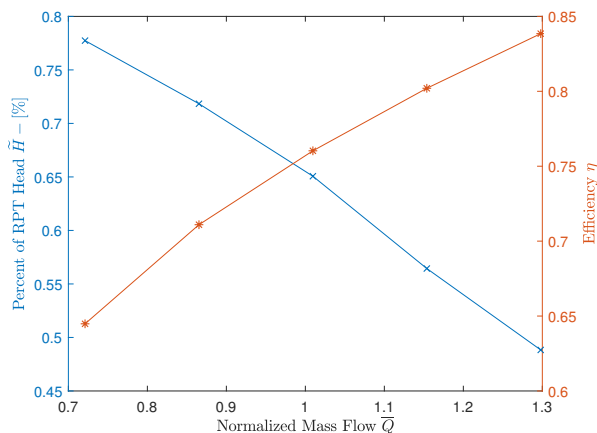


**Figure B.2:** Pump curves for the axial booster-pump

For the design of the booster-pump, efforts were made to follow the guidelines for creating axial pumps given by *Gulich* in [13]. Due to issues with choosing an applicable non-symmetric *NACA* profile this turned out to be challenging. However, by using only velocity diagrams, *BladeGen* was able to produce a pump that can represent some of the issues present in an axial pump. A particular problem for the pump visualized in Fig. B.1 was separation near the hub of the impeller. This separation created a disturbance in the flow, which led to back-flow vortices at the outlet domain of the pump.

## B.2 Large Diameter Mixed-Flow Booster-Pump

If more lift than what an axial pump can produce is required, one has the option to go for a mixed-flow pump instead of an axial pump. As mentioned earlier, mixed-flow pumps do not utilize a volute, and therefore, in terms of space, the pump can be relatively small. That is, compared to a centrifugal pump with a volute. However, if one decides to fit the pump at the outlet of the draft tube, one must decide on a couple of crucial factors. Since mixed-flow pumps rely on centrifugal forces to generate pressure, there must be a difference in the diameter of the pump to achieve that. The width of the impeller outlet needs to be bigger than the impeller inlet, ( $D_2 > D_1$ ). Since the draft tube is designed as a diffuser for the RPT in turbine mode, the diameter of the outlet will be quite large. To utilize centrifugal forces, one must choose to either make the pump larger or smaller than the draft tube outlet.

In Fig. B.3, a proposed design has been given, where the inlet of the booster-pump is the same diameter as the draft tube. To utilize centrifugal forces, the diffusers need to be larger than the impeller outlet. Given that the width of the draft tube is already quite large, this gives a rather bulky machine.

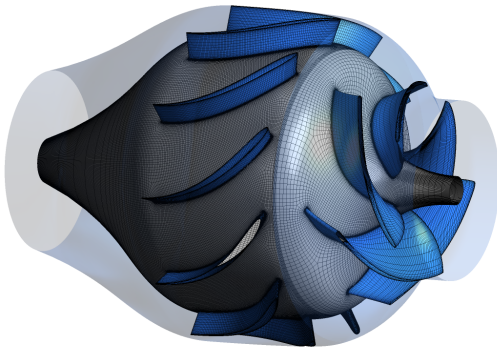


**Figure B.3:** Design of mixed-flow booster-pump. Here, the inlet and the outlet of the booster-pump has the same diameter as the outlet of the draft tube. Rotational speed:  $n = 150rpm$

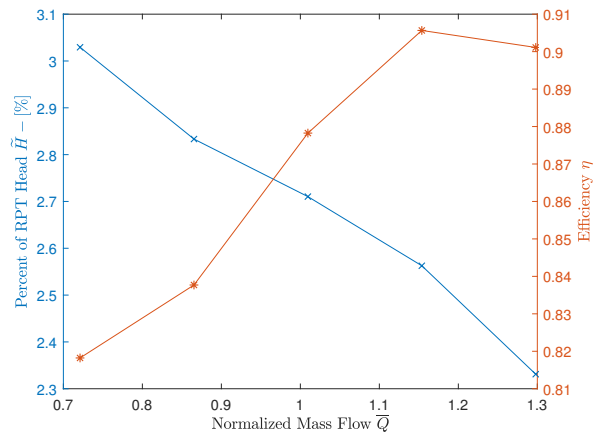


**Figure B.4:** Pump curves for the large mixed-flow booster-pump

The rotational speed was set such that the velocity diagrams at the inlet of the impeller would fit with the inlet angle of  $\beta_1 = 22.5^\circ$  at the midspan of the impeller. This angle gave a rotational speed of  $150rpm$ , which lead to the pump curves given in Fig. B.4. Because of the low rotational speed, the net head of the booster pump is quite low compared to the RPT. The head of the booster-pump could increase by giving the pump longer impeller blades or increasing the rotational speed of the runner. Another way of increasing the head of the booster pump was to make the inlet area of the impeller smaller, thereby increasing the rotational speed needed to fit the velocity triangles at the inlet of the impeller.



Appendix C

Nepal Conference Paper

# Pre-rotation of inlet flow in a reversible pump turbine in pump mode

Rune H. Larsen\*, Petter Østby and Pål-Tore Selbo Storli

Waterpower laboratory, Department of Mechanical Engineering, NTNU, Alfred Getz' vei 4, 7034 Trondheim, Norway

\*Corresponding author: runehl@stud.ntnu.no

March 2019

**Abstract.** Norway has 50% of the European hydro reservoir energy storage, and many of these sites are highly suitable for retrofitting of pump-storage capabilities. To be able to reuse existing power plants by retrofitting with Reversible Pump Turbines (RPTs), the problem of cavitation in pumping mode must be solved. This has been proposed solved by the use of an axial booster pump in front of the RPT. A booster pump will create a rotational component in the flow leaving the booster pump. How this component will evolve as the flow approaches the RPT is uncertain, and how the rotation actually is at the inlet of the RPT is important for the operation and characteristics of the RPT, especially since it affects the cavitation properties of the unit, and might counteract the initial suggested solution by using the booster pump in the first place.

Steady-state CFD simulations on the full geometry of an RPT, including a spiral casing, draft tube, and guide vanes, have been performed using the commercial ANSYS CFX software and pump performance curves with and without pre-rotation have been obtained and investigated. The results suggest that pre-rotation in the opposite direction of the impeller rotation creates additional lifting height, according to the Euler machinery equation. However, efficiency does not increase.

## Keywords

*Reversible pump turbine, pump mode, pre-rotation, booster-pump, CFD, hydropower*

## 1. Introduction

### 1.1. Motivation

In an ever-evolving, technological world it is key to keep on improving existing technology. Hydropower is the world's largest source of renewable energy production [1]. Moreover, hydropower is clean, efficient and has a long lifetime compared to other forms of energy production. Another form of energy production comes from wind energy. In 2017, the average wind generating capacity in the US had increased by 224% since 1998

and is continuing to grow rapidly [2]. Decreased prices for installing wind power has made it the least-cost option for new power capacity in a large number of countries [3]. Enabling efficient collaboration between hydropower and wind power is the driving force behind this paper. *Renewables Global Status Report (REN21)* emphasizes the need for balancing energy production from intermittent renewable energy resources. That is, to utilize the surplus energy when production is higher than demand, and to store energy for times when energy production is too low [3]. RPTs (Reversible Pump Turbines) in pumped hydropower plants are an excellent tool for doing just so. According to the *Norwegian Water Resources and Energy Directorate (NVE)*, only nine out of 1676 hydropower plants in Norway are pumped hydro power plants. In order to help balance the European energy production, more pumped hydro power plants are needed. Norway has 50% of Europe's hydropower reservoir capacity and much of this capacity is suitable for retrofitting RPTs in existing Francis power plants [4]. Consequently, replacing Francis turbines with RPTs is a task that is being reviewed by the *Norwegian Research Centre for Hydropower Technology (HydroCen)*.

When replacing Francis turbines with RPTs, the problem of cavitation in pump mode needs to be solved. In pumping mode, there is a need for added lifting height due to the opposing friction in the waterways. This, along with other factors, leads to pressure zones below vapor pressure at the suction side of the impeller, and hence, cavitation occurs. In order to avoid cavitation in pump mode, the RPT would normally have had to be submerged further down, leading to the creation of new waterways. According to NVE, this implies that the project of replacing Francis turbines with RPTs would not be economically beneficial [5]. A proposed solution, which sidesteps the costly procedure of building new waterways, is to add an axial booster pump in front of the draft tube (when seen in pump mode). The hope is that the solution gives cost savings large enough to make the project profitable. Regardless of the economics involved in the project, an axial booster pump may produce a rotational component in the flow. How this rotational component at the inlet of the draft tube will affect the pump curve is of interest because it may alter the pump's characteristics. This paper will investigate how the rotational component will affect the performance of an RPT in pump mode.

## *1.2. Theory and previous work*

An RPT is essentially a radial pump in one rotational direction and a turbine in the opposite rotational direction [6]. For this paper, only pump mode will be of interest. A rotational component in the inlet of a pump is often referred to as pre-rotation, pre-whirl or pre-swirl when studying turbomachinery, and the phenomenon occurs in other cases than with just a booster pump. It can, for example, occur at flow rates considerably below BEP (Best Efficiency Point) in normal single stage pumps. The pre-rotation occurs because of an important type of secondary flow which can be present in pumps, namely backflow. This is caused by a leakage flow between the tip of the blades of an

impeller and the pump casing. Below a certain mass flow, the pressure difference driving the leakage flow becomes sufficiently large so that the tip leakage jet penetrates upstream of the inlet plane of the impeller, and forms a region of backflow on the impeller inlet duct [7]. Pre-rotation can also occur from secondary flows induced by bends, or from geometry which alters the flow towards the impeller and adds a rotational component to the flow. According to the Euler turbo machinery equation, the head,  $H$ , is given by:

$$H = \frac{1}{g}(U_2 C_{\theta_2} - U_1 C_{\theta_1}) \quad (1)$$

where  $U$  represents the circumferential velocity of the impeller,  $C_{\theta}$ , represents the absolute peripheral velocity of the fluid,  $g$  represents the gravitational constant and the subscripts  $_1$  and  $_2$  represents inlet and outlet of the pump, respectively [6]. If there is not anything obstructing the flow in front of the impeller, one normally assumes that the inlet of the pump is rotation free [8], meaning  $C_{\theta_1} = 0$ . In this paper, this will not be the case.

Controlling the inlet angle of the flow is desirable, meaning that regulation of the inlet angle of the flow could be a suitable measure for regulating the flow and increase efficiency over the entire operating range. Pre-whirl regulation on centrifugal pumps with IGVs (Inlet Guide Vanes) has been investigated by Liu and Amjad [9], [10]. These reports show that pre-whirl with IGVs can greatly increase or decrease the performance curves of a centrifugal pump in a wide operational region. For the pump investigated in these papers, the improvement was up to 2.0% increase in efficiency at certain operational points. This is a substantial increase and suggests that the idea is worth pursuing. Another research paper that investigates the possibility of pre-whirl regulation on a full-scale pump-turbine is given by Keith [11]. In his paper, the pre-rotation is induced by water jets in the draft-tube cone. However, though the paper is thorough, the results of the paper are inconclusive due to the fact that the blowing intensity was not enough to alter the angular momentum in the flow for this particular pump turbine.

### 1.3. Hypothesis and objective

It is hypothesized that pre-rotation will change the characteristics of an RPT in pumping mode. In this paper, pre-rotation will be induced in front of the draft tube. How the rotational component evolves throughout the draft tube and how this affects the performance curves of the RPT will be investigated.

## 2. Numerical Setup

The RPT used in this paper is a model including a draft tube, a runner with 9 blades, 26 guide vanes, 26 stay vanes, and a spiral casing. The RPT has a specific speed,  $\Omega_s$ , of 0.575 according to the dimensionless number given by:

$$\Omega_s = \frac{\Omega \sqrt{Q}}{(gH)^{3/4}} \quad (2)$$

where  $\Omega$  is the rotational speed of the impeller,  $Q$  is the volume flow and  $H$  is the head over the entire domain [12]. The specific speed is calculated at BEP in pumping mode. In the present work, the computational fluid dynamics software ANSYS CFX 19.1 and the RNG k-epsilon turbulence model has been applied for steady state calculations. The boundary conditions have been set as a mass flow inlet with tangential velocity components in order to induce pre-rotation, and static pressure outlet condition was set at the outlet of the spiral casing. No-slip wall conditions have been utilized on all the walls, stationary and rotating, and the  $y^+$  values have been kept under 300 in all domains with an average of below 130 following the criteria given by Gulich [13]. For modeling the interface between the stationary and rotating domains, the frozen rotor interface model has been applied to serve as initial conditions, while the mixing plane model has later been applied for precision. The simulations have been performed in such a way that all operating points have had enough iterations to reach oscillatory convergence with mean root square residuals below  $10^{-4}$ . It should be noted that some oscillatory behavior in the head and efficiency was present at the end of the simulations.

ANSYS  
R19.1  
Academic

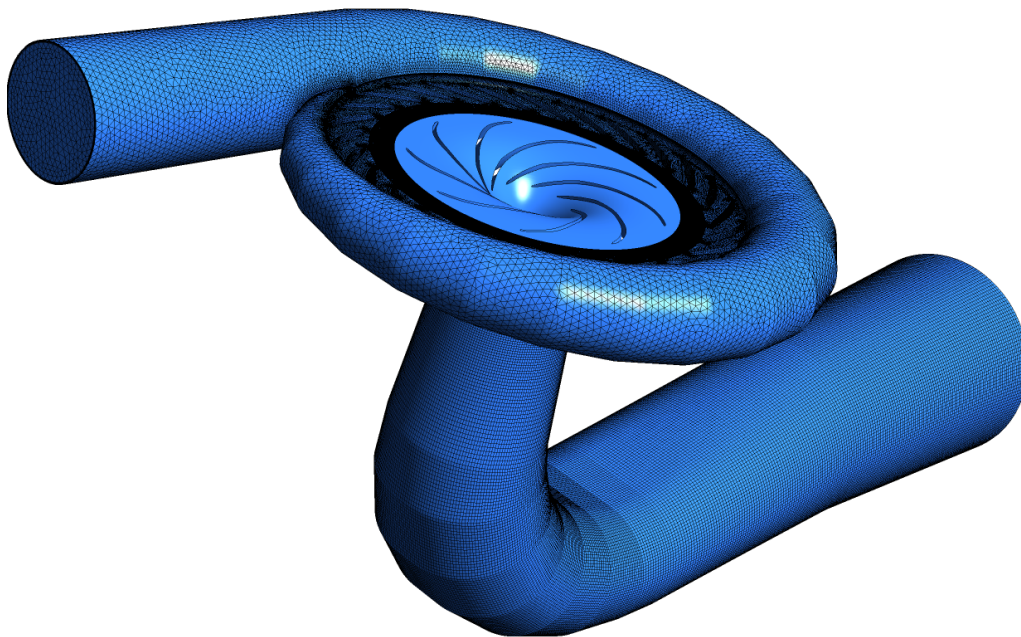


**Figure 1.** The RPT used, including spiral casing, stay vanes, guide vanes, runner and draft tube.

## 2.1. Computational mesh

The meshing of the guide vanes and the impeller is done using Turbogrid, creating a fully structured hexahedral mesh. The draft tube is meshed using ANSYS Meshing and with use of the Multizone method, creating an unstructured hexahedral mesh. The mesh in the draft tube includes an inflation layer with 15 layers with the first element height being controlled for holding the  $y+$  values down. The spiral casing, including the stay vanes, is meshed using ANSYS Meshing using the patch conforming method. Here, eight inflation layers have been applied, also controlling the first element height for  $y+$  considerations. The quality criteria recommended by ANSYS CFX for aspect ratio, expansion factor, and orthogonal quality has been upheld for all domains, except for a small percentage of elements containing expansion factor of above 50 at the leading and trailing edge of the stay vanes. Since the percentage of these elements are well below 1% the quality of the mesh is deemed sufficient. The geometry, along with the structured surface mesh in the draft tube and the unstructured mesh in the spiral casing, can be seen in figure 1.

## 2.2. Mesh independence study

To validate the independence of the mesh, a mesh independence study has been performed in accordance with the guidelines set by the *Fluids Engineering Division of ASME* [14]. For validation of the independence of mesh density, three sets of meshes with element count from 8 million elements to 30 million elements were investigated. Further details can be seen in table 1. For the study, BEP with no pre-rotation was investigated and set as a baseline for mesh verification. How the values for the torque and head varied with the mesh size can be seen in figure 2. From the mesh independence study, it was decided that the medium mesh would be sufficient for further calculations. The decision was based on the computational resources available and also the level of accuracy needed for this research.

**Table 1.** Mesh independence study at Best Efficiency Point

Item	Mesh 1	Mesh 2	Mesh 3
Draft Tube	3,738,726	1,926,000	952,666
Runner	9,487,350	4,408,560	2,150,010
Guide Vanes	8,370,648	4,244,604	2,122,302
Spiral Casing and Stay Vanes	9,460,379	4,883,139	2,819,084
Total number of elements	30,712,124	15,462,303	8,044,062
$H/H_3$	0.9935	0.9946	1
$T/T_3$	0.9943	0.9972	1
$H - GCI$	0.57%	2.77%	
$T - GCI$	1.42%	1.43%	

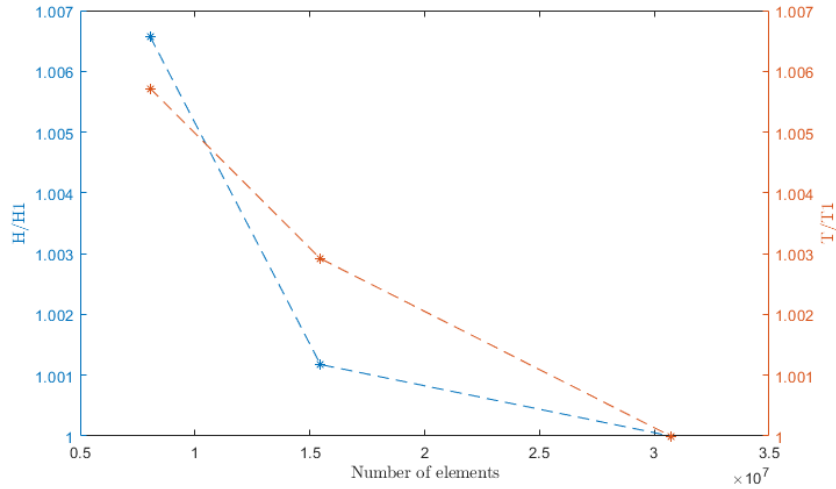


**Figure 2.** Mesh independence study at BEP. The values are normalized with respect to the finest grid.

### 2.3. Inlet boundary condition

Specification of the correct boundary conditions in a CFD calculation remains as one of the most critical tasks in order to get physical results [15]. Therefore, great care was taken when considering the inlet condition. For inducing the pre-rotation, a mass flow inlet boundary condition was used. The tangential component was set such that the inlet would have four different inlet angles;  $-24^\circ$ ,  $-12^\circ$ ,  $12^\circ$  and  $24^\circ$ , in addition to no pre-rotation. How the pre-rotation was imposed can be seen in figure 3. In figure 3, the circumferential velocity component of the inlet boundary condition is plotted as a vector field. This inlet angle will not accurately model an axial booster pump, nor will it accurately model an inlet flow from IGVs. When imposing pre-rotation to the flow, one will also add energy to the flow, compared to what it would be without any pre-rotation. This must be taken into account when considering the results. Positive pre-rotation is defined as an angle that add circumferential velocity component in the reverse direction of the runner rotation, while negative pre-rotation would be the opposite. That is if one assumes that the swirl will continue in the same direction through the bend in the draft tube. Hence, positive pre-rotation would add energy to the flow according to the Euler turbo machinery equation (1).

## 3. Results and discussion

From figure 4, one can see that the overall trend seems reasonable compared to experimental data. The simulated data has a bit lower gradient than the experimental data, meaning that the simulations, in general, overpredict the simulations at 1.2 BEP and at BEP. At 0.8 BEP, the results seem to hit spot on. This results in a lower overall gradient for the simulations than for the experiment. Here, a simple spline function in

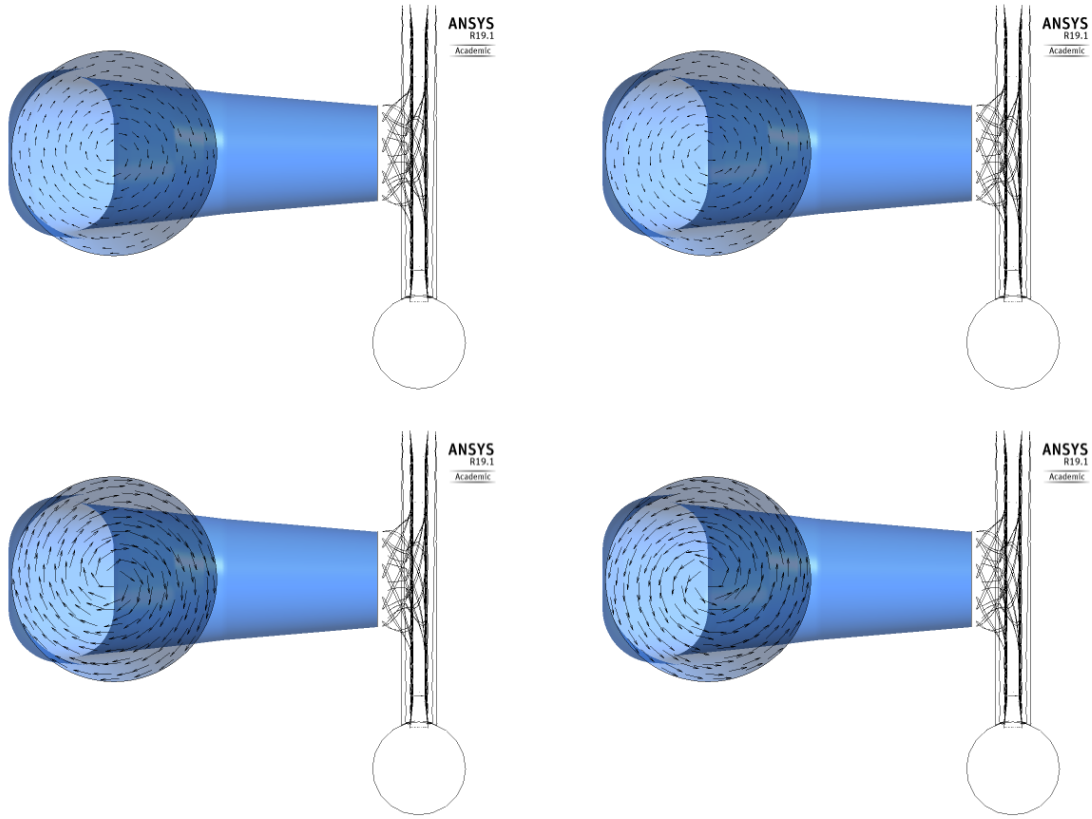


**Figure 3.** Inlet angle for the different simulations; top-left: 12°, bottom-left: 24°, top-right: -12°, bottom-right: -24°

MATLAB has been utilized in order to compare and visualize the trends compared to a linear line between the different operational points. Further, one can see that in general, pre-rotation in the opposite direction of the impeller rotation creates additional lift over the whole operating range. This is in accordance with equation (1), and it can be argued that with added pre-rotation, the impeller has the possibility to generate more torque because of the altered inlet angle. However, as mentioned earlier, it is tricky to estimate how much energy is added to the system by adding pre-rotation and hence how this will alter the characteristic curve in itself. This must be taken into account when comparing the different curves. The head is calculated in ANSYS CFX by:

$$H = \frac{p_{s2} - p_{s1}}{\rho g} + \frac{C_2^2 - C_1^2}{2g} \quad (3)$$

where  $p_s$  represents the static pressure and  $C$ , represents the absolute velocity.

By investigating figure 5, one can see that the added lifting height does not correlate with increased efficiency. Firstly, one can see that the general trend is also captured by the simulations. However, overprediction of the efficiency is evident for all operating points. This is as expected since the steady-state simulation is not able to predict several losses that may occur in different domains. Therefore, overall efficiency is larger than the experiments for all operating points. However, all is not lost, it is assumed that the



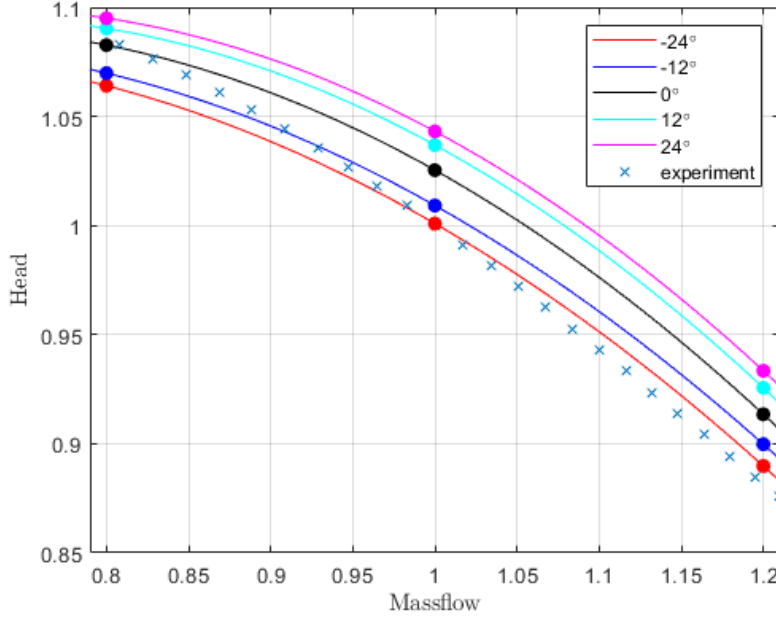


**Figure 4.**  $Q - H$  plot with normalized values for different pre-rotation values

simulation with no pre-rotation is most similar to the actual experimental data since the pre-rotation is not induced intentionally in the experimental data. Pre-rotation can be present at the inlet of the draft tube. Although, occurring because of bends or other obstacles in the water path prior to the draft tube. Pre-rotation can also occur from the pumps in the lab. However, if one assumed that zero pre-rotation is the most natural, one can see from figure 5 that efficiency actually is highest for zero pre-rotation for both 0.8 BEP and BEP. For 1.2 BEP one can see a slight advantage for 12° pre-rotation in the opposite direction of the impeller rotation, but this is only marginal. By this reasoning, one can say that pre-rotation is not beneficial for the pumps efficiency, at least for the situation investigated in this paper. Efficiency,  $\eta$ , is given by:

$$\eta = \frac{P_{out}}{P_{in}} = \frac{\rho g H Q}{\Omega T_{shaft}} \quad (4)$$

where  $P$  represents power,  $\Omega$  represents the impeller rotational speed,  $\rho$  represents density and  $T$  represents torque on the impeller [11].

#### 4. Conclusion

A numerical analysis was carried out to investigate the effects of pre-rotation prior to the draft tube on a pump turbine in pump mode. The results strengthen the hypothesis that pre-rotation will change the pump's characteristics. The simulations suggest that pre-rotation in the opposite direction of the impeller rotation creates additional lift for the entire pump range, while pre-rotation in the same direction as the pump impeller creates lower lift. This is in accordance with the Euler equation (1). Pre-rotation

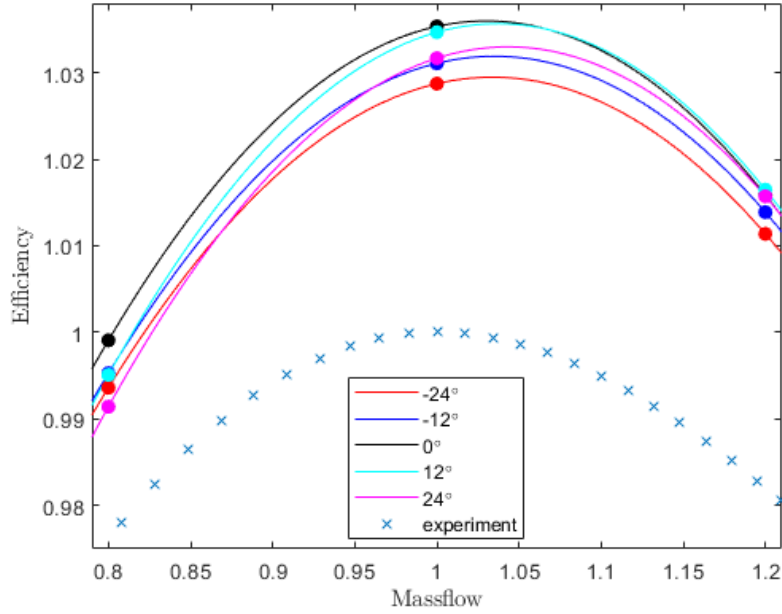


**Figure 5.**  $Q - \eta$  plot with normalized values for different pre-rotation values

does not, however, give higher efficiency. On the contrary, the simulations suggest that pre-rotation will decrease efficiency compared to the simulations with no pre-rotation. Compared to the experimental data, the simulated efficiency is higher. This is believed to be due to numerical inaccuracy and not the added pre-rotation.

## 5. Further work

More operating points should be simulated in order to validate that the trend is according to the splined function showed in this paper. Instead of imposing a uniform circumferential velocity field as an inlet condition it would be interesting to impose an actual velocity field from an axial booster pump. Further, simulating the actual booster pump in series with the RPT would be interesting, though the design of the booster pump still remains unfinished.

## References

- [1] C. H. St, N. Way, Y. Datuk, *et al.*, “Hydropower Status Report,” International hydropower association, Tech. Rep., 2018.
- [2] R. H. Wisler and M. Bolinger, “2017 Wind Technologies Market Report,” Tech. Rep. 12, 2016, pp. 26–30.
- [3] REN21, “Renewables 2018 - Global Status Report,” REN21 Secretariate, Paris, Tech. Rep., 2018, p. 41.
- [4] Hydrocen, “Pump turbines in existing power plants,” [Online]. Available: <https://www.ntnu.edu/hydrocen/2.3-pump-turbines-in-existing-power-plants>.
- [5] NVE/Vattenfall, “Pumpekraft i Noreg - Kostnader og utsikter til potensial,” Tech. Rep., 2011, p. 258.
- [6] H. Brekke, *Pumps and Turbines*. Trondheim: Vannkraftlaboratoriet NTNU, 2003.
- [7] E. C. Brennen, “Prerotation,” in *An Internet Book on Fluid Dynamics*, Danksat Publishing, 2016.
- [8] H. Brekke, *Introduction to hydraulic machinery*. Vannkraftlaboratoriet NTNU, 2000.
- [9] Y. Liu, L. Tan, M. Liu, Y. Hao, and Y. Xu, “Influence of prewhirl angle and axial distance on energy performance and pressure fluctuation for a centrifugal pump with inlet guide vanes,” *Energies*, vol. 10, no. 5, p. 695, May 2017.
- [10] S. Amjad Ahmed, A. Muiz, M. Mubashir, and W. Ahmed, “Efficiency Enhancement of Centrifugal Water Pump by Using Inlet Guided Vanes,” Tech. Rep. 10, 2016, pp. 1–4.
- [11] Keith A. Martin, “Analysis of the Effects of Pre-whirl on the Efficiency and Operating Range of Hydro Pumps used in Pumped Storage Facilities,” *Research Summary*, 2015.
- [12] S. L. Dixon and C. A. Hall, *Fluid mechanics and thermodynamics of turbomachinery*, 14th ed. ELSEVIER, 2014, p. 537.
- [13] J. F. Gülich, “Numerical Flow Calculations,” in *Centrifugal Pumps*, Berlin, Heidelberg: Springer Berlin Heidelberg, 2014, pp. 499–574.
- [14] ASME, “Procedure for Estimation and Reporting of Uncertainty Due to Discretization in CFD Applications,” *Journal of Fluids Engineering*, vol. 130, no. 7, 2008.
- [15] H. Keck and M. Sick, “Thirty years of numerical flow simulation in hydraulic turbomachines,” *Acta Mechanica*, vol. 201, no. 1-4, pp. 211–229, 2008.



